



NBS TECHNICAL NOTE 945

U.S. DEPARTMENT OF COMMERCE / National Bureau of Standards

An Investigation of the Fire Environment in the ASTM E 84 Tunnel Test

An Investigation of the Fire Environment in the ASTM E 84 Tunnel Test

William J. Parker

Center for Building Technology
Institute for Applied Technology
National Bureau of Standards
Washington, D.C. 20234



U.S. DEPARTMENT OF COMMERCE, Juanita M. Kreps, Secretary

Dr. Sidney Harman, Under Secretary

Jordan J. Baruch, Assistant Secretary for Science and Technology

NATIONAL BUREAU OF STANDARDS, Ernest Ambler, Acting Director

Issued August 1977

National Bureau of Standards Technical Note 945

Nat. Bur. Stand. (U.S.), Tech Note 945, 75 pages (Aug. 1977)

CODEN: NBTNAE

U.S. GOVERNMENT PRINTING OFFICE
WASHINGTON: 1977

For sale by the Superintendent of Documents, U.S. Government Printing Office, Washington, D.C. 20402
Price \$2.20 (Order by SD Catalog No. C13.10:46:945) Stock No. 003-003-01819-8

CONTENTS

	Page
LIST OF FIGURES	v
LIST OF TABLES	vii
NOMENCLATURE	viii
ABBREVIATIONS	ix
CONVERSION OF UNITS	ix
Abstract	1
1. INTRODUCTION	1
1.1. General	1
1.2. Hazard Classification and Reproducibility	2
1.3. Comparison with Corner and Room Fire Tests	3
1.4. Diagnostic Measurements in the Tunnel	4
2. DESCRIPTION OF ASTM E 84 Tunnel Test Method	5
2.1. Test Apparatus	5
2.2. Operation	6
2.3. Classification	7
3. INSTRUMENTATION	8
3.1. General	8
3.2. Temperatures	8
3.3. Oxygen Concentration	9
3.4. Air Velocity	9
3.5. Heat Flux	9
4. RESULTS AND DISCUSSION	10
4.1. Noncombustible Specimens	10
4.1.1. Temperature	10
4.1.2. Oxygen Concentration	11
4.1.3. Air Velocity	14
4.1.4. Pressure Drop in Tunnel	15
4.1.5. Heat Flux	17
4.2. Experiments with Auxiliary Burner	20
4.2.1. General	20
4.2.2. Flame Distance	20
4.2.3. Oxygen Depletion	21
4.2.4. Temperature	22
4.2.5. Velocity	23
4.2.6. Heat Flux	23
4.2.7. Smoke	23
4.3. Experiments with 0.92-Meter (3-ft) Combustible Specimens	23
4.3.1. General	23
4.3.2. Heat Release Rates	24
4.3.3. Flame Distance	26
4.4. Combustible Specimens of Standard Length	28
4.4.1. General	28
4.4.2. Flame Distance	29
4.4.3. Temperature	29

CONTENTS (cont'd)

	Page
4.4.4. Oxygen Concentration	30
4.4.5. Air Velocity	30
4.4.6. Burning Rate	31
4.4.7. Smoke	31
4.5. Effect of Air Velocity on Flame Spread in the Tunnel	31
4.6. Effect of Ceiling-Wall Mounting of Specimens in the Tunnel	31
5. SUMMARY	33
6. RECOMMENDATIONS	36
7. ACKNOWLEDGMENT	38
8. REFERENCES	39

LIST OF FIGURES

	Page
Figure 1. Details of Test Furnace.	40
Figure 2. Cross Section of Furnace at BB of Figure 1	41
Figure 3. Time-Temperature Curve for the Fuel Contribution Thermocouple for an ACB Specimen.	42
Figure 4. Centerline Air Temperature Profiles at Various Distances in the Tunnel for an ACB Specimen at 10 Minutes	42
Figure 5. Temperatures on Rear Wall and on Floor at 14 Feet for an ACB Specimen at 4 Minutes.	43
Figure 6. Temperature Distribution Along Exposed and Unexposed Surfaces of AMB Specimen at 20 Minutes and in the Air One Inch below It at 10 Minutes	43
Figure 7. Temperature Distributions Across Exposed and Unexposed Surfaces of AMB and 25 mm below It at 2.5 Feet at 20 Minutes.	44
Figure 8. Chart Record of the Oxygen Concentration in the Duct 22 Feet Downstream from the End of the Tunnel for an ACB Specimen.	45
Figure 9. Oxygen Concentration Versus Distance Along the Floor with an ACB Specimen at 5 Minutes.	45
Figure 10. Vertical Oxygen Concentration Profile at Nine Feet with an ACB Specimen at 5 Minutes.	46
Figure 11. Oxygen Depletion Profiles at 3, 9, 14 and 23 Feet for an ACB Specimen at 5 Minutes.	46
Figure 12. Horizontal Velocity Distribution of the Ambient Air Along the Midheight at the End of the Tunnel	47
Figure 13. Vertical Velocity Profile through the Centerline at Nine Feet with the Burner Off	47
Figure 14. Vertical Velocity Profile through the Centerline at Nine Feet with the Burner On for 4 Minutes.	48
Figure 15. Vertical Velocity Profile through Centerline at 14 and 20 Feet for ACB with the Burner On for 4 Minutes and for 20 Feet with Burner Off	48
Figure 16. Chart Record of the Inflow Velocity for ACB Measured with the Thermoanemometer	49
Figure 17. Pressure Distribution on the Floor of the Tunnel with the Burner Off	49
Figure 18. Location of Pressure Points Discussed in Section 4.1.4	50
Figure 19. Variation in Incident Heat Flux with Time at Two Feet.	50
Figure 20. Incident Heat Flux Distribution Along an AMB Specimen at 20 Minutes.	51
Figure 21. Convective Heat Flux Distribution Along an AMB Specimen at 10 Minutes.	51
Figure 22. Flame Distance Versus Time at Different Flow Rates of Methane in Auxiliary Burner	52
Figure 23. Flame Spread Distance Versus Total Methane Flow Rate in Auxiliary Burner	52
Figure 24. Oxygen Depletion in the Duct 22 Feet Downstream from the End of the Tunnel Using the Auxiliary Burner.	53

LIST OF FIGURES (cont'd)

	Page
Figure 25. Oxygen Concentration on Floor of Tunnel at Nine Feet Using Auxiliary Burner.	53
Figure 26. Temperature Rise of Fuel Contribution Thermocouple as a Function of Gas Flow	54
Figure 27. Vertical Temperature Profiles at 9 Feet at 5 Minutes Using Auxiliary Burner.	54
Figure 28. Vertical Temperature Profiles at 16 Feet at 5 Minutes Using Auxiliary Burner	55
Figure 29. Temperature Distribution Along Wall at 14 Feet at 5 Minutes Using Auxiliary Burner.	55
Figure 30. Temperatures for AMB Under Full Flame Exposure at 20 Minutes Using Auxiliary Burner.	56
Figure 31. Vertical Velocity Profiles at 9 Feet at 5 Minutes Using Auxiliary Burner.	56
Figure 32. Incident Heat Flux Distribution Along an AMB Specimen Fully Covered with Flame at 20 Minutes.	57
Figure 33. Flame Distance Versus Fuel Generation Rate in the Tunnel.	57
Figure 34. Air Temperatures at Called Flame Distances for Three-Foot Specimens .	58
Figure 35. Flame Spread Distance Versus Time for Four Materials.	58
Figure 36. Relationship Between Flame Front and Pyrolysis Zone for Red Oak Deck in the Tunnel.	59
Figure 37. Temperature Versus Time on Heat Contribution Thermocouple for Five Materials	59
Figure 38. Temperature Distribution Along Wall at 14 Feet at 5 Minutes for Type B Specimen	60
Figure 39. Vertical Temperature Profiles at 9 Feet at 5 Minutes for Specimens of ACB and Type B (F.R. Polyurethane FSC 28).	60
Figure 40. Vertical Temperature Profiles at 16 Feet at 5 Minutes for Specimens of ACB and Type B	61
Figure 41. Chart Record of Oxygen Concentration on the Floor of the Tunnel at 10 and 18 Feet for a Type B Specimen	61
Figure 42. Chart Record of Oxygen Concentration on Floor and Ceiling at 22 Feet for a Type B Specimen	62
Figure 43. Chart Record of Oxygen Concentration on the Floor of the Tunnel at 10 and 18 Feet for an Oak Specimen	62
Figure 44. Chart Record of Oxygen Concentration on the Floor of the Tunnel at 10 and 18 Feet for an Oak Specimen	63
Figure 45. Chart Record of Oxygen Concentration at the Ceiling of the Tunnel at 22 Feet for an Oak Specimen.	63

LIST OF FIGURES (cont'd)

	Page
Figure 46. Chart Record of Oxygen Concentration on the Floor of the Tunnel at 10 and 18 Feet for a Type O Specimen.	64
Figure 47. Chart Record on Inflow Velocity Data for a Type O Specimen	64
Figure 48. Average Burning Rate Distribution Along a Type B Specimen for a 5-Minute Period.	65
Figure 49. Decomposed Depth Versus Distance for Type B Specimen Over a 5-Minute Period	65

LIST OF TABLES

	Page
Table 1. Property Data Used in the Calculations	5
Table 2. Heat Produced per Volume of Oxygen Consumed for Some Common Polymeric Materials.	12
Table 3. Peak Heat Release Rates Deduced from the Oxygen Depletion in the Duct Compared with Those from the NBS Heat Release Rate Calorimeter at 3 W/cm ²	25
Table 4. Flame Distances in the Tunnel for 3-Foot and 24-Foot Specimens . . .	26
Table 5. Flame Distance in the Tunnel Versus Air Velocity for Three Low FSC Foam Plastics.	32
Table 6. Effect of Ceiling-Wall Mounting on Distance and Time in the Tunnel .	33

NOMENCLATURE

C	Heat capacity of air
d	Maximum distance of flame travel beyond the end of the burner flame
D	Hydraulic diameter = 4 times the cross sectional area divided by the perimeter
E	Ratio of eddy diffusivities for heat and momentum
f	Friction factor for the tunnel surface
FC	Fuel contribution classification
FSC	Flame spread classification
G	Mass flow rate
h	Surface heat transfer coefficient
H	Total incident heat flux
H _C	Convective component of the heat flux
K	Thermal conductivity
L	Length
ΔP	Pressure difference
q	Heat release rate per unit area
Q	Total rate of heat production in the tunnel
Q _B	Rate of heat production from the burner
Q _L	Total rate of heat loss in the tunnel
S	Number of volumes of oxygen required for the complete combustion of one volume of fuel
SDC	Smoke development classification
t	Time
T	Absolute temperature
T _O	Ambient absolute temperature
T _S	Absolute temperature of the exposed face of the specimen
T _R	Absolute temperature of the back face of the specimen
ΔT	Temperature difference
V	Air velocity
V _a	Volumetric flow rate of air
V _g	Volumetric flow rate of gas
x	Thickness of specimen
Y	Oxygen concentration in the tunnel
Y _O	Oxygen concentration of normal air (20.8 percent)

NOMENCLATURE (cont'd)

- ϵ Emittance of specimen surface
- ϕ Oxygen depletion = $\frac{Y_o - Y}{Y_o} \times 100$ percent
- ϕ_B Oxygen depletion in duct due to regular burner only
- ρ Air density
- σ Stefan Boltzmann constant
- ν Kinematic viscosity

ABBREVIATIONS

- ACB Asbestos Cement Board
- AMB Asbestos Millboard
- ASTM American Society for Testing and Materials
- NBS National Bureau of Standards
- UL Underwriters' Laboratories

CONVERSION OF UNITS

- 1 Btu = 1.054 kJ
- 1 Btu/s = 1.054 kW
- 1 Btu/ft²s = 1.14 W/cm²
- 1 ft = 0.305 m
- 1 in = 25.4 mm
- 1 mil = 25.4 μ m
- 1 cfm = 0.473 dm³/s = 0.473 l/s
- 1 cfh = 7.88 cm³/s
- 1 lb = 0.454 kg
- 1 lbf = 4.45 N
- 1 in of water = 249 Pa
- 1 °F = 0.555 °C
- T (°F) = 1.8 T (°C) + 32

AN INVESTIGATION OF THE FIRE ENVIRONMENT IN THE ASTM E 84 TUNNEL TEST

William J. Parker

Measurements were made of heat flux, oxygen concentration, temperature, velocity and pressure in a series of instrumented ASTM E 84 tunnel tests using (1) standard length specimens, (2) 0.91-m (3-ft) long specimens, and (3) a reference specimen consisting of asbestos-cement board and an auxiliary controlled supply of methane. Five different flow rates of methane to the auxiliary burner provided constant and known heat inputs simulating the gaseous decomposition products from regular test specimens. Incident heat fluxes on an inert specimen surface as high as 6.3 W/cm^2 ($5.5 \text{ Btu/ft}^2 \cdot \text{s}$) were measured within the flame impingement zone with a water-cooled heat flux meter 0.61 m (2 ft) downstream from the burner. While oxygen depletion in the tunnel did not appear to be a dominating factor in controlling the flame spread, the oxygen depletion measured in the exhaust duct beyond the tunnel correlated with the total rate of heat production of the specimens. It appears that the differences in the observed burning behavior of materials in the tunnel test and in a room may be mainly due to differences in the incident heat flux distribution in the two cases. These distributions reflect the different geometries, orientations, and ignition sources. The potential for rapid flame spread of some low flame spread classification (FSC) low density materials is evident from observations of the flame propagation along these materials during the tunnel test, but is not adequately reflected in the flame spread classification.

Key words: ASTM E 84; fire tests; flame spread; heat flux; heat release rate; smoke; Steiner Tunnel Test; oxygen depletion.

1. INTRODUCTION

1.1. General

Prior to 1950 fire protection of buildings dealt primarily with (1) the prevention of fire, (2) early detection and warning, (3) confinement with fire resistant structural components (e.g. walls, partitions, floors, ceilings, doors, etc.), and (4) extinguishment. Major fires which spread rapidly along interior surfaces causing large property losses and high death tolls due to the effects of smoke and toxic gases alerted the fire protection community to the need for a test which could be used to regulate interior finish materials with respect to their burning characteristics (e.g. flame spread, heat release, and smoke production).

The tunnel test was originally developed at Underwriters' Laboratories (UL) by A. J. Steiner for determining the fire hazard classification of building materials [1]¹.

¹ Numbers in brackets refer to the literature references listed at the end of this paper.

The three classifications determined in the Steiner tunnel are flame spread, fuel contribution, and smoke production. The first formal test standard (UL 723) was published by UL in 1950 with revised editions in 1958, 1960, and 1971. The test was adopted by the American Society for Testing and Materials (ASTM) as a tentative standard (E 84) in 1950 and formally adopted in 1961 with revised editions in 1960, 1970, and 1972. It was adopted as a standard of the National Fire Protection Association (NFPA No. 255) in 1955 with revised editions in 1958, 1961, 1966, 1969, and 1972. It was approved as an American National Standard (A 2.5) by the American National Standards Institute (ANSI) in 1963 with a revised edition in 1970. The tunnel test has been adopted by all four of the model building codes and is used by regional and local code authorities.

Prior to 1960 the tunnel test was used primarily for the evaluation of the surface burning characteristics of interior finish materials for walls and ceilings. In the late 1960's an appendix entitled, "Guide to Mounting Methods" was added to the Standard to permit the testing of materials which were not self-supporting. These materials include acoustical panels, adhesives, cementitious mixtures, sprayed fiber, batt or blanket insulation, loose fill insulation, coatings, piping, floor coverings, etc.

The tunnel test has thus been used to examine a large range of materials with a specimen area of sufficient size to include joints and other construction details and to be affected by delaminations and deformations which might be expected to occur in an actual fire. The 7.3-m (24-ft) long specimen which forms the ceiling surface of the tunnel has an exposed width of 0.46 m (1.5 ft) and is exposed to a 1.4-m (4.5-ft) long igniting flame with a total heat release rate of 88 kJ/s (5000 Btu/min) based on the gross heat of combustion of methane. The tunnel is lined on the floor and walls with fire brick. The igniting flame, which covers approximately 0.65 m² (7 ft²) of the specimen surface, is of an area that might typically be encountered by a wall exposed to a fire in a large waste container or a small upholstered chair. Air at a velocity preset prior to test at 1.2 m/s (240 ft/min) is drawn through the tunnel by means of a fan at the exhaust end.

1.2. Hazard Classification and Reproducibility

The flame spread classification described and used in this report is based on ASTM E 84-70 which was in effect at the time of this research. The three classifications derived in the tunnel test are each expressed on a scale which rates red oak flooring as 100 and asbestos-cement board, which is noncombustible, as zero. 1) The flame spread classification (FSC) is based on the time required for the flame to progress beyond the end of the tunnel or on the maximum distance reached during the 10-minute exposure period if the flame fails to reach the end. 2) The fuel contribution (FC) is based on the area under the temperature versus time curve over the 10-minute exposure period for the thermocouple located in the hot combustion product laden air 0.31 m (1 ft) upstream from the vent end of the tunnel and 2.5 cm (1 in) below the surface of the specimen. 3) The smoke development classification (SDC) is

based on the area under the light absorption versus time curve over the 10-minute exposure period measured by the smoke meter located in the duct some distance beyond the end of the tunnel.

Concern over the reproducibility of the test led Endicott and Bowhay [2] to perform a statistical evaluation of the effect of relative humidity, draft velocity, brick temperature, section length, specimen thickness, and preheat time on the three hazard classifications. The two materials used in this evaluation were Douglas fir plywood and particle board. The FSC was found to depend strongly on moisture content, brick temperature, preheat time, and specimen thickness, but had no significant dependence on draft velocity. On the other hand the smoke classification was highly dependent on velocity. However, the velocity was only varied between 1.17 and 1.27 m/s (230 and 250 ft/min).

While the above evaluation was performed by varying the test conditions on a single tunnel, Lee and Huggett [3] performed an interlaboratory evaluation involving nine materials and eleven tunnels each utilizing its normal operating conditions. For a series of eight specimens, the maximum coefficient of variation between laboratories was 43% for flame spread, 85% for smoke, and 117% for fuel contribution. These variations were due to differences in tunnel construction and in the operating procedure and illustrated a need to tighten up the standard to minimize these differences.

Changes in the standard are considered by the tunnel operators through the ASTM subcommittee E05.04. A new procedure for determining the FSC has been included in ASTM E 84-76a.

1.3. Comparison with Corner and Room Fire Tests

The evaluations described above dealt with the reproducibility of the fire hazard classifications measured by the tunnel test. They did not address the question as to the applicability of the classification to the growth of fires in rooms. Materials with FSC \leq 25 have generally been regarded by the building codes as providing a high degree of fire safety. Serious fires involving cellular plastics of undetermined FSC and demonstrations of rapid and extensive fire buildup in corners involving some low FSC cellular plastics at the University of California at Berkeley [4] and at Factory Mutual [5] have raised concern as to the applicability of the test for these materials.

The question of the applicability of the FSC of an interior finish material to its potential hazard in a full-scale fire was investigated by UL [6] in a series of vertical panel, open corner, corridor and room fire tests involving 31 different building materials whose FSC was measured in the tunnel and five different size ignition sources. Most of the experiments were performed with 9.1-kg (20-lb) wood cribs in the open corner configuration. Under these conditions the extent of the fire buildup in the open corner tests was roughly correlated with the FSC for the whole range of materials, but the rapidity of the fire buildup depended more on the density of the material than on its FSC. The results of the limited number of room fire tests indicated that a 9.1-kg (20-lb) wood crib, which is roughly equivalent in burning rate to

a small upholstered chair or a large waste container was a sufficiently large ignition source to cause full involvement of a 2.4 x 3.7 x 2.4 m (8 x 12 x 8 ft) room lined with a FSC \leq 25 material. When the material was a low density foam plastic, this buildup time was of the order of a minute and a half. It thus appears that an FSC \leq 25 is no assurance that a surface finish material is safe to use in a critical location. These low density materials are particularly serious because of their short buildup time to full room involvement. In the UL tests [6] a FSC 22 low density, 37 kg/m³ (2.3 lb/ft³), cellular plastic caused full involvement of a room in one-third of the time required for a FSC 178 medium density, 527 kg/m³ (31 lb/ft³), cellulosic. Full involvement occurred in one minute and 20 seconds for the low density material and four minutes and 20 seconds for the medium density material. Since a FSC 22 material has a maximum flame spread distance of only 2.7 m (9 ft) in the tunnel it is natural to inquire about differences in burning behavior between the tunnel and the room. It is also desirable to see if there are differences in burning behavior between cellulose and plastics in the tunnel. Clearly there is a need for analytical models for flame spread in the tunnel and in the room to provide guidance in the utilization of the tunnel data. The flame spread along a material depends on its environmental conditions which include the incident heat flux and the temperature, oxygen concentration, and the velocity of the air passing over its surface. There have been no extensive measurements made on the environment in the tunnel.

1.4. Diagnostic Measurements in the Tunnel

The present investigation was concerned with the characterization of the environment in the tunnel and with discovering significant elements of the burning behavior which could serve as a basis for establishing an analytical model for flame spread in the tunnel.

Recent measurements have also been reported by Quintiere and Raines [7] on the variation in the air velocity at the entrance to the tunnel during the test and some internal temperature distributions from which the heat losses along the tunnel could be deduced. These measurements were carried out on four different carpets in the Hardwood Plywood Manufacturer's Association tunnel in Arlington, Virginia. Maximum drops in the inlet air velocity during the tests ranged from 19 to 28 percent for the different materials tested. Approximately half of the heat produced by the burner flame was absorbed by the specimen or lost within the tunnel.

The data presented in this report came from seven groups of instrumented tunnel tests spaced approximately a month apart. Each group consisted of up to 20 tests which took two days to set up and run. The tests were conducted at Underwriters' Laboratories in Northbrook, Illinois and include air velocity, temperature, heat flux, oxygen concentration, pressure drop and specimen weight loss as well as the customary flame distance and smoke measurements. Although a large range of interior finish and insulation materials were included in this program, materials which would cause additional problems because of their melting and dripping during the test were excluded.

The nomenclature appears in the front of this paper (see page viii) and the property data used in the calculations are listed in table 1. This research project was undertaken during 1974 when the author participated in an NBS-UL scientific exchange program. The description of equipment and procedures in this report were current at the time of the research.

Table 1. Property Data Used in the Calculations

	Engineering Units	S.I. Units
Density		
Air 15 °C (60 °F)	0.0763 lbs/ft ³	1.22 kg/m ³
40 °C (105 °F)	0.0702 lbs/ft ³	1.12 kg/m ³
Heat Capacity		
Air 15 °C (60 °F)	0.24 Btu/lb °F	1.0 kJ/kg K
Air (average between 15 °C (60 °F) and 816 °C (1500 °F))	0.26 Btu/lb °F	1.09 kJ/kg K
Thermal Conductivity		
Asbestos Millboard	2.17×10^{-5} Btu/ft °F	0.135 W/m K
Asbestos-Cement Board	5.8×10^{-5} Btu/ft °F	0.36 W/m K
Heat of Combustion		
Methane gross 15 °C (60 °F)	1012 Btu/ft ³	39 J/cm ³
Methane net 15 °C (60 °F)	912 Btu/ft ³	34 J/cm ³
Kinematic Viscosity		
Air 15 °C (60 °F)	1.6×10^{-4} ft ² /sec	15 mm ² /s
Heat of Vaporization		
Water	1072 Btu/lb	2.49 kJ/g

2. DESCRIPTION OF ASTM E 84 TUNNEL TEST METHOD

2.1. Test Apparatus

The Steiner tunnel was developed at the Underwriters' Laboratories and is described in the ASTM book of fire test methods [8] and in the Underwriters' Laboratories standard UL 723. Nevertheless, a brief description of the instrument and its operation may be of value here in order to stress those elements which are most important to the present study. Furthermore, there are slight ambiguities in the write-up of the standard test, such that operational procedures can vary unless agreed upon by the different operators using the tunnel.

Basically, the instrument as used at the Underwriters' Laboratories in Northbrook is a steel duct-shaped enclosure 8.7 m (28.5 ft) long lined with fire brick on the floor and walls to provide a cross section 0.44 ± 0.01 m ($17.5 \pm 1/2$ in) wide and 0.3 ± 0.01 m ($12 \pm 1/2$ in) high. The front wall contains a series of viewing windows. (Refer to figures 1 and 2 for more details.) The specimen forms the ceiling closure

over the final 7.3 m (24 ft). The specimen is preceded by a 0.3-m (1-ft) section of 6.4-mm (1/4-in) thick asbestos-cement board (ACB). The other 1.1-m (3.5-ft) section is permanently closed by the steel shell. The 25-ft steel lid, which is lined with 51-mm (2-in) thick calcium silicate insulation over 6.4-mm (1/4-in) thick ACB, is closed in contact with the top of the specimen. The enclosure is rendered air-tight with a water seal. Methane gas is introduced through two nominal one-inch pipe burners spaced 0.2 m (8 in) apart along a line normal to the airflow. The pipes extend 0.11 m (4.5 in) above the floor, 7.3 m (24 ft) from the end of the tunnel. These burners provide the diffusion flames to expose the first 1.4 m (4.5 ft) of the specimen. All axial distances in the tunnel which are quoted in this report are measured downstream from these burners.

The air is admitted at the floor level of the tunnel through a 0.44-m (17.5-in) long slit with an adjustable height located 1.4 m (4.5 ft) ahead of the burner. The other end of the tunnel terminates in a circular exhaust duct 0.41 m (16 in) in diameter. Just beyond the tunnel the duct takes an upward turn and then a horizontal bend in order to run horizontal at right angles to the tunnel and 1.2 m (4 ft) above it. The duct terminates in a 0.6-m (2-ft) diameter stack with a fan at its base to provide the suction necessary to pull air through the tunnel. The negative pressure at a tap located in the duct approximately 6.7 m (22 ft) from the end of the tunnel is held constant by an automatic damper located downstream. There is a vertical path smoke meter located just ahead of the damper. There is a thermocouple located 25 mm (1 in) below the specimen at 7.0 m (23 ft) from the burner which provides the data for the fuel contribution index. There is a buried thermocouple 3.2 mm (1/8-in) below the surface of the floor of the tunnel at 4.3 m (14 ft) that is used to establish the starting temperature for each test.

2.2. Operation

Prior to test, the average air velocity is measured with a thermal anemometer at seven points across the width of the tunnel along the midheight 7.0 m (23 ft) beyond the burner. The velocity can be varied by changing the negative pressure at the pressure tap or by changing the height of the entrance slit. However, once these settings were established to get an average air velocity of 1.2 m/s (240 ft/min) with the tunnel preheated to 41 °C (105 °F), they have been fixed at a negative pressure drop of 18 Pa (0.072 in of water) and a slit height of 83 mm (3.25 in). With a methane flow to the burner of 2.3 dm³/s (4.9 cfm), corresponding to 8.8 x 10⁴ J/s (5000 Btu/min) (using the gross heat of combustion), red oak spreads flame past the end of the tunnel in approximately 5.5 minutes. The gas flow rate to the burner is measured by the difference in gas meter readings over the duration of the test.

Calibration runs are conducted approximately once a month to check the air velocity and the time at which flame passes over the end of the tunnel for red oak. Significant departures from the normal lead to trouble shooting rather than to the readjustment of the pressure, slit height, or gas flow which remain as fixed parameters of this tunnel. Leaks in the tunnel are sometimes found and repaired during this calibration process.

The time of flameover of the oak also depends on the degree of turbulence developed in the tunnel. Changes in tunnel construction through the years such as using flush rather than recessed viewing windows have caused a reduction in the turbulence which resulted in a corresponding reduction in flame spread. Five bricks have been placed on the floor of the tunnel at strategic locations to increase the degree of turbulence to the point that the red oak flamed over once again at 5.5 minutes. The location of these bricks are now fixed at 1.4, 2.3, 3.5, 5.0, and 5.9 m (4.5, 7.5, 11.5, 16.5 and 19.5 ft) from the burner. Their positions are alternated between the front and rear walls and they protrude into the tunnel 50 mm (2 in) horizontally and 200 mm (8 in) vertically.

The cold tunnel is preheated to 66 °C (150 °F) and then cooled to 43 °C (110 °F), as indicated by the buried thermocouple at 4.3 m (14 ft), before a specimen is inserted. The burner must be turned on and the test started while this temperature lies between 38 °C (100 °F) and 43 °C (110 °F). This may require heating or cooling between tests. The nominal starting temperature is taken to be 41 °C (105 °F). The windows are cleaned as necessary between tests and high temperature burnouts are conducted when the tunnel accumulates deposits such as those from dripping specimens.

The tunnel is operated by a technician who loads the specimen and electrically ignites a pilot flame which in turn ignites the burner gas when it is turned on. The gas meter reading is recorded before and after the test. A timer is started at the instant of ignition of the burner gas. The technician, records the time of ignition of the specimen for particular tests and monitors the pressure during all tests. The actual control of the pressure, and thus the airflow, through the tunnel is by means of the automatic damper in the duct. The temperature of the fuel contribution thermocouple and the light transmission through the smoke are recorded on a strip chart recorder. The technician records the times at which the engineer observes, through the observation ports, that the flame has reached various distances in the tunnel. The distance is reported to the nearest 0.15 m (0.5 ft).

The reading of the flame distance is done by trained personnel. This requires some judgment since much of the time the end of the flame is composed of brief flashes and detached flamelets. The observation can also be complicated by obscuration of the viewing ports by smoke from some materials. Although there is no written definition of what constitutes flame length, it is probably best defined as the distance at which there is flame present approximately one-half of the time over a time interval of several seconds. As will be brought out later, the reported flame distance appears to coincide with an abrupt decrease in the extent of the damage to the specimen.

2.3. Classification

At the time of the research the FSC was calculated from one of four formulas depending on how soon the flame reaches the end of the tunnel or where the flame stops within the tunnel. 1) If the flame spreads over in 5.5 minutes or less, the $FSC = 550/t$ where t is in minutes. This gives red oak which is the reference standard a FSC 100.

2) If the flame spreads over within the 10-minute test period, but takes greater than 5.5 minutes, the $FSC = 50 + 275/t$. 3) If the flame stops between 5.5 m (18 ft) and the end of the tunnel, the $FSC = 50 + 4.62 d$ where d is the maximum distance in meters traveled beyond the burner flame whose designated distance is 1.4 m (4.5 ft). 4) If the flame stops at 5.5 m (18 ft) (4.1 m (13.5 ft) past the burner flame) or less, the $FSC = 16.7 d$.

An important discontinuity was noted in this calculation procedure. If the flame were to spread to a point just short of the end of the tunnel in 0.55 minutes, the $FSC = 77.5$. If it passes over in the same time, $FSC = 1000$. Both situations could occur in the case of duplicate runs of the same material. A new calculational method in which the FSC is proportional to the area under a modified flame distance versus time curve has been included in ASTM E 84-76a to resolve this discontinuity.

3. INSTRUMENTATION

3.1. General

During the course of this project seven groups of instrumented tunnel tests were performed in order to establish the environment in the tunnel. Although the operation of the tunnel was usually the same as it would have been during a normal run, the presence of the monitoring instrumentation obviously had some effect on the environment it was attempting to measure. This instrumentation included pitot tubes, gas sampling tubes, and water-cooled heat flux meters all of which had copper tubing running along the floor of the tunnel and out through the entrance slit. Thermocouple support rods and their lead wires could also have affected the flow pattern. However, the inflow velocity and the times and distances of flame spread in the tunnel did not appear to be affected significantly. Nevertheless, it is well to keep in mind that these disturbances did exist to some degree. There was a drop in the air velocity of about 20%, however, when the rather massive auxiliary burner was added for the experiments described in section 4.2.

3.2. Temperatures

The temperatures in the tunnel were measured with 0.25 mm (10 mil) (#30 gage) Chromel Alumel and 0.25 mm (10 mil) Iron-Constantan thermocouples. Air temperature profiles were obtained at different distances with trees of either ten or twelve thermocouples spaced vertically and held in place on ring stands with high temperature cement. Wall and floor temperatures were measured with similar thermocouples held to the surface of the brick with plaster. The thermocouple leads were run along the floor out through the entrance slit of the tunnel and were connected to a 24-point temperature recorder with a 48-second print cycle (2 seconds between prints). Thermocouples on the exposed surface of the specimen or 25 mm (1 in) below it were mounted by drilling two holes 25 mm (1 in) apart and bringing the lead wires through the specimen and securing them to the unexposed surface. At that point the 0.25 mm (10 mil) wires were generally welded to 1.3 mm (50 mil; #16 gage) wires and then led along the top of the specimen

and back into the tunnel 0.31 m (1 ft) upstream of the burner and out through the slit. The lead wires on either side of the exposed thermocouple junction ran parallel to the specimen surface for 13 mm (1/2 in) in order to minimize heat conduction losses. Selected thermocouples at critical locations were connected to continuous pen recorders in order to obtain a better time response.

Temperature data were also taken with the 1.0 mm (40 mil; #18 gage) chromel alumel thermocouple at 7.0 m (23 ft) which is used to measure the fuel contribution in all of the regular tests.

No corrections to the thermocouple readings were made for radiation.

3.3. Oxygen Concentration

The oxygen concentration at various distances in the tunnel and in the exhaust duct was measured with a chemical oxygen cell which uses a KCl solution with gold and zinc electrodes. It has an output voltage which is directly proportional to the oxygen concentration. It nominally produces 180 mv for a 20.8 percent oxygen concentration. However, the output depends on the condition of the cell and decreases with age, requiring rejuvenation in six months or less depending on the usage.

A fiber glass filter was used to remove particulates, a charcoal filter was used to remove organic vapors, a silica gel filter was used to remove water and a pumice filter loaded with sodium hydroxide was used to remove acids. An adjustable flow meter between the cell and the vacuum line was set to produce a flow rate of 39 cm³/s (5 cfh) through the cell. The inlet to the series of filters was connected to a 6.4-mm (1/4-in) copper tube whose other end terminated at the sampling point. During the later phases of this project oxygen concentrations were also measured with a high temperature oxygen cell which oxidized any unburned fuel prior to the measurement.

3.4. Air Velocity

Velocities of the ambient air were measured with a hot film thermoanemometer and with pitot tubes. The pitot tube system alone was used at the elevated temperatures. The vertical velocity profiles were obtained with a bank of ten pitot tubes mounted on a ring stand. They were connected to a rotary fluid switch by means of 6.4 mm (1/4-in) copper tubing running along the floor of the tunnel and out through the entrance slit. This switch was used to connect the pitot tubes in sequence to the pressure transducer which was connected to a continuous pen recorder. Thermocouples were located near the tip of each pitot tube.

3.5. Heat Flux

The heat flux into the surface of the specimen or the floor of the tunnel was measured with heat flux meters either attached directly to an ACB specimen with a high temperature cement or mechanically attached to a water-cooled plate. Silicon stop cock

grease was used to reduce the thermal contact impedance between the meter and the underlying surface. The term heat flux meter as used in this report refers to a flat plate device which consists of a sandwich of three ceramic wafers. The center one is wound with alternate lengths of dissimilar wires welded together to form a thermopile which measures the temperature difference across the wafer. The output voltage is proportional to the heat flux conducted through the meter. This is sometimes called a thermal ammeter. The exposed face of the meter was given a coat of velvet black paint whose absorptance is 0.97.

The second method of measuring the incident heat flux was approximate but permitted the measurement at many different locations simultaneously. Thermocouples were located on the front and rear surface every 0.1 m (4 in) along two 1.2 m (4 ft) lengths of asbestos millboard (AMB). After a steady difference in temperature between the rear and front surface was achieved, the heat flux conducted into the specimen at each location was calculated from this temperature difference and the known thermal conductivity of the material. The heat flux radiated from the exposed surface was calculated from its temperature assuming an emittance of unity. The incident heat flux at equilibrium was considered to be equal to the sum of the radiation from the exposed surface and the conduction losses through the specimen. An emittance of 0.96 at 38 °C (100 °F) has been reported for asbestos board [9].

4. RESULTS AND DISCUSSION

4.1. Noncombustible Specimens

4.1.1. Temperature

In all of the standard tunnel tests the temperature is measured at a point 25 mm (1 in) below the specimen and a point 7.0 m (23 ft) from the burner and midway between the sides of the tunnel. The integral of the temperature rise over the ten-minute exposure period compared to that of an ACB specimen determines the heat contribution of the test specimen. This temperature history for an ACB specimen as recorded in UL 723 is reproduced in figure 3. During one of the instrumented tunnel tests on an ACB specimen the vertical temperature profiles were measured with an array of 10 thermocouples located at 0.92, 2.7, 4.3, 6.1 and 7.0 m (3, 9, 14, 20 and 23 ft). In figure 4 these profiles are compared at 10 minutes into the test. A peak temperature of about 800 °C (1500 °F) 25 mm (1 in) below the specimen is noted in the region of the burner flame. This is in the range of temperatures occurring 25 mm (1 in) from the ceiling of a room at the time of flashover. The temperature profile flattens as the air moves down the tunnel. Apparently the heat gained by the air in the lower part of the tunnel by mixing compensates for the heat losses to the floor so that the temperature near the floor doesn't change very much with distance.

Figure 5 shows the vertical variation of temperature along the wall for an ACB specimen at 4.3 m (14 ft) at four minutes. The data are badly scattered but they do indicate an average temperature of about 160 °C (340 °F) on the upper part of the wall.

This data was taken in order to estimate the expected radiation to the specimen. Note that a 160 °C (320 °F) black body surface will only radiate about 0.21 W/cm² (0.18 Btu/ft²·s).

The temperature of the lower exposed and upper unexposed surfaces of a 13-mm (1/2-in) thick AMB specimen is plotted as a function of distance after a 20-minute exposure in figure 6. The maximum exposed surface temperature of about 650 °C (1200 °F) occurs 0.61 m (2 ft) downstream from the burner. The calculation of the heat flux from these temperature distributions was described in subsection 3.5. The temperature distribution 25 mm (1 in) below an AMB specimen after 10 minutes is also shown in figure 6 in order to provide an estimate of the expected temperature gradient in the gas phase for heat transfer considerations. The gas temperature was nearly constant after 5 minutes. The lateral distribution of temperature across the exposed and unexposed surfaces of the AMB specimen and 25 mm (1 in) below it at 0.76 m (2.5 ft) is shown in figure 7 after a 20-minute exposure. The rear wall is the wall opposite to the one containing the viewing windows. These profiles covering one-half of the tunnel width show the degree of error incurred by assuming that the centerline temperature is the average over the total width. The reduction in the area under the curves due to heat losses at the wall was less than 5 percent. Data was not taken on the window side to check the effect of symmetry.

4.1.2. Oxygen Concentration

The decrease in oxygen concentration of the air leaving the tunnel provides an approximate measure of the heat released by the specimen. This is based on the assumption that for a given volume of oxygen consumed there will be a fixed amount of heat released regardless of the type of fuel. While this amount does vary, the variation is relatively small over a wide range of materials which are tested in the tunnel as seen in table 2. The values tabulated for the polymeric materials are calculated from the table appearing in an article by Throne and Griskey [10]. The tabulated heats of combustion are based upon complete combustion with all the carbon and hydrogen present in the reactants appearing in water and carbon dioxide in the products. The heat of combustion of cellulose is taken from Johnson [11] while the heats of combustion for hydrogen, carbon, and methane, included for reference purposes are taken from the Handbook of Chemistry and Physics [12]. The differences between the net and gross heats of combustion for the various materials were determined by multiplying the mass of water formed by its heat of vaporization which was taken to be 2.49 kJ/g (1072 Btu/lb). In calculations involving the air temperature rise in the tunnel or in a room fire we are concerned with the net heat of combustion since the water formed during the combustion process remains in the gaseous state in the region of interest. It is noted in the table that methane produces 16.4 MJ/m³ (441 Btu/ft³) of oxygen consumed and that this value represents all of the entries in the table to within ± 15% (Hydrogen excluded). If the chemical composition and heat of combustion of the material are known then its heat produced per unit volume of oxygen consumed can be calculated. However, the real value may deviate some from the calculated value if combustion is not complete.

Table 2. Heat Produced per Volume of Oxygen Consumed for Some Common Polymeric Materials

Materials	Heat of Combustion		Oxygen Requirement at 25 °C		Heat Produced per Volume of Oxygen Consumed at 25 °C					
	Heat of Combustion		Oxygen Requirement at 25 °C	Heat Produced per Volume of Oxygen Consumed at 25 °C	Heat Produced per Volume of Oxygen Consumed at 25 °C	Net				
	Gross (MJ/kg) (Btu/lb)	Net (MJ/kg) (Btu/lb)					(m ³ /kg) (ft ³ /lb)	(MJ/m ³) (Btu/ft ³)	(MJ/m ³) (Btu/ft ³)	
Polyethylene	46.6	20,050	43.4	18,670	2.63	41.9	17.8	479	16.5	446
Polypropylene	46.5	20,030	43.3	18,650	2.63	41.9	17.7	478	16.5	445
Polystyrene	41.5	17,850	39.7	17,110	2.36	37.6	17.6	474	16.9	455
Polyvinyl Chloride	17.9	7,720	16.9	7,260	1.08	17.2	16.6	449	15.7	422
Polymethyl Methacrylate	26.7	11,470	25.2	10,830	1.47	23.5	18.1	488	17.1	461
Phenol-formaldehyde (1:1)	27.9	12,000	26.7	11,480	1.86	29.7	15.0	404	14.3	386
Urea-formaldehyde (1:2)	17.8	7,680	16.8	7,220	1.02	16.3	17.5	471	16.4	443
Melamine-formaldehyde (1:3)	19.3	8,310	18.4	7,950	1.14	18.1	17.0	459	16.3	439
Polyurethane, ester based	23.7	10,180	22.4	9,650	1.32	21.1	17.9	482	17.0	457
Unsaturated polyesters	29.8	12,810	28.4	12,220	1.58	25.2	18.8	508	18.0	484
Butadiene/styrene (25.5%) Copolymer (GRS rubber)	44.2	19,010	41.9	18,020	2.46	39.3	18.0	484	17.0	459
Butadiene/acrylonitrile (37%) Copolymer	39.9	17,180			2.21	35.3	18.1	487		
Natural rubber	45.3	19,490			2.53	40.3	18.0	484		
Cellulose	16.6	7,160	15.2	6,560	0.91	14.5	18.3	494	16.8	452
Carbon	32.8	14,100	32.8	14,100	2.05	32.7	16.0	431	16.0	431
Hydrogen	143.0	61,550	120.6	51,900	6.14	98.0	23.3	628	19.6	529
Methane	55.8	24,000	50.2	21,590	3.07	49.0	18.2	490	16.4	441

Actually this deviation may be small because the reduction in heat produced is accompanied by a roughly equivalent drop in oxygen consumed. The heats of pyrolysis, dehydration, and evaporation for the material are included in its measured gross heat of combustion in the oxygen bomb calorimeter. The release of volatiles from the specimen surface and chemical reactions in the gas phase lead to volume changes in the flow which can also affect the oxygen concentration. This source of error, not considered to be large, is not considered here. In spite of these effects it is expected that the measured oxygen depletion would yield approximate values of the heat released in the tunnel which are better than those obtained by calorimetric methods because of the significantly high rate of heat losses in the tunnel.

The oxygen depletion is defined by

$$\phi = \frac{Y_o - Y}{Y_o} \times 100 \text{ percent} \quad (1)$$

where Y is the oxygen concentration during the test and Y_o is the concentration prior to the test. The determination of the oxygen consumed depends on knowing the mass flow rate of the air as well as the oxygen depletion and it is assumed that the depletion is constant over the cross section of the duct. The mass flow is nominally 0.207 kg/s (27.5 lbs/min) but drops by as much as 20 percent during the test for some materials in some tunnels [7]. The rate of air inflow should be monitored during the test. In fact it is hoped in the upgrading of the tunnel by the tunnel operators that the air velocity into the tunnel would be controlled rather than the pressure drop across the tunnel and the duct, thereby providing better uniformity between tunnels and a constant inflow air velocity in all of them. The gases are well mixed by the time they reach the sampling point near the pressure tap in the duct. This was verified by traversing the duct in the vertical direction with the sampling probe. Figure 8 shows the oxygen concentration measured at the centerline of the duct for an ACB specimen. The sampling point is at the location of the pressure tap approximately 22 ft downstream from the end of the tunnel. The 13-percent depletion is due to the consumption of oxygen by the burner flame. However, this value is reached relatively slowly due to lags in the measurement system. This poor time response is the source of some error in the peak oxygen depletion measured during short duration burns. However, the small cost and relative ruggedness of the cells justified their use in the preliminary investigation. In most of the cases this response was enough. The high temperature oxygen cell used later in the project provided a faster responding system.

The variation of oxygen concentration with distance on the floor of the tunnel due to mixing is shown in figure 9. The concentration is reduced about 0.6 percent at 3.1 m (10 ft) and about 1.8 percent at 5.5 m (18 ft). In a room fire the oxygen concentration is near normal in the free stream but drops as the flaming region is approached. In the tunnel the airflow near the floor should represent the free stream conditions of airflow temperature, and oxygen concentration insofar as possible. The additional drop in oxygen concentration caused by combustible specimens will be presented in subsection 4.4.4. Figure 10 shows the vertical oxygen concentration profile at 2.7 m (9 ft) in

the tunnel with an ACB specimen. The oxygen depletion profiles obtained at five minutes with the high temperature oxygen cell at 0.92, 2.7, 4.3, and 7.0 m (3, 9, 14, and 23 ft) midway between the walls of the tunnel are shown in figure 11. The oxygen depletion measured in the duct was 12.8 percent while the average depletion at 0.92 m (3 ft) was 18 percent. This difference can qualitatively be accounted for by the reduced mass flow rate of the heated air in the upper part of the tunnel.

4.1.3. Air Velocity

A knowledge of the air velocity profiles as well as the temperature profiles in the tunnel are necessary for computing the quantity of heat being carried along by the air and for estimating the heat transfer to the ceiling, walls, and floor. The rate of heat transfer to the specimen forming the ceiling controls its fuel production rate which in turn determines the flame distance and hence its FSC. Figure 12 shows the ambient velocity distribution measured across the tunnel at midheight and 7.2 m (23.75 ft) from the burner using a hot film anemometer. This profile is taken during the normal calibration runs of the tunnel to establish the average air velocity. In order to obtain the velocity profiles at elevated temperature it was necessary to use pitot tubes. Two factors limit the accuracy of these measurements. First, the velocities are below the optimum operating range of the pressure sensor producing pressure differentials in many cases of less than 2.5 Pa (0.01 in of water). Second, the introduction of the air through a slit near the floor of the tunnel, the location of the seven bricks purposely used to increase turbulence, and even the thermocouple tree and the ten pitot tubes along with their copper tubing running the length of the tunnel produced eddies which could cause a misalignment of the direction of airflow and the axis of the pitot tube. Nevertheless these distributions were determined and they are of the proper magnitude to roughly account for the total mass flow rate of the air. The vertical velocity profile of the ambient air measured with pitot tubes at 2.7 m (9 ft) from the burner is shown in figure 13. The relatively flat profiles of both figures 12 and 13 are characteristic of turbulent flow. The Reynolds number is approximately 30,000.

When the burner was turned on the profile shown in figure 14 was obtained. If there were no vertical transfer of momentum and the mass inflow of air were to remain constant, the velocity would be proportional to the absolute temperature of the air. The dashed curve was obtained by dividing the velocity by the ratio of the absolute temperature and the ambient absolute temperature, T/T_0 . The departure of this dashed curve from the distribution in figure 13 demonstrates the presence of such momentum transfer. The slope of the velocity profile should decrease with distance down the tunnel due to momentum transfer. Figure 15 shows the velocity profiles at 4.3 and 6.1 m (14 and 20 ft) with the burner on and at 6.1 m (20 ft) with the burner off.

In order to look for changes in the mass inflow rate the thermoanemometer was positioned just in front of the entrance slit to the tunnel where the relative change in inflow velocity could be recorded. A record of the output of this probe versus time is shown in figure 16. Initially there is a drop in the inflow velocity as the burner

is turned on. This transient lasts long enough for the expanded hot air to follow the slower moving ambient air through the tunnel and out the duct. The original inflow velocity was restored in about six seconds. While the average inflow rate does not seem to be changed, the instantaneous inflow shares some of the turbulence developed in the tunnel.

The volumetric air inflow rate, V_a can also be calculated from the oxygen depletion in the stack with the methane burner serving as the only source of fuel.

$$V_a = \frac{SV_g}{0.01 \phi Y_o} \quad (2)$$

where S is the number of volumes of oxygen needed for complete combustion of one volume of fuel, and V_g is the volumetric delivery rate of the gas. $S=2$ for methane and V_g is $2.3 \text{ dm}^3/\text{s}$ (4.9 cfm) for the tunnel. The oxygen concentration in normal air, Y_o , is 0.208 . Using the 13 percent oxygen depletion measured in the exhaust duct with the ACB specimen (figure 8) V_a is estimated to be $0.17 \text{ m}^3/\text{s}$ (362 cfm). The cross sectional area of the tunnel is 0.14 m^2 (1.46 ft^2), so the average linear velocity at ambient temperature is 1.3 m/s (248 ft/min). This average velocity is close to that estimated from the velocity profile obtained with the pitot tubes in figure 13, 1.3 m/s (250 ft/min), and the thermoanemometer in figure 12, 1.2 m/s (245 ft/min). The velocity averaged over both vertical and horizontal directions could be somewhat lower. The nominal velocity is 1.2 m/s (240 ft/min) at $41 \text{ }^\circ\text{C}$ ($105 \text{ }^\circ\text{F}$) which would be reduced to 1.1 m/s (225 ft/min) at ambient temperature.

The 10 percent difference could be due to errors in velocity and oxygen concentration measurements, incomplete combustion, air leakage into the tunnel, or actual variations in mass inflow of air through the tunnel.

4.1.4. Pressure Drop in the Tunnel

In order to estimate the effective friction factor inside of the tunnel and the flow impedance of the entrance slit, the pressures were monitored at several points. These parameters are important in estimating the heat transfer and the variation in velocity with the air temperature and the pressure differential across the tunnel. According to the UL flammability studies [6] the variation in velocity appears to have a small effect on flame spread distances in the tunnel but a large one on the smoke concentration in the duct. The negative pressures as determined from the side port of a pitot tube aligned with the axis of the tunnel and located on the floor with the burner off are shown as a function of distance from the burner in figure 17. These measurements were made at ambient temperatures. The variation in pressure is small compared with the scatter. Nonetheless a slope was estimated to be 0.20 Pa/m (2.4×10^{-4} in of water/ft) using a least squares fit. The friction factor, f , is calculated from the relationship [12]:

$$f = gD(\Delta P/L)/(2 \rho V^2) \quad (3)$$

where g is the newton constant (1 m kg/Ns²; 32.2 ft lb/lbfS²), ΔP is the pressure difference (lbf/ft²) over the length L (feet), ρ is the air density (1.22 kg/m³; 0.0763 lb/ft³), V is the velocity (1.22 m/s; 4 ft/sec), and D is the hydraulic diameter (0.37 m; 1.2 ft). The hydraulic diameter is equal to 4 times the cross sectional area divided by the perimeter. A pressure of 249 Pa (1 in of water) is equal to 249 N/m² (5.2 lbf/ft²). The calculated value of f from equation (3) is 0.020. The accuracy of this calculation suffers from the scatter of the data, but the result leads to a prediction of the heat transfer which is roughly in agreement with the other methods which will be discussed.

The Reynold's number, $Re = \frac{VD}{\nu}$, is 30,000 based on a velocity, V , of 1.2 m/s (4 ft/sec), a kinematic viscosity, ν , of 0.15 cm²/s (1.6 x 10⁻⁴ ft²/sec, and a hydraulic diameter of 0.37 m (1.2 ft). For smooth tubes,

$$f \approx (0.046)/(Re)^{0.2} \quad (4)$$

so the smallest value f could assume is 0.006. A typical value for concrete surfaces is 0.01 [13]. The value derived from figure 17 is twice as high but there are large scale irregularities in the tunnel including the added turbulence bricks. It is clear from the figure that a large fraction of the pressure drop is across the entrance region of the tunnel. This large flow impedance which is independent of temperature has a stabilizing effect on the mass inflow rate of air in the tunnel particularly since the impedance of the tunnel itself increases with air temperature.

The measurement of the pressure drop in the tunnel can be used to estimate the effect of the distance and location of the pressure tap on the change in the mass inflow rate of the air during a regular tunnel test. Figure 18 is a simplified sketch of a vertical cross section of the tunnel, riser, and exhaust duct showing the specific pressure points needed for this development. The following relationship between the pressures must hold:

$$(P_0 - P_1) + (P_1 - P_2) + (P_2 - P_3) + (P_3 - P_4) + (P_4 - P_5) = P_0 - P_5 = P_0gz$$

or

$$\Delta P_{slit} + \Delta P_{tunnel} + \Delta P_{riser} + \Delta P_{duct} + \Delta P_{tap} = P_0gz \quad (5)$$

The drop in pressure across the slit is proportional to the kinetic energy of the flow so that $\Delta P_{slit} = k\rho_0 V_0^2$. The pressure drop across the tunnel and the exhaust duct are given by equation 3. The pressure drop in the riser is given by ρ_0gz and Δp_{tap} is controlled at a fixed negative value throughout the test. Then equation 5 can be written

$$k\rho_0 V_0^2 + 2\rho_T V_T^2 \frac{f_T}{g} \frac{L_T}{D_T} + 2\rho_D V_D^2 f_D \frac{L_D}{D_D} = -\Delta P_{\text{tap}} + (P_0 - P) gz$$

Since $G = \rho_0 V_0 = \rho_T V_T = \rho_D V_D$ and $\rho = \frac{T_0}{T} \rho_0$,

$$\frac{G^2}{\rho_0} = \frac{-\Delta P_{\text{Tap}} + (1 - T_0/T_R) P_0 gz}{k + \frac{2}{g} (f_T \frac{L_T}{D_T} \frac{T_T}{T_0} + f_D \frac{L_D}{D_D} \frac{T_D}{T_0})}$$

$$G = \sqrt{\rho_0} \left[\frac{-\Delta P_{\text{tap}} + (1 - T_0/T_R) \rho_0 gz}{K + \frac{2}{g} (f_T \frac{L_T}{D_T} \frac{T_T}{T_0} + f_D \frac{L_D}{D_D} \frac{T_D}{T_0})} \right]^{1/2} \quad (6)$$

where the subscripts T, D, and R refer to the average values of these parameters in the tunnel, exhaust duct, and riser respectively. Taking $f_T = f_D = 0.02$ and measuring G at ambient temperature a value of 15.5 was calculated for K.

Since all tunnels do not share the same differences in height between the tunnel and the pressure tap, z, there will be differences in the effective pressure across the tunnel when the temperature of the air in the duct is rising during a test. This means that there may be significant mass inflow velocity differences between tunnels during their operation which may cause some changes in flame spread and larger changes in smoke transmission. For uniformity between tunnels either (1) the pressure taps should be at the same elevation and distance from the end of the tunnel, (2) the airflow should be controlled directly from the measured velocity at the entrance slit or (3) the pressure tap should be located upstream of the burner where the air temperature is not changing during the test. In updating existing tunnels the latter alternatives would be more feasible.

4.1.5. Heat Flux

The response of a material to a fire environment, as measured by its ignitability, heat release rate, and rate of flame spread, depends on its incident heat flux. The comparison between the heat fluxes in a room fire and those in the tunnel are of the utmost importance.

It is difficult to measure the heat flux without altering the quantity being measured. The incident heat flux is due to both radiation and convection. The latter depends on the difference between the gas and surface temperature. Since the surface temperature of a burning specimen will be in excess of 315 °C (600 °F) the heat absorbed at the surface of the specimen will be less than that for a water-cooled Gardon heat flux gage or water-cooled heat flux meter flush with the surface. Nevertheless, measurements with a water-cooled heat flux meter were collected so that a direct comparison could be made with the water-cooled Gardon total heat flux gage used in the full-scale corner and room tests. Measurements made on the surface of an ACB specimen

0.61 m (2.0 ft) from the burner, with a water-cooled heat flux meter yielded a maximum flux of 6.3 W/cm^2 ($5.5 \text{ Btu/ft}^2 \cdot \text{sec}$) as seen in figure 19. This is in the region of flame impingement from the burner. The range of incident heat fluxes measured 1.2 m (4 ft) above the floor in the UL corner tests with the 9.1-kg (20-lb) crib [6] ran between 6.0 and 8.4 W/cm^2 (5.3 and $7.4 \text{ Btu/ft}^2 \cdot \text{sec}$) by the time the flames had covered the ceiling. The 1.2-m (4-ft) elevation was chosen so that the flux measurement would be well within the area of impingement of the crib flame.

In another measurement made at 0.76 m (2.5 ft) with the heat flux meter attached directly to the ACB without water cooling, the flux conducted into the specimen was observed to be 4.0 W/cm^2 ($3.5 \text{ Btu/ft}^2 \cdot \text{sec}$). When the ACB surface rose in temperature, there was a reduction in the heat transferred to the surface and furthermore, part of the incident heat flux was radiated away so that the actual incident heat flux was greater than 4.0 W/cm^2 ($3.5 \text{ Btu/ft}^2 \cdot \text{sec}$) but less than 6.3 W/cm^2 ($5.5 \text{ Btu/ft}^2 \cdot \text{sec}$).

As was explained in subsection 3.5 the heat flux distribution along a 13-mm (1/2-in) thick AMB specimen over the entire length of the tunnel was estimated by attaching 0.25 mm (10 mil) thermocouples every 0.1 m (4 in) along the length of two 1.2-m (4-ft) sections on both the exposed and unexposed surfaces. Twenty-minute runs were made with the boards between 0 and 2.4 m (0 and 8 ft), then 2.4 and 4.9 m (8 and 16 ft), and finally between 4.9 and 7.3 m (16 and 24 ft). This time was sufficient to establish nearly steady flow through the specimen. The temperature data is presented in figure 6. The thermal conductivity of the AMB was measured to be $0.135 \text{ W/m} \cdot \text{K}$ ($2.17 \times 10^{-5} \text{ Btu/sec} \cdot \text{ft} \cdot \text{°F}$). The incident heat flux, H , which was partly conducted through the specimen with the remainder radiated from its surface, was calculated from the formula

$$H = \frac{K}{x} (T_s - T_r) + \epsilon \sigma T_s^4 \quad (7)$$

where K is the thermal conductivity, x is the thickness, T_s is the front surface temperature, T_r is the rear surface temperature, ϵ is the emittance which is assumed to be unity, and σ is the Stefan Boltzmann constant.

The results of this calculation are plotted in figure 20. The magnitude of the heat flux will depend on the material. The distribution for AMB is taken as a typical one. The amplitude will actually increase somewhat for materials of higher thermal conductivity. For the AMB it is seen to be a peaked distribution which drops to essentially half of its maximum value at the end of the burner flame.

This is consistent with the general principle of calling the flame distance the furthest point at which flame is present half of the time. Note that the flux at 0.76 m (2.5 ft) was calculated to be 3.75 W/cm^2 ($3.3 \text{ Btu/ft}^2 \cdot \text{s}$) for AMB whereas for ACB which had a thermal conductivity of $0.36 \text{ W/m} \cdot \text{K}$ ($5.8 \text{ Btu/sec} \cdot \text{ft} \cdot \text{°F}$) and a thickness of 6.4 mm (1/4-in) it was measured to be between 4.0 and 6.3 W/cm^2 (3.5 and $5.5 \text{ Btu/ft}^2 \cdot \text{sec}$).

In order to estimate the convective component of the heat flux to the surface, the momentum heat transfer analogy [13] was used. The surface heat transfer coefficient, h , is given according to this analogy by

$$h = \frac{Ef}{2} \rho CV \quad (8)$$

where E is the ratio of the eddy diffusivities for heat and momentum (approximately unity for air), f is the friction factor, measured to be 0.020, ρ is the density, C is the heat capacity and V is the air velocity. The product ρV is approximately constant and equal to its ambient value ($1.5 \text{ kg/m}^2 \cdot \text{s}$ ($0.31 \text{ lb/ft}^2 \cdot \text{sec}$)). The average value of C between $20 \text{ }^\circ\text{C}$ ($70 \text{ }^\circ\text{F}$) and $800 \text{ }^\circ\text{C}$ ($1500 \text{ }^\circ\text{F}$) is $1.1 \text{ kJ/kg} \cdot \text{K}$ ($0.26 \text{ Btu/lb} \cdot \text{ }^\circ\text{F}$). Hence $h = 16.5 \text{ W/m}^2 \cdot \text{K}$ ($0.00081 \text{ Btu/ft}^2 \cdot \text{sec} \cdot \text{ }^\circ\text{F}$). The convective heat flux, H_C , is given by

$$H_C = h\Delta T \quad (9)$$

From figure 6 the air temperature 25 mm (1 in) below the AMB at 7.0 m (23 ft) is $338 \text{ }^\circ\text{C}$ ($640 \text{ }^\circ\text{F}$). The temperature of the surface is $204 \text{ }^\circ\text{C}$ ($400 \text{ }^\circ\text{F}$). Putting this temperature difference in equation (7) yields a convective heat flux of 0.22 W/cm^2 ($0.19 \text{ Btu/ft}^2 \cdot \text{sec}$). The estimated total incident heat flux from figure 19 at 7.0 m (23 ft) was 0.38 W/cm^2 . While both of these numbers contain considerable approximation, the convective component is of the correct order of magnitude to account for most of the total heat flux near the end of the tunnel. Radiation from the wall and floor will also provide some contribution. For example, if the average temperature of the walls and floor were half that of the AMB surface the radiation contribution would be 0.14 W/cm^2 ($0.12 \text{ Btu/ft}^2 \cdot \text{sec}$).

A plot of the convective component of the heat flux distribution between 1.2 m (4 ft) and 6.1 m (20 ft) based on the momentum-heat transfer analogy using the air and exposed surface temperatures in figure 6 is given in figure 21. Comparison with the total heat flux distribution indicates that beyond 2.4 m (8 ft) in the tunnel the heat transfer might be accounted for by using the above analogy for convection and by taking wall radiation into account. However, flame radiation and other heat transfer mechanisms must be considered in order to take the large difference between these curves into account in the flame region. Figure 6 indicates a temperature difference of $288 \text{ }^\circ\text{C}$ ($550 \text{ }^\circ\text{F}$) between the AMB surface and the temperature 25 mm (1 in) below it at 0.76 m (2.5 ft). Equation (9) yields a convective heat flux of only 0.48 W/cm^2 ($0.42 \text{ Btu/ft}^2 \cdot \text{sec}$) whereas the estimated total heat flux was 3.75 W/cm^2 ($3.3 \text{ Btu/ft}^2 \cdot \text{sec}$).

Yet another way to estimate the heat flux to the surface is to determine the rate of loss of the enthalpy of the air as it passes down the tunnel.

$$Q_L = \rho V_a C \Delta T \quad (10)$$

This would result in a total rate of heat transfer of 3.5 kW (3.3 Btu/sec). If the flow is assumed to be two-dimensional, then the losses would be only through the specimen and the floor of the tunnel. The area of the floor and the specimen between 6.1 and 7.0 m (20 and 23 ft) is 0.84 m² (9 ft²). The average rate of heat transfer would be 0.41 W/cm² (0.36 Btu/ft²·sec). Between 2.7 and 4.3 m (9 and 14 ft) the average temperature difference was 45 °C (80 °F) which yields an average heat flux to the surface of 0.66 W/cm² (0.58 Btu/ft²·sec). These estimated heat fluxes are plotted in figure 21 for comparison with the other methods.

The heat flux measured on the ceiling of the tunnel by a water-cooled heat flux meter at 4.3 m (14 ft) was 0.64 W/cm² (0.56 Btu/ft²·sec). Because of the lower surface temperature this value would be expected to be somewhat higher than that to the specimen surface. The heat flux measured on the floor of the tunnel at 4.3 m (14 ft) with a water-cooled heat flux meter was 0.34 W/cm² (0.30 Btu/ft²·sec) or approximately one-half of that on the ceiling. The latter measurement was made with the AMB specimen.

The purpose of trying to determine the heat flux by as many methods as possible was to put its distribution on firmer ground in order to provide a basis for the flame spread model. The heat fluxes obtained by the various methods are all included in figure 21.

4.2. Experiments with the Auxiliary Burner

4.2.1. General

In the previous sections, the temperatures, velocities, oxygen depletion, heat fluxes, and pressures were reported for inert specimens. Before proceeding with combustible specimens a set of experiments was conducted with an auxiliary burner which delivered known flow rates of methane to simulate the gaseous decomposition products, "fuel," that would be released by a combustible specimen. The purpose of these experiments was to examine:

- (1) the relationship between the flame distance and the rate of fuel production,
- (2) the validity of using the oxygen depletion in the duct as a measure of the rate of fuel production of the combustible specimens, and
- (3) the effect of the rate of fuel production and flame length on the oxygen, temperature, velocity, and heat flux distributions in the tunnel.

4.2.2. Flame Distance

The reported flame distance versus time is shown in figure 22. The rate of flow delivered by the auxiliary burner is marked on each plateau of this plot. The regular burner with 2.3 dm³/s (4.9 cfm) is started at time zero and is left on during the run. Note that as the flow to the auxiliary burner is increased, the maximum flame distance

takes some time to establish. In particular at a flow of 2.4 dm³/s (5.0 cfm) through the auxiliary burner it takes 1.5 minutes for the flame to reach its maximum distance even with a steady flow of methane. This effect was not explored further, but was merely noted because of the bearing that it might have in the development of a flame spread model for the tunnel. No attempt was made to examine the buildup time of the regular burner flame. The maximum flame distances are plotted against the total flow rate of methane in figure 23. The total flow rate includes the 2.3 dm³/s (4.9 cfm) flow to the regular burner plus the flow rates to the auxiliary burner. The flame distance is the distance from the burner to the downstream end of the flame.

Beyond the burner flame the distance increases linearly with the flow rate with a slope of 19 s/dm² (3.0 ft/cfm). It is seen, however, that the 2.3 dm³/s (4.9 cfm) contributed by the regular burner was not nearly as effective in contributing to the flame length in the tunnel. This is probably because the burner fuel is delivered from ports 0.10 m (4 in) above the floor and much of the fuel is burned before it reaches the specimen 0.3 m (1 ft) or more downstream of the burner. On the other hand, the fuel from the auxiliary burner was delivered at the specimen surface in a region already supplied by the regular burner so that its burning would take place in the proximity of the surface and some distance downstream. The fuel delivered or generated at the specimen surface has access to oxygen from one side only and is in the proximity of a heat sink. Both of their effects tend to reduce the burning rate and thus extend the flame area. The heat production rate of the flame from the auxiliary burner is 3.9 W/cm² (3.4 Btu/ft²·sec) assuming a net heat of combustion for methane of 34 MJ/m³ (912 Btu/ft³), a flame width of 0.46 m (1.5 ft), and the above slope of 19 s/dm² (3.0 ft/cfm).

4.2.3. Oxygen Depletion

Figure 24 shows that the relationship between the oxygen depletion in the duct and the total flow rate of methane is essentially linear with a slope of 6.8%/dm³ (3.2%/cfm). Since the auxiliary burner introduced some impedence there was a decrease in airflow of about 20 percent as indicated by an increase in oxygen depletion with the auxiliary burner in place but not turned on. Without the auxiliary burner installed, the regular burner flow of 2.3 dm³/s (4.9 cfm) produced a depletion of 13 percent or 5.7%/dm³ (2.7%/cfm). Taking a net heat of combustion of 34 MJ/m³ (912 Btu/ft³) for methane and assuming that a given volume of oxygen consumed produces the same amount of heat regardless of the material, the total rate of heat generation including that from the regular burner is given approximately by

$$Q = 6.0 \varnothing \text{ kW} = 340 \varnothing \text{ Btu/min} \quad (11)$$

where \varnothing is the oxygen depletion in percent.

Equation (11) provides a means of determining the heat generated by a specimen during the test. This is superior to the use of the regular fuel contribution thermocouple at 7.0 m (23 ft) because the heat losses upstream of the thermocouple limit the temperature rise particularly when large concentrations of smoke are present in the tunnel.

The oxygen concentration on the floor of the tunnel at 2.7 m (9 ft) as a function of fuel flow is given in figure 25. At the highest flow rate the flame exceeds the length of the tunnel, but the oxygen concentration on the floor has been reduced by only about two percent of its initial value. This low value of oxygen depletion is important in establishing the similarity between burning in the tunnel and in the room. A high oxygen concentration at the floor level of the tunnel should be equivalent to a high oxygen concentration in the free stream some distance away from the burning surface in the room.

4.2.4. Temperature

The temperatures recorded at the end of four minutes by the standard fuel contribution thermocouple located at 7.0 m (23 ft) are plotted as a function of total methane flow in figure 26. The tunnel is preheated and cooled to 41 °C (105 °F) before starting each test, hence the 41 °C (105 °F) intercept of the curve which appears to be fairly linear with a slope of 88 K·s/dm³ (75 °F/cfm) of methane. If it is assumed that the temperature 25 mm (1 in) below the surface represents the average value, through the cross section of the tunnel this slope would correspond to a 6.4 kJ/s (363 Btu/min) increase in enthalpy flow for each 0.47 dm³/s (1 cfm) of methane. Since the methane has a net heat of combustion of 34 J/cm³ (912 Btu/ft³) and the average temperature is actually lower than that recorded by the thermocouple, over 60% of the heat is conducted through the ACB specimen or lost through the walls of the tunnel. This absorption of heat within the tunnel would tend to be less for a lower thermal conductivity specimen but more for a smoke producing specimen because of thermal radiation from the smoke particles to the interior surfaces of the tunnel.

Figure 27 shows the increase in temperature at 2.7 m (9 ft) for an additional flow of 2.4 dm³/s (5 cfm) of methane. Figure 28 shows the temperature profiles for a series of flow rates at 4.9 m (16 ft). The similarity of the profiles is noteworthy and it is of significance to the model development that increasing the total flow from 4.7 to 5.4 dm³/s (9.9 to 11.5 cfm) causes essentially the same increase in temperature as the other steps even though a flow of 4.7 dm³/s (9.9 cfm) extended the burner flame 1.8 m (6 ft) past the 4.9 m (16 ft) location where the measurement was made. In figure 29 the vertical temperature profile is shown along the wall at 4.3 m (14 ft) for an auxiliary gas flow of 2.4 dm³/s (5 cfm). The temperature of the upper part of the wall is of the order of 315 °C (600 °F) which would give rise to a radiation level of about 0.7 W/cm² (0.6 Btu/ft²·sec). The distribution for the burner alone is included for comparison.

The temperature distribution on the exposed and unexposed surfaces along the length of the tunnel for an AMB specimen fully covered with the flame from an auxiliary burner with 2.8 dm³/s (6 cfm) of methane is seen in figure 30. The purpose of these measurements was to deduce the incident heat flux distribution along a specimen fully covered with flame.

4.2.5. Velocity

The velocity profiles at 2.7 m (9 ft) are compared with the burner off, burner on, and burner on with 2.4 dm³/s (5 cfm) of methane delivered by the auxiliary burner in figure 31.

4.2.6. Heat Flux

The heat flux distribution along an AMB surface covered with flame was deduced by the same methods as that used for the burner flame alone in section 4.1.5. It can be seen in figure 32 that these fluxes are considerably higher than for the burner flame alone. In fact the flux level at the end of the tunnel has only fallen to 2.7 W/cm² (2.4 Btu/ft²·sec). This is after a constant 20-minute exposure to the flame from the auxiliary burner and will contain some radiation from the walls and floor which builds up with time.

4.2.7. Smoke

No attempt was made to measure the smoke density inside the tunnel but it is measured in the duct during the regular tunnel runs. It has also been recorded on the various instrumented tunnel tests. Because smoke affects the heat transfer in the tunnel it is an important part of the environment. The introduction of methane into the auxiliary burner has caused a small but measurable amount of smoke production. Methane is normally not a smoky flame but there are two conditions existing that could lead to smoke production. One is a reduced oxygen atmosphere and the other is flame quenching against the cold ceiling. In the case of combustible specimens both conditions are operating. For 3.1 dm³/s (6.6 cfm) of methane delivered to the auxiliary burner and 2.3 dm³/s (4.9 cfm) to the regular burner, the optical density produced in the duct was 0.14 per meter. The optical density is essentially zero with the regular burner alone.

4.3. Experiments with 0.92-Meter (3-ft) Combustible Specimens

4.3.1. General

The next step in the project was to introduce combustible specimens but to confine them to the region of the burner flame so that uniform exposure conditions could be achieved as nearly as possible. Their location between 0.31 and 1.2 m (1 and 4 ft) beyond the burner ruled out any consideration of flame spread across the surface since the complete specimen would be involved almost at once. Although the peak heat flux to the surface does not change appreciably when the specimen begins to generate fuel, the rate of drop-off of this flux with distance (see fig. 20) would be decreased so that there will be some difference in the exposure for different materials. Nevertheless, in order to have adequate sensitivity a 0.92-m (3-ft) specimen length was chosen and the variation in the exposure was ignored for the present stage of the investigation.

The primary objective of this part of the project was to determine the fuel generation or heat release rates of the materials due only to their exposure to the burner flame. This rate was to be measured by the oxygen depletion in the duct according to equation (11). The second objective was to learn how the flame distance varied with the fuel production rate among the various combustible materials.

The predicted flame spread distance in the tunnel might then be expressed as a product of (1) the total rate of fuel production from the specimen and (2) the flame distance required to consume the fuel produced at a unit rate.

4.3.2. Heat Release Rates

In order to determine the heat release rate per unit area equation (11) has to be divided by the area of the specimen so that

$$q = 1.44 (\delta - \delta_B) \text{ W/cm}^2 = 1.27 (\delta - \delta_B) \text{ Btu/ft}^2 \cdot \text{sec} \quad (12)$$

where q is the heat release rate and δ_B is the oxygen depletion produced by the burner alone. This value of δ_B will be about 0.13 but does vary slightly so that it is measured in each series of tests with an ACB specimen. Table 3 lists the heat release rates for a number of materials used in the UL full-scale tests [6]. The heat release rates were obtained from equation (13) and are compared with those measured with the NBS heat release rate calorimeter at a radiant flux of 3 W/cm^2 ($2.6 \text{ Btu/ft}^2 \cdot \text{sec}$). The materials tested in this way were broken up into four groups for discussion purposes. The distribution of the materials among the groups was based only on the data comparisons. Even though the incident heat flux varies across the face of the specimen in the tunnel, the agreement is quite good for the materials in group 1. In group 2 the values in the tunnel were much higher. In the calorimeter only materials A and B ignited and in these cases the flaming was probably limited to the gas phase above the specimen and hence contributed no heat feedback to the specimen. This speculation is based on observations of the burning of these materials in a 3 W/cm^2 ($2.6 \text{ Btu/ft}^2 \cdot \text{sec}$) radiation field outside of the calorimeter. Unfortunately the exposed surface of the specimens is not visible in the NBS heat release rate calorimeter. In the tunnel all of the specimens are exposed to the burner flame. In group 3 the values produced in the tunnel were lower due to the limited time response of the oxygen measuring system which may not have been fast enough to follow the short duration peaks of these materials. The materials in group 4 are inordinately high smoke producers. This smoke tends to radiate the heat away rapidly. This may account for these lower measured values of heat release rate in the calorimeter. Some evidence for this radiation loss is seen in the temperature records for the 7.0 m (23 ft) thermocouple in the tunnel which indicate $290 \text{ }^\circ\text{C}$ ($555 \text{ }^\circ\text{F}$) after five minutes for an ACB specimen and only $117 \text{ }^\circ\text{C}$ ($350 \text{ }^\circ\text{F}$) for a 0.92-m (3-ft) type "O" specimen even though it produced a considerable amount of heat.

Table 3. Peak Heat Release Rates Deduced from the Oxygen Depletion in the Duct Compared with those from the NBS Heat Release Rate Calorimeter at 3 W/cm²

Material Designation	Thickness (mm)	Density (kg/m ³)	Material Type	FSC	Tunnel (W/cm ²)	Calorimeter (W/cm ²)	Group
S	50	37	F.R. Polyisocyanurate	26	2.0	2.1	1
C	50	30	F.R. Polyurethane	28	2.3	2.3	1
J	13	290	Wood Fiberboard	54	3.6	4.0	1
Q	50	32	F.R. Polyurethane	28,59	7.6	7.4	1
AE	20	620	Red Oak Flooring	100	9.1	9.4	1
U	13	759	Wood Particle Board	156	11	11	1
H	6	530	Prefinished Luan Plywood	178	14	12	1
B	50	30	F.R. Polyurethane	28	3.1	2.3	2
A	50	30	F.R. Polyisocyanurate	22	4.1	0.8	2
I	13	300	F.R. Treated Wood Fiber-board	18	1.7	<0.3	2
T	13	800	F.R. Treated Wood Particle Board	18	2.0	<0.3	2
E	89	10	Fiber Glass	18	3.1	<0.3	2
R	50	37	Foil Faced F.R. Polyisocyanurate	26	4.1	<0.3	2
G	13	590	Treated Plywood	23	4.6	<0.3	2
W	16	1230	Gypsum Wallboard	13	0.5	<0.3	2
F	89	10	Paper Faced Fiber Glass	2540	9.7	13	3
D	50	29	F.R. Polyurethane	925	6.7	19	3
O	50	40	F.R. Polyurethane	1735	23	12	4
M	1.6	1340	Glass Fiber Reinforced Polyester	367	84	14	4

The agreement between the heat release rates based on oxygen depletion for the group 1 materials with their heat release rates measured directly in the calorimeter indicates the potential of the oxygen depletion in the duct as a measure of the fuel generation rate of a specimen in the tunnel.

4.3.3. Flame Distance

The flame spread distances for 0.92 m (3 ft) specimens of a number of the materials used in the full-scale tests at UL [6] are given in table 4 along with the flame spread distances for full size specimens of the same materials. The similarity of the flame distances for the 0.92-m (3-ft) and the 7.9-m (24-ft) specimens of the low flame spread materials is quite striking. It indicates that most of the fuel which contributes to the extension of the flame for these materials is generated in the region exposed directly to the burner flame. Flame distance does not depend on the environmental conditions in the vicinity of the flame front for low FSC materials.

Table 4. Flame Distances in the Tunnel for
3-Foot and 24-Foot Specimens

Material*	FSC	Called Flame Distance (ft)**	
		3-Foot	24-Foot
E	18	6.5	8
W	13	7	7
I	18	7.5	8
T	18	7.5	8
G	23	8.5	9
C	28	8.5	9.5, 10.5
A	22	9	8.5, 9.9
S	26	9	9.5
B	28	9	10
Q***	28, 59	9	9.5, 10, 16
R	26	10	9.5
J	54	10	15
AE	100	12	24
D	925	12	24
O	1735	12	24
H	178	13	24
U	156	14.5	24
F	2540	15	24

* See description in table 3.

** 1 foot = 0.305 meters

*** Material is highly variable in its flame distance in the tunnel.

The 0.92-m (3-ft) tests may be a useful way to compare the flame spread potential of materials, since even the high flame spread materials have flame extensions which terminate within the tunnel. Those materials which spread flame a distance of over 3.1 m (10 ft) in the 0.92-m (3-ft) test, spread flame over the end of the tunnel in the regular test and hence are normally rated for time of flame spread rather than distance. The 0.92-m (3-ft) specimen test would allow the comparison of all materials on the same scale. For flame spread distances of less than 3.1 m (10 ft) on the 0.92-m (3-ft) test, the distances were only 0.15 m (0.5 ft) less on the average than for the 7.9-m (24-ft) test. Specimen Q is a special case. Because of the variability of this material as evidenced by the different flame spread distances in the regular tunnel tests it was difficult to make a comparison.

It appears that the flame spread in the tunnel can be considered to be an extension of the burner flame due to the total rate of fuel production along the specimen up to the end of the flame extension. The total rate of fuel production depends (1) on the rate of heat release of the material as a function of incident flux and (2) the distribution of incident flux along the specimen up to the end of the flame extension. It is necessary to know the flame distance, burner flame plus flame extension, required to burn all of the fuel from the burner and the specimen. The burner flame is 1.4 m (4.5 ft) long and the flame extension is plotted as a function of the total fuel production from the specimen in figure 33 for all of the 0.92-m (3-ft) specimens tested. This includes all of the materials listed in table 3. The fuel production was determined by multiplying the average heat release rates measured in the tunnel by the specimen area of 0.42 m² (4.5 ft²). Also included in the plot are the values for a red oak deck where the flame distances are those reported as the flame progressed down the tunnel and the fuel production rate was determined from the oxygen depletion in the duct at the time each of these distances were reached. The oxygen depletion was converted to fuel production by use of equation (11). The points for methane were taken from figure 23 where the flow rate was converted to fuel production by assuming 34 J/cm³ (912 Btu/ft³) of gas.

While there is an appreciable scatter of the points, they can be represented, to within ± 25 percent with some exceptions by the empirical equation,

$$d = (0.61 + 49 Q) \text{ meters} = (2 + 0.17 Q) \text{ feet} \quad (13)$$

where d is the flame extension and Q is the total rate of heat production in MW when SI units are used and Btu/sec when engineering units are employed.

There is no reason at the outset to assume that all of the materials would fall on a single curve. When the properties of the individual materials are properly taken into account, the relationship between the flame extension and the heat release rate should be considerably improved. Nevertheless equation (13) may still be adequate for the preliminary stage of the model development.

The most significant deviation from the curve is exhibited by the F.R. Polyurethane "O" which has an FSC 1735. There are several possible explanations. It produces a very large soot deposition in the tunnel which can obscure the maximum flame spread

distance or may oxidize on the surface by non flaming combustion to produce additional heat without an increase in flame length. The copious rate of volatile production may reduce the oxygen concentration in the duct by dilution and thus result in a false contribution to the estimated heat release. It is noted that if the heat release rate of 12 W/cm^2 ($11 \text{ Btu/ft}^2 \cdot \text{sec}$) observed with the NBS heat release rate calorimeter were correct, the total heat release rate would be 50 kW (47 Btu/sec) and the point would be within the 25% range for the curve.

An interesting feature of equation (11) is that the flame extension reaches 0.6 m (2 ft) beyond the normal burner flame as soon as a significant amount of fuel is produced. This would appear to set an FSC of 10 as essentially the lower limit of the flame classification range. This phenomenon takes place because although the designated flame distance for the burner is 4.1 m (4.5 ft), based on the presence of the flame about 50% of the time, pulsating flamelets do occur as far as 2.0 m (6.5 ft). A very small amount of specimen fuel added to the burner fuel is required to bring the called distance out to 2.0 m (6.5 ft) resulting in the minimum flame extension of 0.61 m (2 ft) observed in figure 33. It should be pointed out, however, that values of the FSC between 0 and 10 have been reported in special cases.

It would be convenient to replace the visual observations of the flame distance in the tunnel by a thermocouple measurement. This would be a viable alternative if the gas temperature in the neighborhood of the maximum flame distance were a fixed quantity. Figure 34 shows the measured air temperature 25 mm (1 in) below the ACB at the called flame distance for all of the materials which were exposed in 0.92-m (3-ft) lengths. The figure illustrates the fall-off of this temperature with distance and with different classes of materials. However, it does portray an interesting distinction between the behavior of the cellulosic and the plastic materials that might be useful to examine later. The higher rate of fall-off with distance may be related to radiation losses due to their high smoke concentration. Due to differences in thermal conductivity between the test material and ACB, the temperatures would be somewhat different for full length specimens even when the flame distances are the same.

4.4. Combustible Specimens of Standard Length

4.4.1. General

The full length specimens actually tested on this project were limited to red oak, a high flame spread foam plastic ("O"), and two low flame spread foam plastics ("A" and "B"). However, non-instrumented tunnel runs were made on all of the materials used in the UL full-scale test series [6]. All of the normal data, which included distance versus time, temperature at 7.0 m (23 ft), and smoke transmission in the duct, taken on that program were available to this project.

4.4.2. Flame Distance

Figure 35 shows the flame spread distance versus time for 7.9-m (24-ft) specimens of some representative materials: Oak ("AE"), treated plywood ("G"), a high FSC foam plastic ("O"), and a low flame spread foam plastic ("A"). These data were taken during regular uninstrumented tunnel tests. Although material A has a low FSC because of its short flame distance, it reaches this distance in a very short time. If this time or the initial slope were reported as well as the FSC there should be less misunderstanding about the short buildup time of this material in a room fire. The extent of this buildup would depend on the size of the ignition source in the room.

The question sometimes arises as to whether the flame is attached to the surface or simply burning in the upper volume of the tunnel. For many materials, including the treated cellulose, the separation of the flame from the surface is clearly seen. However, there is some tendency to think of the flame spreading along untreated wood products as being attached. In order to shed some light on this question, 0.25 mm (10 mil) alumel chromel thermocouples were attached to the surface of a red oak deck at 0.61-m (2-ft) intervals along its length. The times at which the temperature reached 350 °C (660 °F), taken to be the temperature at which pyrolysis becomes rapid enough to support flaming, at each of the thermocouples is plotted in figure 36. This provides a distance versus time curve for the advancing pyrolysis front which is compared with the observed flame distance versus time curve. It can be seen that the flame leads the region of fuel production by an average distance of 1.5 m (5 ft), and thus is not attached to the surface in the region where its distance is measured.

4.4.3. Temperature

Figure 37 shows the temperature versus time recorded by the fuel contribution thermocouple at 7.0 m (23 ft) during regular tunnel runs. Note that the treated plywood ("G") results in a higher temperature than that of ACB while the foam plastic ("B") has a slightly lower temperature. The high FSC foam ("O") has an even lower temperature at 10 minutes. This apparent anomaly may be due to the increase in radiation losses of the smoke laden air when the plastic specimen is present. Note that the peak temperature of the type "O" foam plastic occurred in two minutes while the flame spread over the end of the tunnel in 19 seconds.

In figure 38 the temperature distribution along the wall and floor at 4.3 m (14 ft), is shown at two minutes for a full length type B specimen. The maximum flame spread distance was 3.1 m (10 ft). Note that a 204 °C (400 °F) surface radiates about 0.3 W/cm² (0.26 Btu/ft²·sec).

The air temperature profiles are compared at 2.7 and 4.9 m (9 and 16 ft) for full length specimens of B and ACB in figures 39 and 40. The flame distance was 3.2 m (10.5 ft) for B.

4.4.4. Oxygen Concentration

The oxygen concentration at floor level in the tunnel at 3.1 and 5.5 m (10 and 18 ft) for a low FSC foam plastic is shown in figure 41. The depletion is quite small particularly at 3.1 m (10 ft) where it is less than three percent. Since the maximum flame spread distance was 2.9 m (9.5 ft), the oxygen depletion is not seen to be a limiting factor. Figure 42 shows the oxygen concentration at the ceiling and floor locations for the same material at 6.7 m (22 ft) in the tunnel. The oxygen depletion of nine percent at the floor level was similar to that at 5.5 m (18 ft). Just under the specimen it was up to 31 percent. The oxygen depletion ahead of the flame traveling up a wall or across a ceiling in a room would also be expected to be high.

Figure 43 shows the oxygen concentration in the duct for a red oak deck. This deck which had been constructed for an earlier test flamed over in 3.6 minutes. The high FSC was attributed to a loosening up of the deck due to drying during the three-week delay. The flameover time is indicated on the chart. There was a depletion of 25 percent at the time of flameover.

The depletions at the floor of the tunnel at 3.1 and 5.5 m (10 and 18 ft) for the oak are shown in figure 44. Even at 5.5 m (18 ft) the depletion on the floor is only eight percent. On the ceiling at 6.7 m (22 ft) the depletion reaches 69 percent at the time of flameover as seen in figure 45 and becomes nearly complete by the end of the 10-minute test.

Even on the floor of the tunnel the oxygen depletion becomes essentially complete in the case of the 1735 FSC foam plastic as seen in figure 46. At the time of flameover the depletion at 5.5 m (18 ft) was 26 percent on the floor. While this oxygen depletion is high, it does not prevent the flame from spreading over the end of the tunnel in 19 seconds.

4.4.5. Air Velocity

The output voltage of the thermoanemometer at the entrance slit is shown in figure 47 for a full length type "O" specimen (F.R. Polyurethane with FSC 1735). After the initial drop and recovery characteristic of a non-combustible specimen, there was a measurable drop of 25 percent in the velocity by the end of the test. This is taken to be the approximate drop in the volumetric rate of air inflow to the tunnel. It will not be exactly that since there could be some change in the velocity distribution across the slit or in the contraction factor at the location of the probe. There was a 12 percent reduction by the time of flameover. The data curves for the full length oak and type B (F.R. Polyurethane with FSC 28) specimens did not show a measurable drop in the inlet velocity. Because of the low time resolution the velocity distribution was not measured in the tunnel for the combustible specimens.

4.4.6. Burning Rate

The average rate of weight loss per unit area as a function of distance along the type B specimen was determined by cutting it up into sections of 0.31 m (1 ft) or less in length after the test. The residual weight was subtracted from the original weight which was calculated from the average density of the specimen determined before the test. This difference was divided by the five-minute exposure time during the test and the exposed area of the specimen. The results are plotted in figure 48. This curve shows the origin of the fuel in relation to the area exposed by the burner and the reported flame spread distance which was 3.1 m (10 ft) in this particular test. There is an abrupt change in the average fuel production rate at the called flame distance as one would expect. In order to demonstrate that the flame did not stop in the tunnel due to burn through of the specimen, the minimum thickness of decomposed material was measured at each distance. These thicknesses were subtracted from the original 5-cm (2-in) thickness of the specimen and are plotted in figure 49 to show the distribution of the depth of the decomposed material with distance in the tunnel.

4.4.7. Smoke

The optical transmission in the duct for a full length type B (F.R. Polyurethane with FSC 28) specimen dropped almost to zero immediately upon ignition and then began to rise fairly rapidly to a plateau at 60 percent. After three minutes it rose again to 87 percent. These two transmissions are equivalent to optical densities per meter of 0.54 and 0.15. These calculations are based on an optical path length of 0.41 m (16 in). The initially high optical density could not be determined because the light transmission had been recorded on a linear instead of a log scale.

4.5. Effect of Air Velocity on Flame Spread in the Tunnel

Table 5 shows the effect of velocity on the flame spread distances observed in the tunnel for three low flame spread foam plastics over a range of 0.5 to 1.6 m/s (95 to 312 ft/min). This experiment was run as part of the UL full-scale test program [6]. Going up or down in air velocity did not result in over a 0.31-m (1-ft) difference in flame spread distance and there was no established trend toward an increase or decrease in this distance. The independence of the distance on the air supply rate indicates that oxygen depletion was not a limiting factor in the maximum flame spread distance of these materials.

4.6. Effect of Ceiling-Wall Mounting of Specimens in the Tunnel

It is readily observed in corner tests [6] that the flame usually spreads further and more rapidly along the intersection between the wall and ceiling than it does over the regions of the ceiling surface remote from a boundary. This corner effect may be due in part to radiation trapping and in part to the concentration of the fuel generated there. In any case this effect, which is important in the room fire buildup process, is demonstrated in the tunnel, as seen in table 6. When the back wall,

Table 5. Flame Distance in the Tunnel Versus Air Velocity for Three Low FSC Foam Plastics

Material *	Velocity (ft/s)	Distance** (ft)
A	95	9.0
A	177	8.5
A	240	8.5
A	240	9.0
A	240	9.0
A	312	7.5
B	95	10.0
B	177	9.0
B	240	9.5
B	240	9.5
B	312	9.0
C	95	8.5
C	177	9.0
C	240	9.5
C	240	10.5
C	312	9.5

* See description in table 3, page 25.

**1 foot = 0.305 meters

opposite the window, as well as the ceiling was lined with the specimen material the spread distances were generally increased and the flameover times decreased. In the most dramatic case the plastic foam labeled "S" (F.R. Polyisocyanurate with FSC 26) had a flame distance of 2.9 m (9.5 ft) in the standard test, qualifying it for an FSC 25, but flamed over the end in 20 seconds in the ceiling-wall configuration. These tests were not instrumented and were not performed as a part of this project, but as part of the UL full-scale test program referred to earlier. However, because of their importance to the considerations of this investigation the results are reported here.

Tentatively it appears that the flame spread properties of a material in a room away from an intersection of two walls or a wall and the ceiling may be characterized by the data obtained during a standard tunnel test but not necessarily by its FSC rating. If the fire buildup in a room is strongly influenced by the enhanced flame spread in the neighborhood of an intersection then perhaps the ceiling-wall configuration should be included along with the ceiling only mounting in the tunnel tests.

The results in table 6 constitute another argument against the concept of oxygen starvation as a controlling factor in the flame spread distance in the tunnel, since increasing the amount of material increases the distance of spread.

Table 6. Effect of Ceiling-Wall Mounting on Distance and Time in the Tunnel

Code	Standard FSC	Material Identification	Distance (ft)*		Flameover Time (s)**	
			Standard	Corner	Standard	Corner
T	18	F.R. treated wood particle board	8	8	—	—
I	18	F.R. treated wood fiber board	8	17	—	—
A	22	F.R. Polyisocyanurate	8.5,9,9	11	—	—
G	23	Treated plywood	9	over	—	350
R	26	Foil faced F.R. Polyisocyanurate	9.5	9.5	—	—
S	26	F.R. Polyisocyanurate	9.5	over	—	20
B	28	F.R. Polyurethane	10	over	—	100
C	28	F.R. Polyurethane	9.5,10.5	over	—	226
J	54	Untreated wood fiber	15	over	—	175
AE	100	Red Oak flooring	over	over	330	166
U	156	Untreated wood particle board	over	over	212	133
H	178	Prefinished luan plywood	over	over	185	100
D	925	F.R. Polyurethane	over	over	44	69

* 1 foot = 0.305 meters

** Time at which the flame passes the end of the tunnel

5. SUMMARY

The present report describes the heat flux, oxygen concentration, temperature, velocity, and pressure measurements made in a series of instrumented tunnel tests. The two most important considerations regarding the environment in the tunnel are the heat transfer to the specimen surface and the availability of oxygen. The temperature and velocity profiles and the smoke density provide insight into the convective and radiative heat transfer mechanisms. Pressure measurements relate to the air velocity and its variation during the test.

The pressure distribution along the length of the tunnel indicated that most of the pressure drop takes place in the region of the entrance slit. Thus, the change in flow resistance in the hot region of the tunnel during the test has only a mild effect on the mass inflow velocity. The actual magnitude of the velocity change during a test is, however, dependent on the relative elevation and distance of the pressure taps in the exhaust duct beyond the tunnel, which varies from one tunnel installation to another. This variation is probably responsible for some of the differences in smoke data on the same material measured in various tunnels. The largest drop in the inflow velocity observed during these tests was 25% for a FSC 1735 polyurethane foam. There was a 12% reduction by the time that the flame spread over the end of the tunnel.

The heat transfer to the exposed surface of the specimen in the tunnel was measured with the following: (1) heat flux meters, (2) deduced from the temperature distributions along the length of the exposed and unexposed surfaces of an asbestos mill-board specimen, and (3) deduced from the temperature and velocity profiles at various locations in the tunnel. The maximum observed heat flux from the burner was 6.3 W/cm^2 ($5.5 \text{ Btu/ft}^2 \cdot \text{sec}$) measured with a water-cooled flux meter flush with the surface of an asbestos-cement board specimen and 0.61 m (2 ft) downstream of the burner. This flux was continually increasing during the whole ten-minute test period. Heat fluxes of 6.0 to 8.4 W/cm^2 were observed in the U.L. corner tests at the time the ceiling became fully involved [6]. The heat flux falls off rapidly in the tunnel with distance. Where differences in the performance of materials in the tunnel and in the room are observed it is reasonable to attribute it in part to the different incident heat flux distributions. More data are needed on the incident fluxes in a room fire to make quantitative comparisons. The heat flux distributions in the room will depend on the size of the flame from the ignition source and also on the room geometry. Thus, one cannot say in general whether the tunnel represents too mild or too severe an exposure. The total incident heat flux deduced from the temperature rise of an AMB specimen at 0.61 m (2 ft) was 4.2 W/cm^2 ($3.7 \text{ Btu/ft}^2 \cdot \text{sec}$). The incident heat flux distribution is a strong function of distance, falling to roughly half of its maximum value at the end of the flame, and will vary significantly with the thermal conductivity of the specimen. The difference in the incident heat flux levels deduced from the temperatures measured on the AMB and that measured by the water-cooled heat flux meter are qualitatively accounted for by the difference in surface temperatures between the flux meter and the specimen. Radiation losses from the smoke-laden gases were evidenced by the reduction in temperature at the fuel contribution thermocouple and by the increased heat flux measured on the floor of the tunnel for materials yielding high smoke densities.

Even in the absence of radiation from the smoke particles the rate of heat absorption in the specimen and in the walls and floor of the tunnel are as much as 60% of the rate of heat production. These high heat transfer rates which depend strongly on the thermal properties, flame spread properties, and the smoking tendency of the specimen, make the temperature registered by the fuel contribution thermocouple at the end of the tunnel a poor measure of the heat release.

The reduction in the oxygen concentration does not appear to be a factor in limiting the flame distance in the tunnel for the materials examined on this project based on the following evidence:

- (1) The flame distance was not a marked function of the inlet air velocity over a range of 0.5 to 1.6 m/s (95 to 312 ft/min) for the three foam plastics tested.
- (2) The oxygen concentration on the floor of the tunnel at 3.1 m (10 ft), which was at the called flame distance for the FSC 28 F.R. Polyurethane foam being tested, was only reduced to 20.3 percent. It was reduced to 19.3 percent at the same location at the time of flameover for a foam plastic with an FSC of 1735 which flamed over the end of the tunnel in

19 seconds. A red oak specimen which flamed over the end of the tunnel in 3.6 minutes had an intermediate value of 19.7 percent at the same place at the time of flameover. A high oxygen concentration of oxygen in the air away from the flames in a well ventilated room fire. (The short flameover time for the red oak was attributed to a loosening of the joints in the specimen which had been stored for three weeks.)

- (3) The fact that the flame spread distances for low FSC materials were nearly the same for 7.9-m (24-ft) and 0.92-m (3-ft) specimens, even though the leading edge of the flame was adjacent to an ACB surface in the latter case, indicated that local conditions near the flame front were not controlling factors in the extent of the spread. (It is clear that the flame spread distance recorded in the tunnel is a flame extension rather than a surface flame spread.)
- (4) Increasing the exposed area of the material as was done in the ceiling-wall mounting tests led to increased flame spread distances.

The oxygen depletion measured in the exhaust duct was proportional to the heat release rates of the specimens. The flame spread distance is roughly proportional to the total rate of heat production in the tunnel. The flame spread distance, for those materials whose flames terminate within the tunnel, can be considered to be an extension of the burner flame due to the fuel generated by the specimen primarily in the region of the burner flame. Thus an FSC 25 material which spreads flames from 1.4 m (4.5 ft) to 2.9-m (9.5 ft) exhibited essentially the same flame spread distance when the specimen material was limited to the region between 0.3 and 1.2 m (1 and 4 feet).

The flame extends beyond the pyrolyzing region for those materials that spread flame over the end of the tunnel. The maximum flame spread distance led the forward extent of the pyrolysis region by about 5 feet over the whole length of the tunnel for red oak. The fuel required for flame propagation comes from the region already covered by flame, not the region ahead of it.

The data presented in this report are taken from a wide variety of tests rather than from repeated experiments aimed at statistical accuracy. However, there is no reason to suggest that repeated experiments would lead to greatly different results. The intention was to provide a large scope of information which must be taken into account in constructing an analytical model of the Steiner tunnel and to make suggestions that might be considered in improving the usefulness of the E 84 tunnel test. When particular areas have been identified for critically testing the theory against experiment, some measurements similar to some of those described in this report will need to be run more carefully and be repeated several times.

6. RECOMMENDATIONS

The following recommendations are presented for consideration as a result of the research described in this report.

1. The oxygen depletion in the duct beyond the tunnel could provide an approximate measure of the rate of heat production by the specimen. It is suggested that an oxygen analyser could be included in the standard tunnel test. This measurement is not affected by the heat losses in the tunnel, as is the temperature recorded by the fuel contribution thermocouple. However, the mass flow rate into the tunnel must be constant or known. A knowledge of the fuel contribution is important for research as well as regulation. This is not offered as a substitute for the heat release rate calorimeter which measures the heat release rate under well-defined and controlled conditions. However, it would be a considerable improvement over the present fuel contribution measurement in the tunnel.
2. The value of the smoke measurement in the tunnel could be vastly improved simply by recording the optical density rather than the absorptivity of the smoke. The optical density of the smoke generated in the tunnel could be compared directly with the optical density of the smoke emerging from a room. It would have the advantage of measuring the optical density of a dynamic rather than a static system as is measured in the smoke density chamber. However, it might be necessary to measure the smoke closer to the end of the tunnel to avoid losses due to deposition. Again this modification is not suggested as an alternative to the smoke density chamber in which the exposure conditions are controlled. It is offered as an improvement over the present system and does offer a more realistic range of exposures than the smoke density chamber. While the present project was primarily concerned with flame spread, a knowledge of the optical density of the smoke in the tunnel is an essential ingredient in accounting for radiation heat losses. These losses affect the heat transfer to the specimen and thus its flame spread.
3. In principle, shifting the airflow control from the pressure drop at the exhaust duct to the inlet air velocity as measured with an anemometer at the entrance slit would ensure a constant mass flow rate of air through the tunnel during a test. The extent of its present variation through a test depends on the temperature increase of the exhaust gases as well as on the construction features of the tunnel particularly the relative height of the tunnel and the pressure tap, the distance of the tap from the tunnel, and the height of the entrance slit. While the indications are that the air velocity has only a minor effect on the maximum flame spread distance it is a significant factor in the smoke measurement.

Any control system for inlet air velocity must be suitably damped to avoid oscillations of the control mechanism due to turbulent fluctuations in the incoming air.

It has been suggested by W.J. Christian [14] that the constant mass flow could be achieved by moving the pressure tap upstream of the burner where only ambient temperature air is involved. Since most of the pressure is dropped across the entrance region of the tunnel as seen in figure 17 this seems to be an attractive alternative to the location of a velocity probe at the entrance slit. (This method has been adopted in ASTM E 84-76a.)

4. Although it appears to be the general practice at the time of this research to measure the air velocity of 1.2 m/s (240 ft/min) at an air temperature of 41 °C (105 °F) at the end of the tunnel, this should be so written in the standard to provide consistency between operators. However, because of temperature gradients in the tunnel at elevated temperature, it would be better to specify that the velocity be measured at ambient temperature. A velocity of 1.2 m/s (240 ft/min) at 20 °C (68 °F) represents a seven percent greater mass flow rate than 1.2 m/s (240 ft/min) at 41 °C (105 °F).
5. The new method of measuring the FSC (ASTM E 84-76a) is based on the area under the distance versus time curve. In order to evaluate the potential for rapid fire buildup in low density materials, the time to ignition and the initial slope of the distance versus time curve should be quoted along with the new FSC. In order to show the potential for maximum extent of fire buildup, the maximum value of the flame spread distance should also be quoted. Neither flame spread distance nor flame spread rate can be determined from the new FSC index.
6. Observation of the maximum flame spread distances for 0.92-m (3-ft) specimens might be an auxiliary use of the tunnel. It appears that for materials with FSC 25 or less, the measured flame spread classification would be the same for a 0.92-m (3-ft) specimen as for a 7.9-m (24-ft) specimen; Much less material would be needed for a test. Furthermore, 0.92-m (3-ft) specimens of the high FSC materials tested on this project have flames which terminate within the tunnel, thus providing a basis for comparing all of the materials on a flame distance scale. This cannot be achieved with 7.9-m (24-ft) specimens. The flame distances in the tunnel may relate to the maximum fire buildup area in a room for a small ignition source. It should be noted, however, that the maximum fire buildup area in a room also depends on the size of the ignition source so that a material with a FSC 25 might produce flameover or flashover in a room if the ignition source is of sufficient size. In fact, the flame travel distances for 0.92 m specimens might rank materials with regard to the size of ignition source needed for flashover. The shorter the distance, the larger the ignition source required.

7. While the flame spread distances could be compared using 0.92-m (3-ft) specimens as discussed in the last paragraph, the flame spread times could be compared by recording the times at which the flame passed the end of the 2.4-m (8-ft) specimens of all of these materials. While there may be an economy to using 2.4-m (8-ft) specimens, the 2.4-m (8-ft) mark along the 7.9-m (24-ft) specimens used for the FSC determination would do as well. These spread times would be indicative of the speed of fire buildup in a room. Flames will spread past 2.4 m (8 ft) for all materials with FSC greater than 18.

8. Measurements made with the ceiling-wall mounting could augment the standard tunnel tests by indicating the flame spread potential of the material in the neighborhood of the intersection between the walls or between a wall and the ceiling. It is possible that the extent of the flame spread under the enhanced incident flux conditions in these areas could make the material more hazardous with respect to flame spread than the standard tunnel test would indicate.

7. ACKNOWLEDGMENT

This research was conducted while the author was serving as a Research Associate at Underwriters' Laboratories, Inc. at Northbrook, Illinois in 1974. I am indebted to the management at UL for making the Steiner tunnel available on the occasions that it was needed and for providing the technical assistance necessary to pursue this project. Many individuals at UL contributed toward its success. In particular I appreciate the encouragement in this work that I received from Tom Castino and Jim Beyreis, the assistance that I got from Bill Metes and Tom Perdue in running the instrumented tunnel tests, and the helpful discussions with Joel Lipsey on the background of the tunnel and the practical considerations concerning its operation.

The crucial element of this project was the instrumentation and its interfacing with the tunnel. For this I am greatly indebted to Dick Bieniarz and his crew, particularly Stan Lesiak and Joe Mack.

I also wish to thank Dan Gross whose thorough review of the original draft led to a considerable improvement of the final version of this report.

8. REFERENCES

- [1] Steiner, A. J., Method of Fire Hazard Classification of Building Materials, ASTM Bulletin, 19-22 (March 1943).
- [2] Endicott, L. E. and Bowhay, R. B., A Statistical Evaluation of the Fire Hazard Classification Furnace (ASTM E84-68), Materials Research and Standards, American Society of Testing and Materials, Philadelphia, Pennsylvania, 19-21,50,52 (May 1970).
- [3] Lee, T. G. and Huggett, C., Interlaboratory Evaluation of ASTM E-84-70 Tunnel Test Applied to Floor Coverings, Journal of Testing and Evaluation, JTEVA, Vol. 3, No. 1, 3-14 (Jan. 1975).
- [4] Williamson, R. B. and Baron, F. M., A Corner Test to Simulate Residential Fires, J. Fire and Flammability, Vol. 4 (April 1973).
- [5] Maroni, W. J., SLRP Analysis of Recommended Protection for Foamed-Plastic Wall-Ceiling Building Insulations, Fire Journal (Sept. 1974).
- [6] Castiño, G. T., Beyreis, J. R. and Metes, W. S., Flammability Studies or Cellular Plastics and Other Building Materials Used for Interior Finishes, Underwriters' Laboratories, Inc., Northbrook, Ill. (1975).
- [7] Quintiere, J. G. and Raines, J. W., Thermal and Flow Characteristics of the ASTM E-84 Tunnel Test Method, Nat. Bur. Stand. (U.S.), NBSIR 75-705, Final Report (Sept. 1975).
- [8] 1974 Annual Book of ASTM Standards, Part 18, American Society for Testing and Materials.
- [9] Gubareff, G. G., Janssen, J. E. and Torborg, R. H., Thermal Radiation Properties Survey, Honeywell Research Center, Minneapolis-Honeywell Regulator Company, Minneapolis, Minnesota, 197 (1960).
- [10] Throne, J. L. and Griskey, R. G., Modern Plastics, 96 (Nov. 1972).
- [11] Johnson, P. R., A General Correlation of the Flammability of Natural and Synthetic Polymers, J. Appl. Polym. Sci. 18, 491-504 (1974).
- [12] Weast, R. C., Editor, Handbook of Chemistry and Physics, 56th Edition, 1975-1976.
- [13] Rohsenow, W. M. and Choi, H., Heat, Mass, and Momentum Transfer (Prentice-Hall, 1961), 57.
- [14] Christian, W. J., Underwriters' Laboratories, Northbrook, Ill. Private Communication.

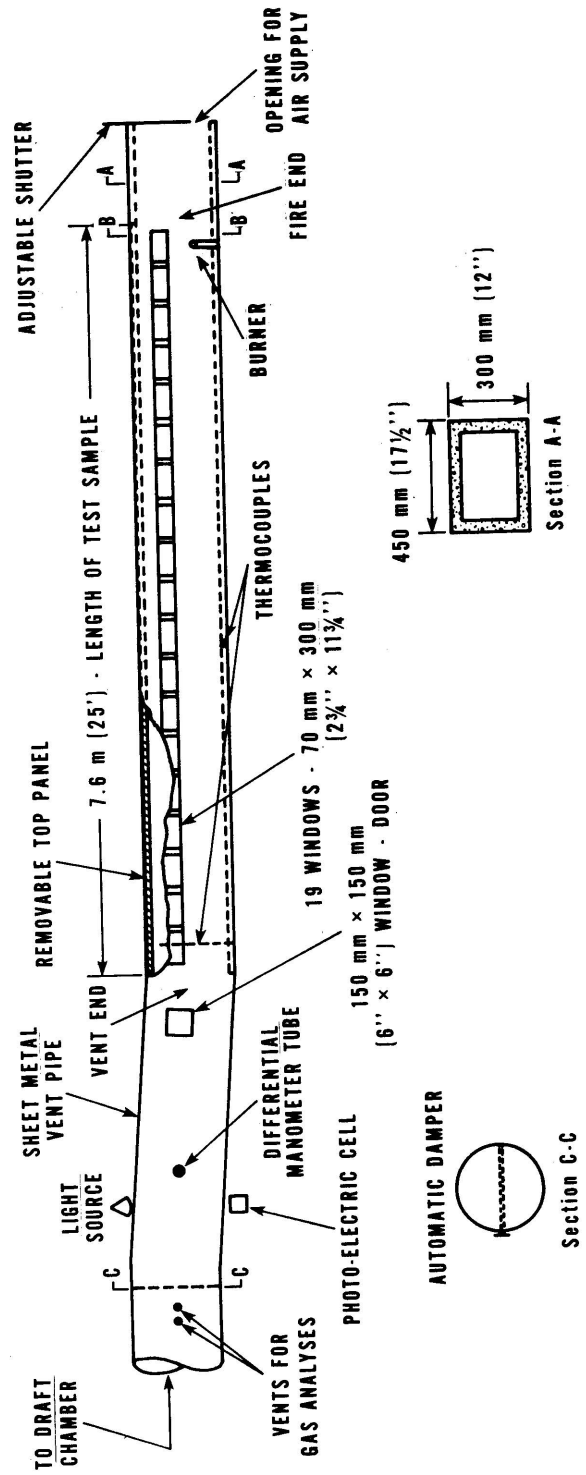


Figure 1. Details of Test Furnace

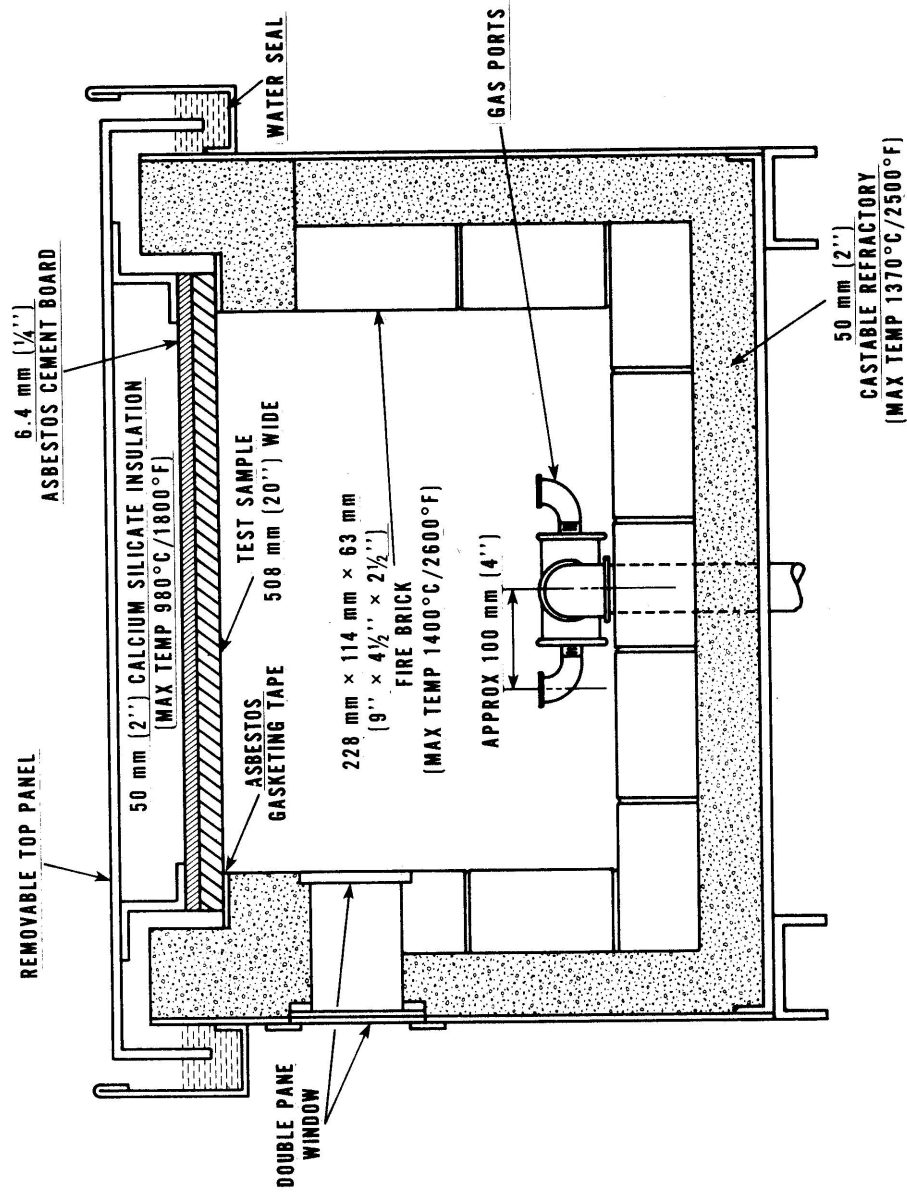


Figure 2. Cross Section of Furnace at BB of Figure 1

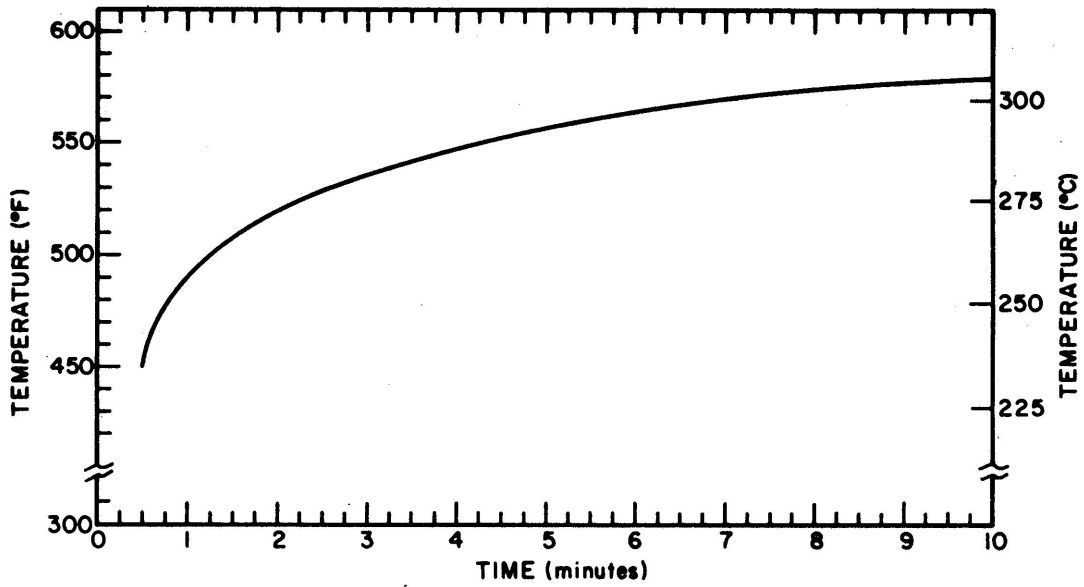


Figure 3. Time-Temperature Curve for the Fuel Contribution Thermocouple for an ACB Specimen

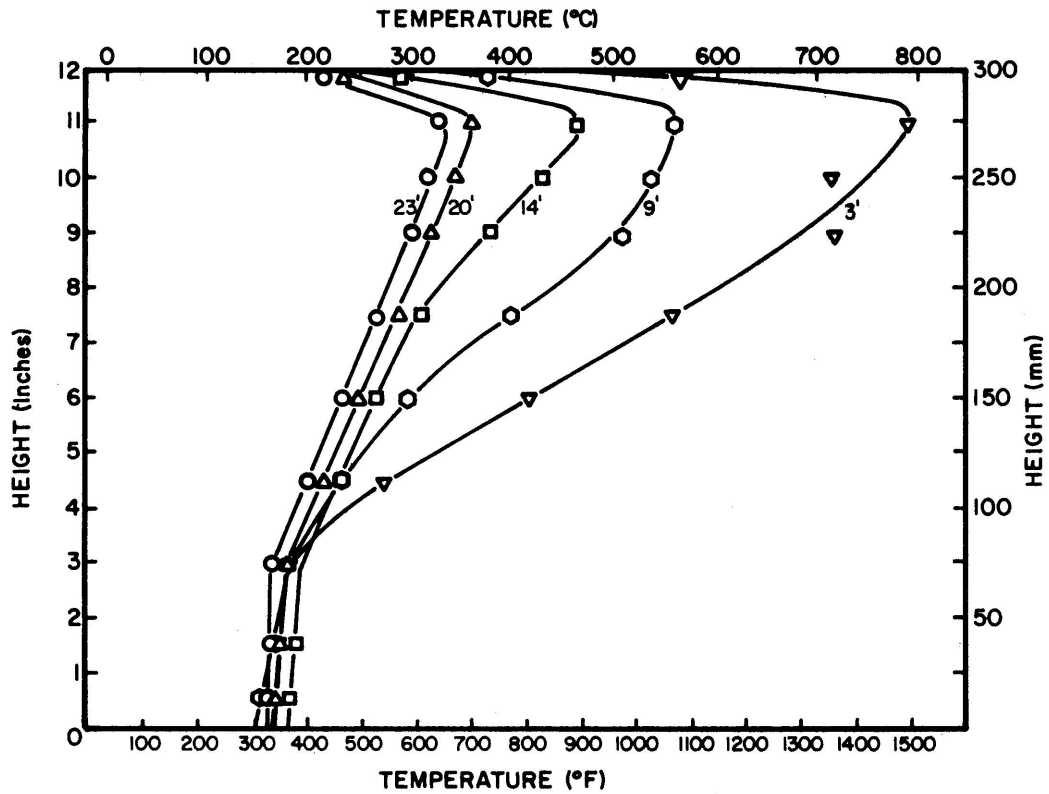


Figure 4. Centerline Air Temperature Profiles at Various Distances in the Tunnel for an ACB Specimen at 10 minutes

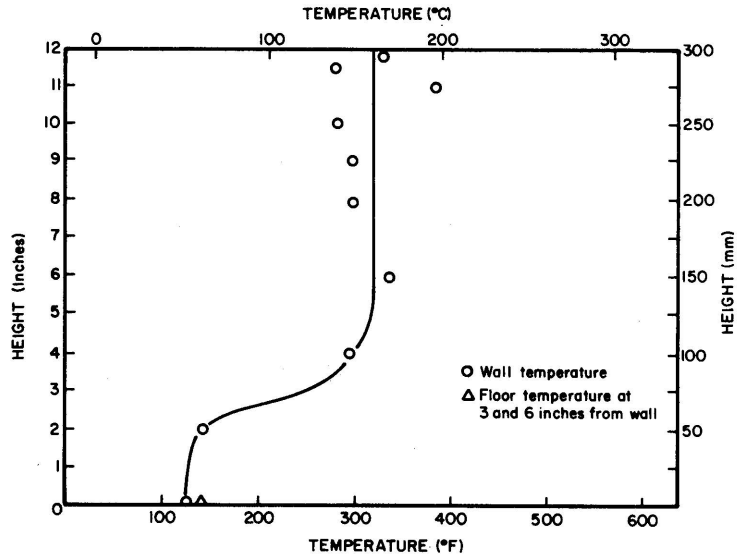


Figure 5. Temperatures on Rear Wall and on Floor at 14 Feet for an ACB Specimen at 4 minutes (1 foot = 0.305 meters)

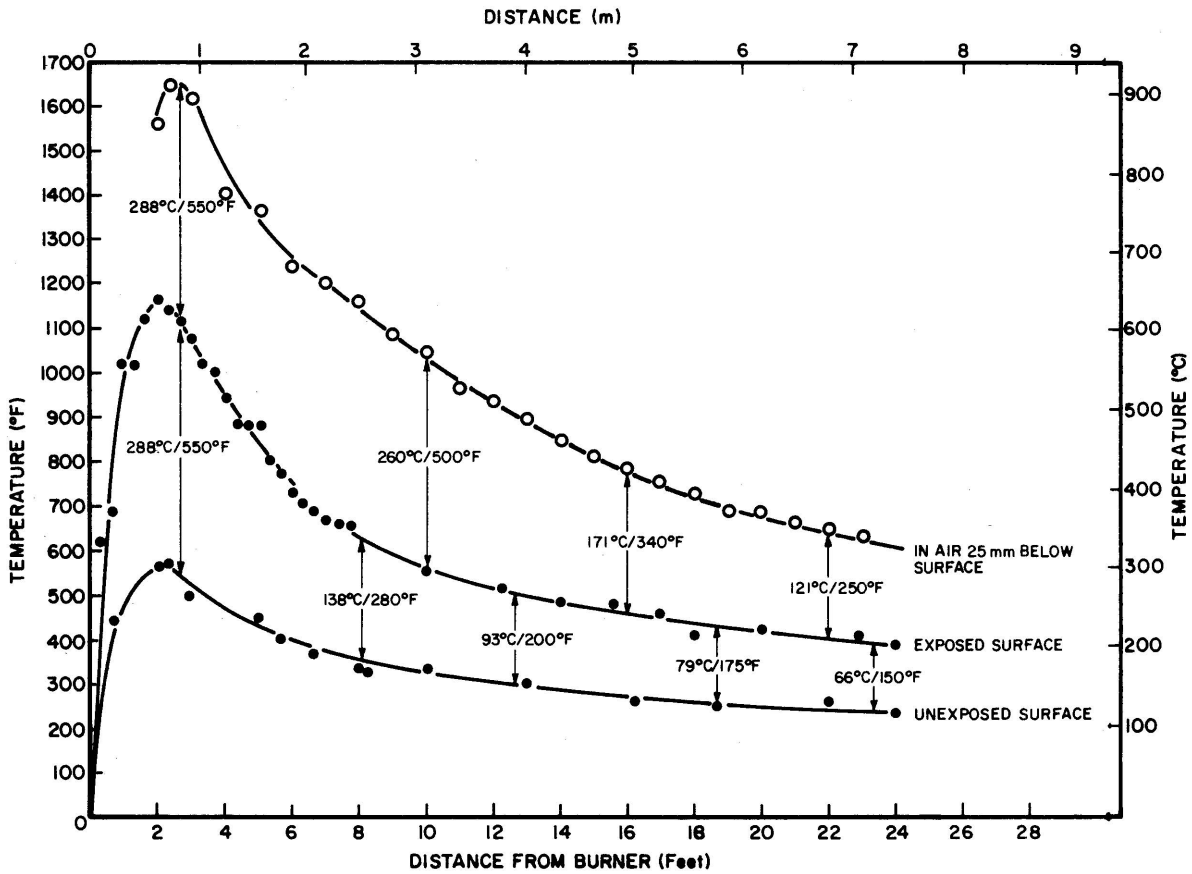


Figure 6. Temperature Distribution Along Exposed and Unexposed Surfaces of AMB Specimen at 20 minutes and in the Air One Inch Below it at 10 minutes

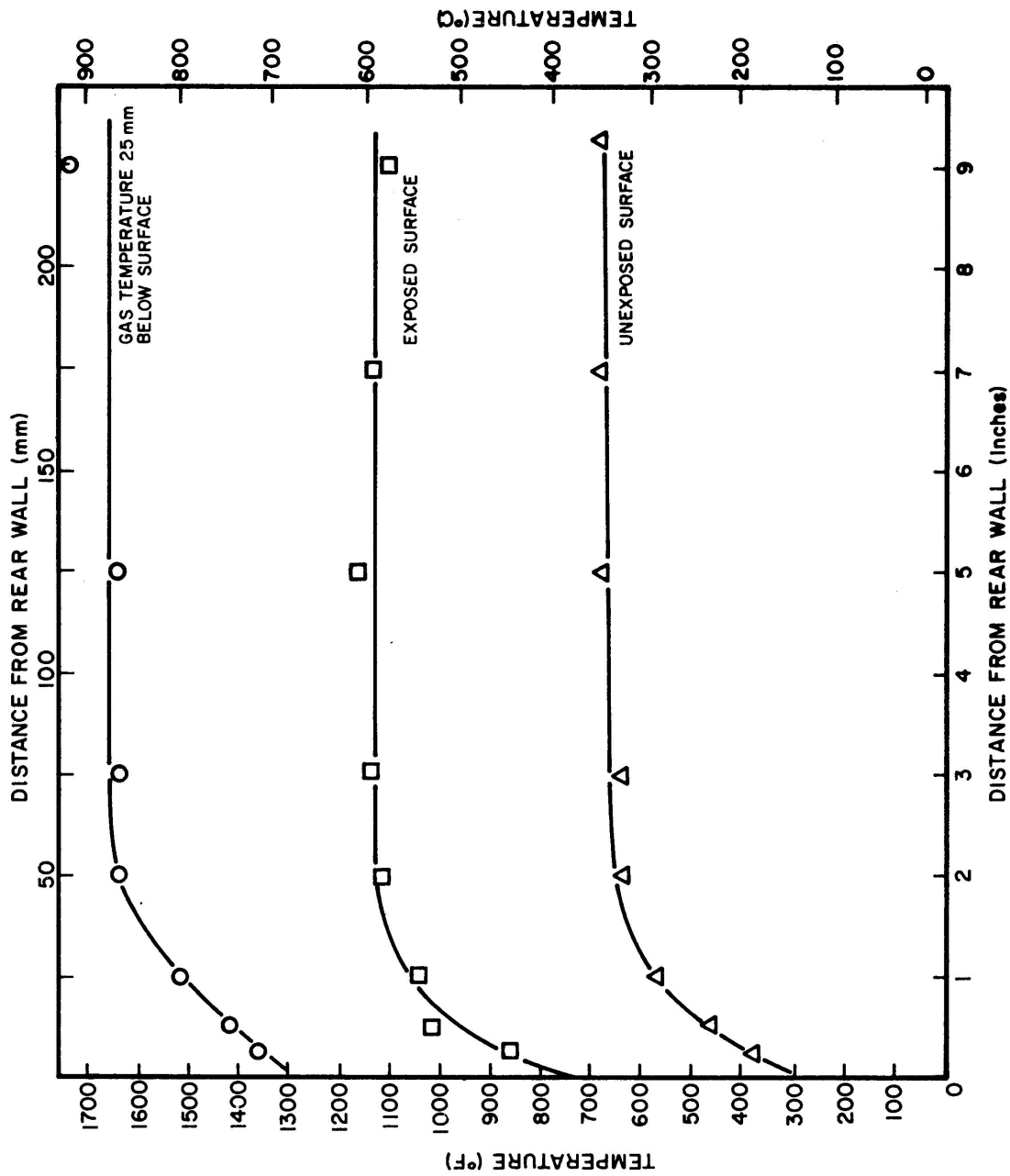


Figure 7. Temperature Distributions Across Exposed and Unexposed Surfaces of AMB and 25 mm Below it at 2.5 Feet at 20 minutes

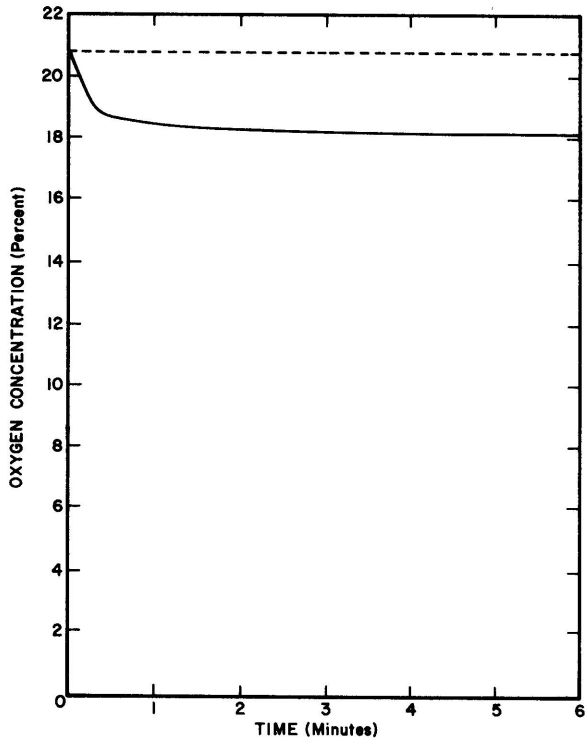
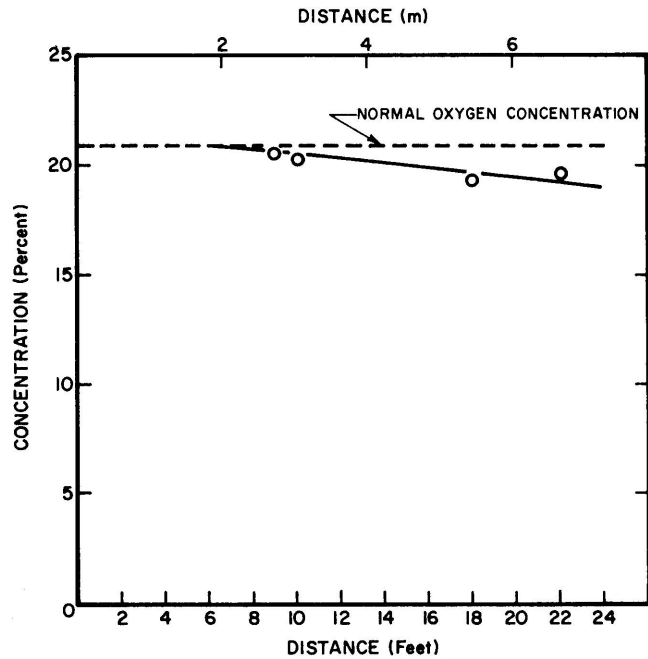


Figure 8. Chart Record of the Oxygen Concentration in the Duct 22 ft Downstream from the End of the Tunnel for an ACB Specimen

Figure 9. Oxygen Concentration Versus Distance Along the Floor With an ACB Specimen at 5 minutes



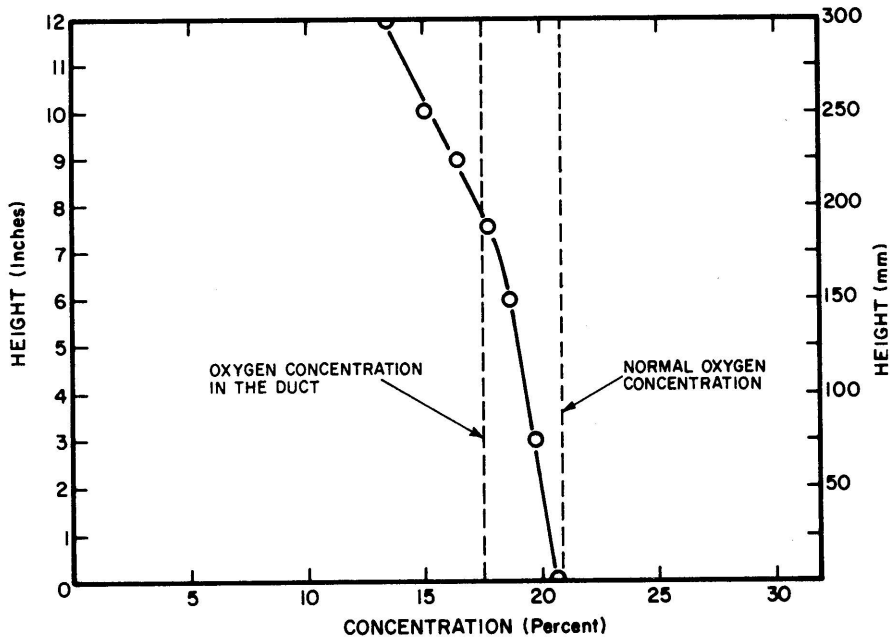


Figure 10. Vertical Oxygen Concentration Profile at Nine Feet with ACB at 5 minutes

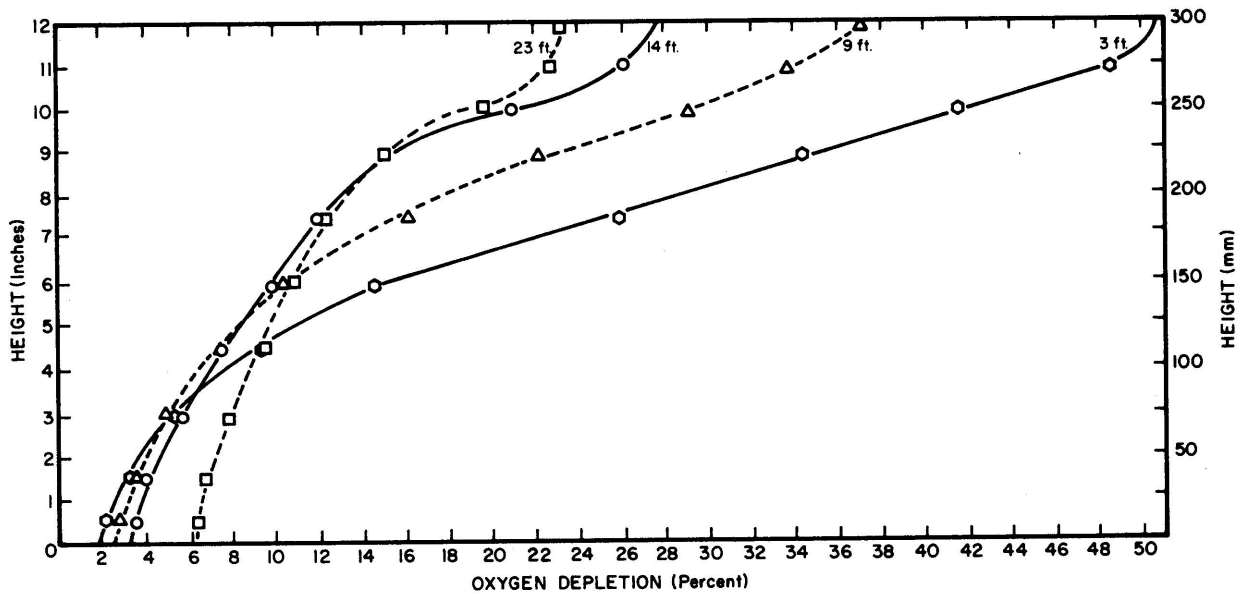


Figure 11. Oxygen Depletion Profiles at 3, 9, 14 and 23 Feet for an ACB Specimen at 5 minutes (1 foot = 0.305 meters)

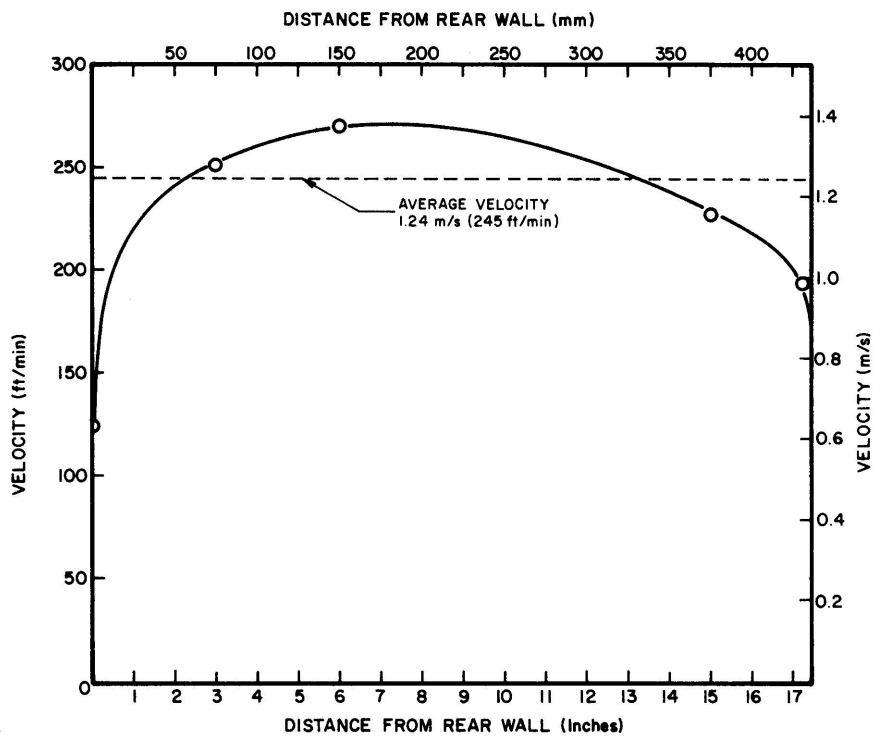


Figure 12. Horizontal Velocity Distribution of the Ambient Air Along the Midheight at the End of the Tunnel

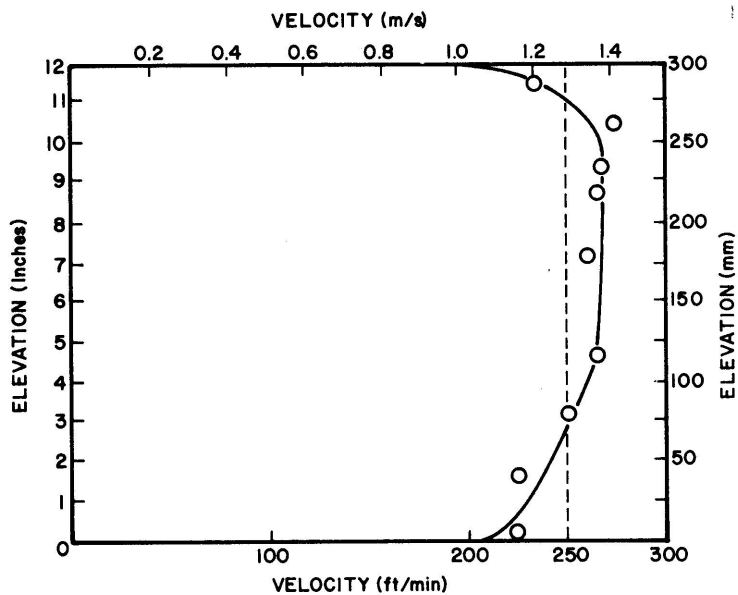


Figure 13. Vertical Velocity Profile Through the Centerline at Nine Feet with the Burner Off (1 foot = 0.305 meters)

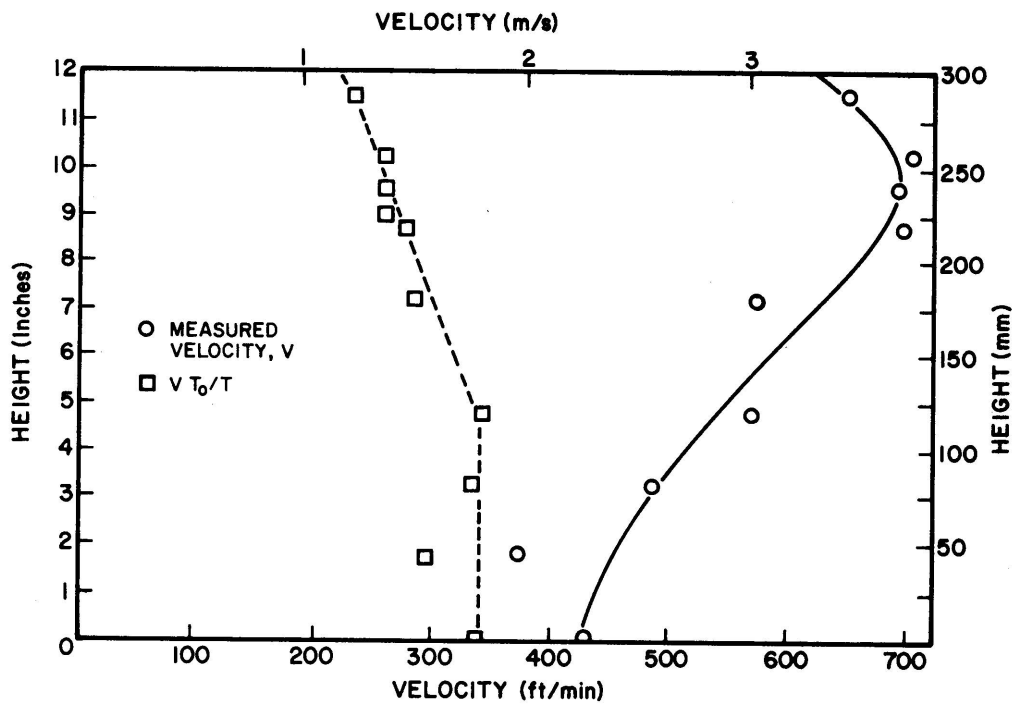


Figure 14. Vertical Velocity Profile through the Centerline at Nine Feet with the Burner On for 4 Minutes

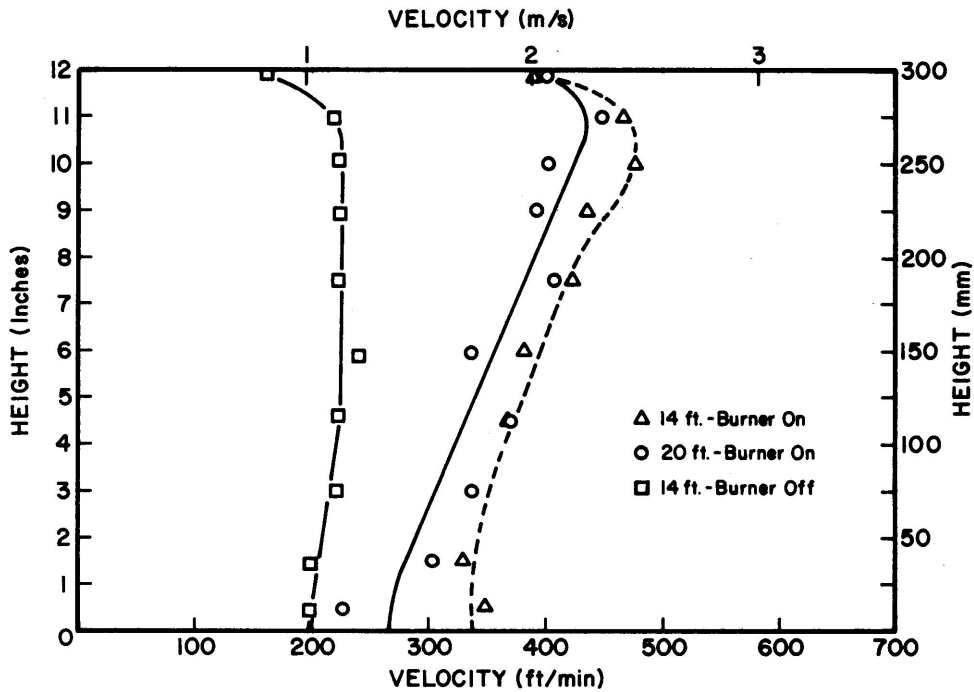


Figure 15. Vertical Velocity Profile through Centerline at 14 and 20 Feet for ACB with the Burner On and for 20 Feet with Burner Off

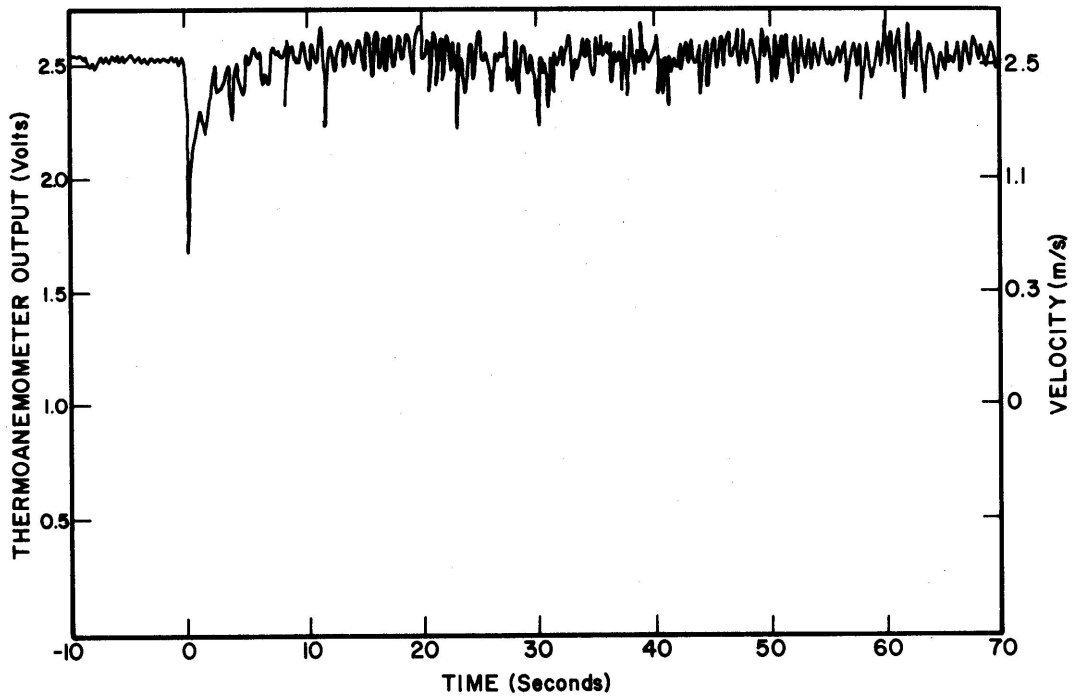


Figure 16. Chart Record of the Inflow Velocity for ACB Measured with the Thermoanemometer

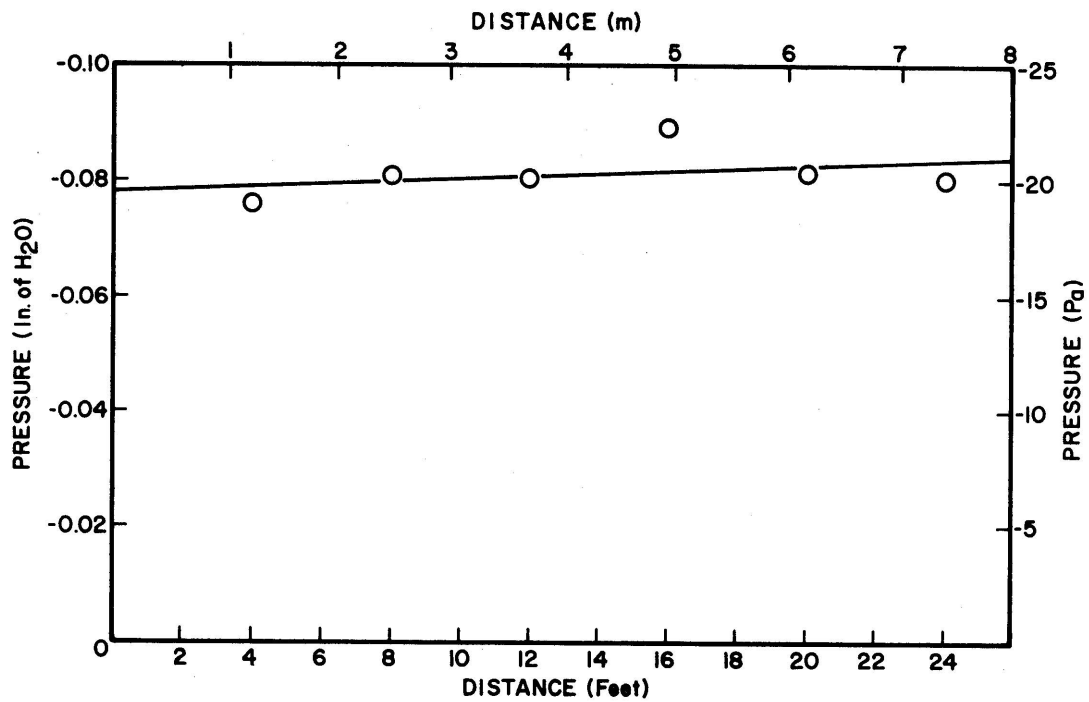


Figure 17. Negative Pressure Distribution on the Floor of the Tunnel with the Burner Off

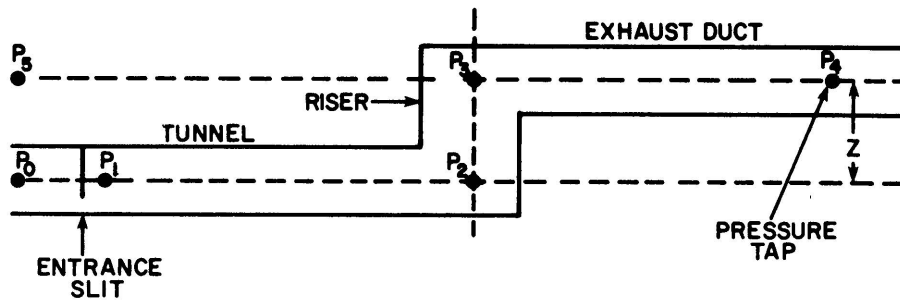


Figure 18. Location of Pressure Points Discussed in Section 4.1.4.

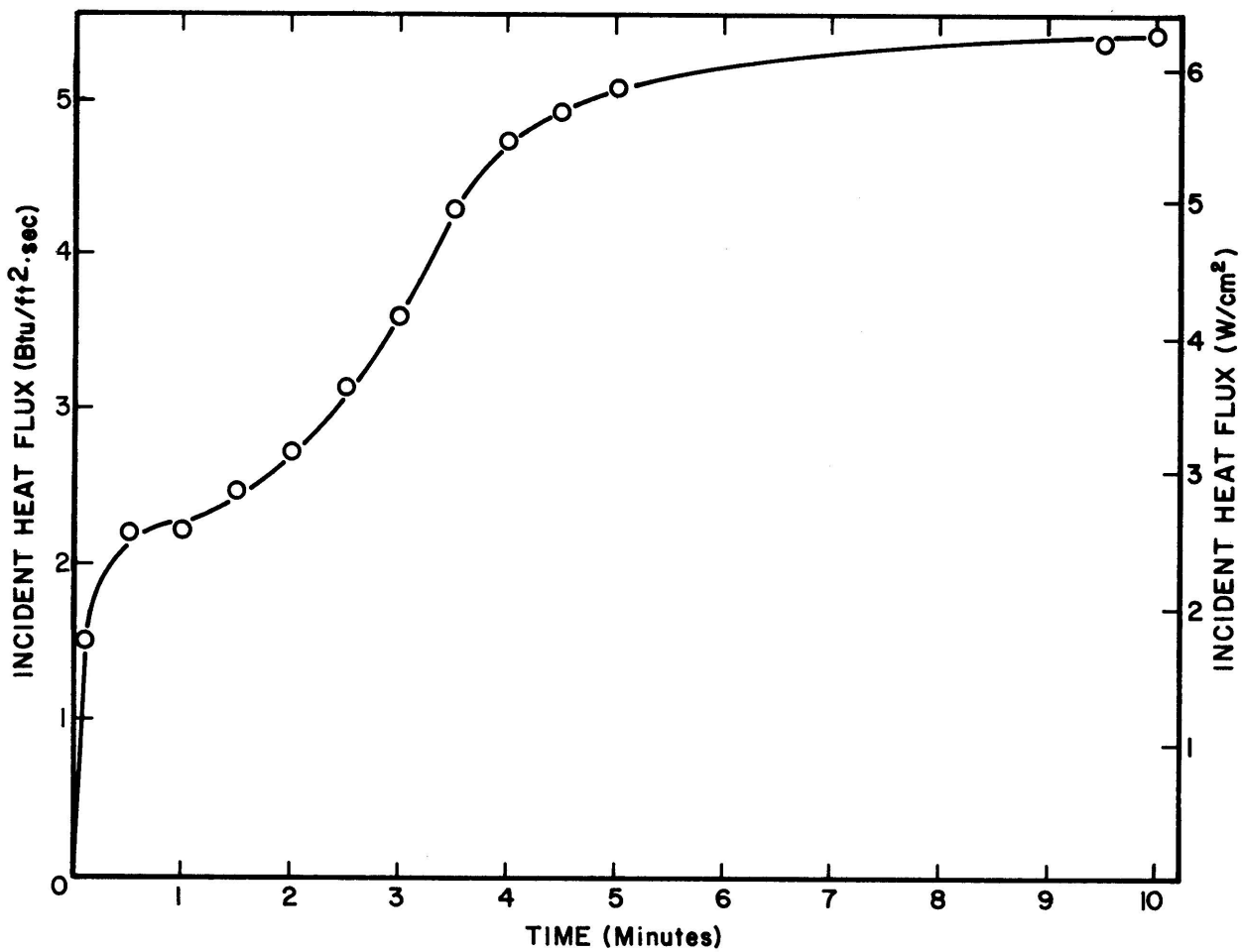


Figure 19. Variation in Incident Heat Flux with Time at Two Feet (1 foot = 0.305 meters)

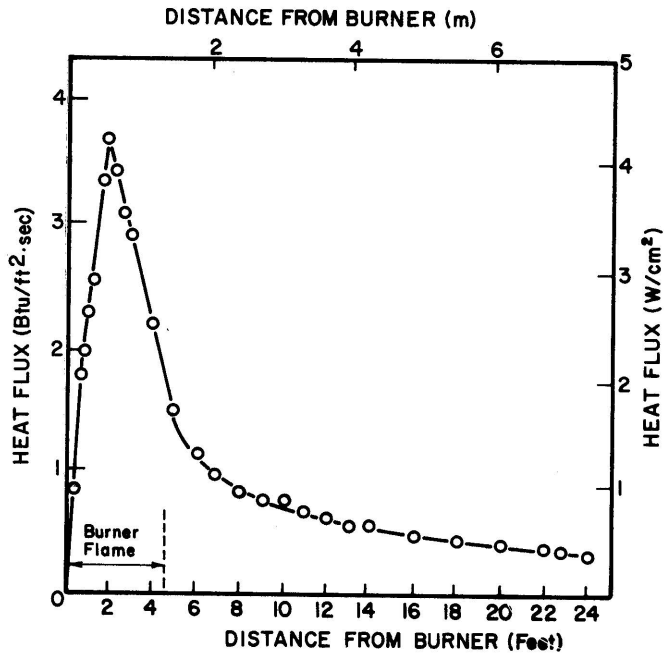


Figure 20. Incident Heat Flux Distribution Along an AMB Specimen at 20 Minutes

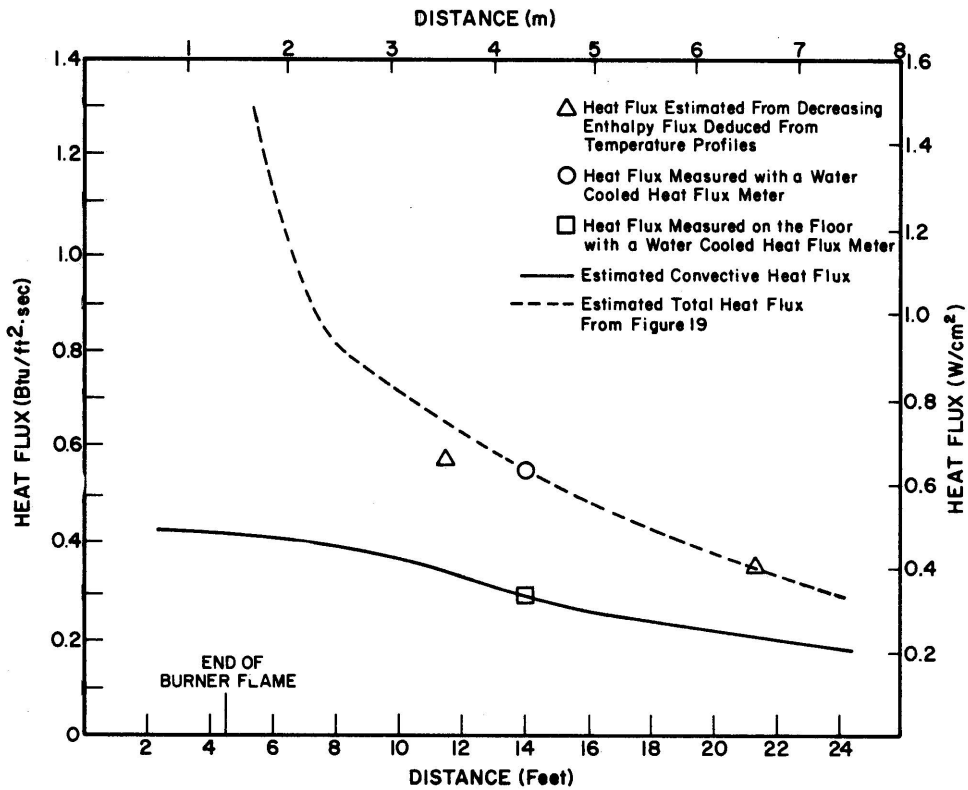


Figure 21. Convective Heat Flux Distribution Along an AMB Specimen at 10 Minutes

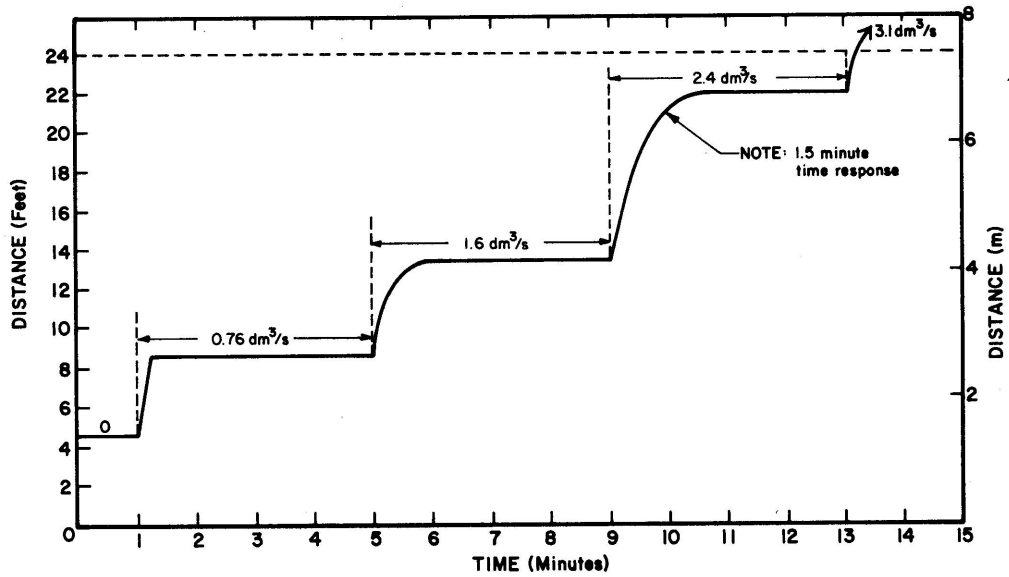


Figure 22. Flame Distance Versus Time at Different Flow Rates of Methane in Auxiliary Burner

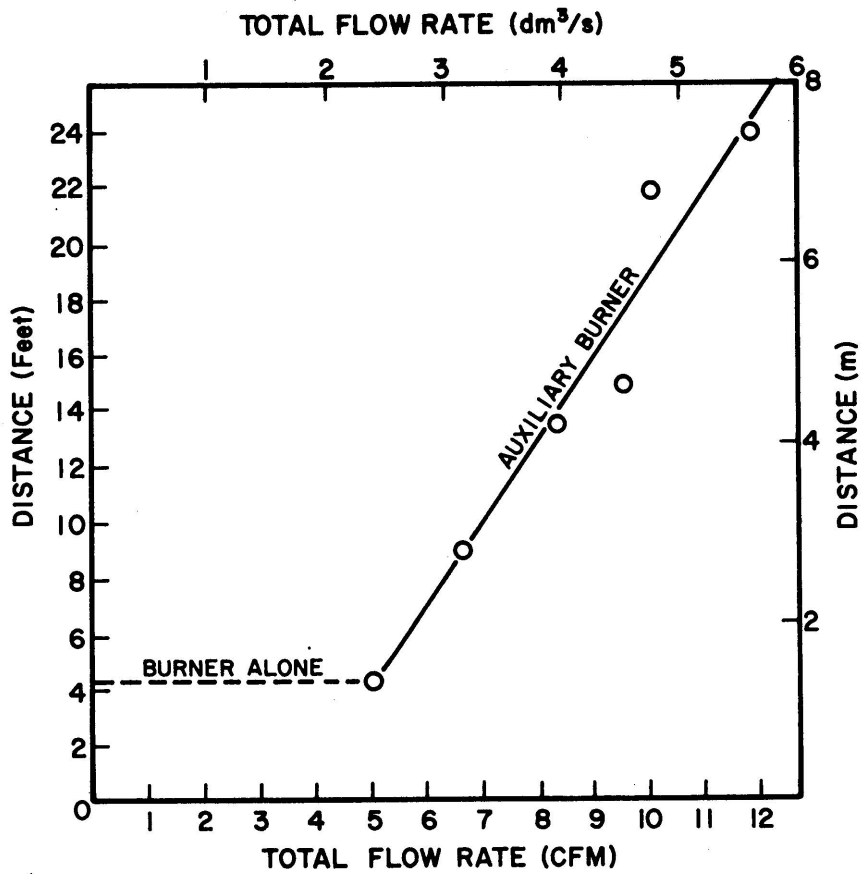


Figure 23. Flame Spread Distance Versus Total Methane Flow Rate in Auxiliary Burner

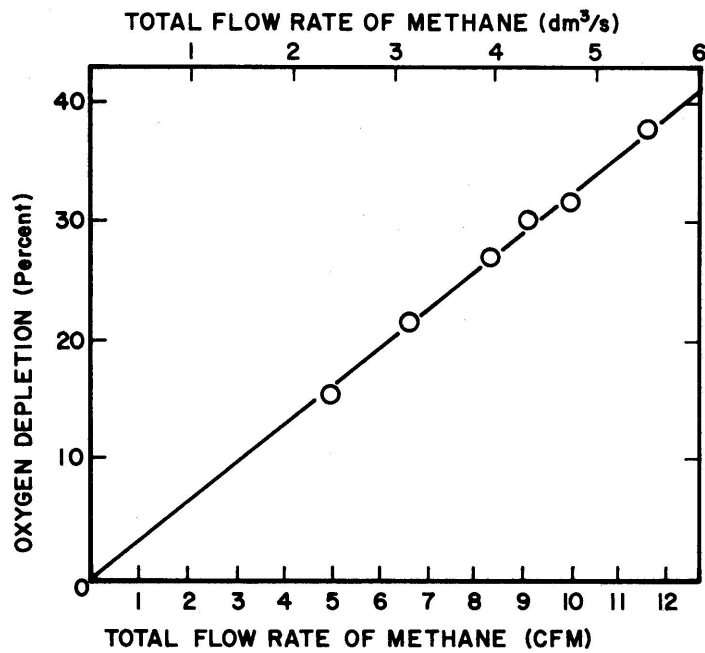


Figure 24. Oxygen Depletion in Duct 22 Feet Downstream from the End of the Tunnel Using the Auxiliary Burner

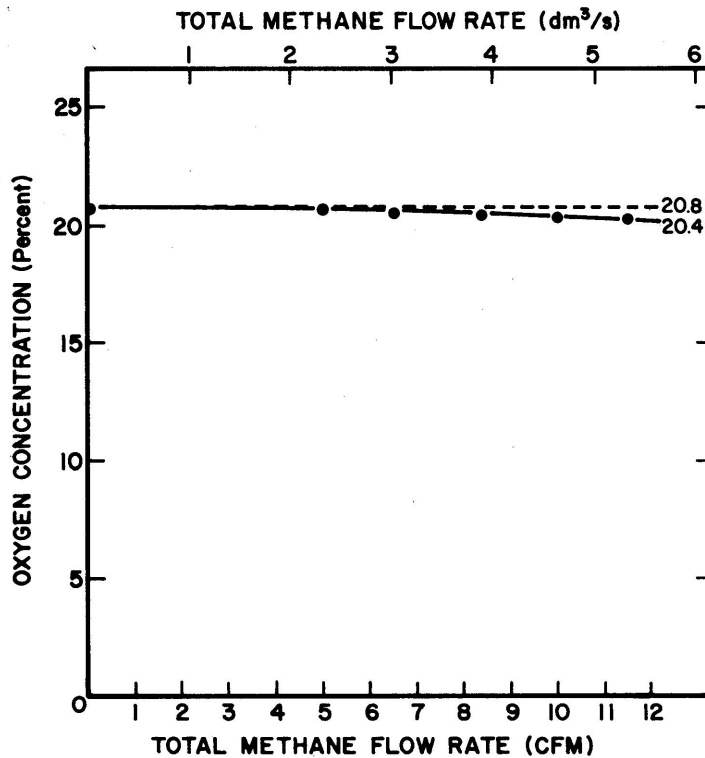


Figure 25. Oxygen Concentration on Floor of Tunnel at Nine Feet Using Auxiliary Burner (1 foot = 0.305 meters)

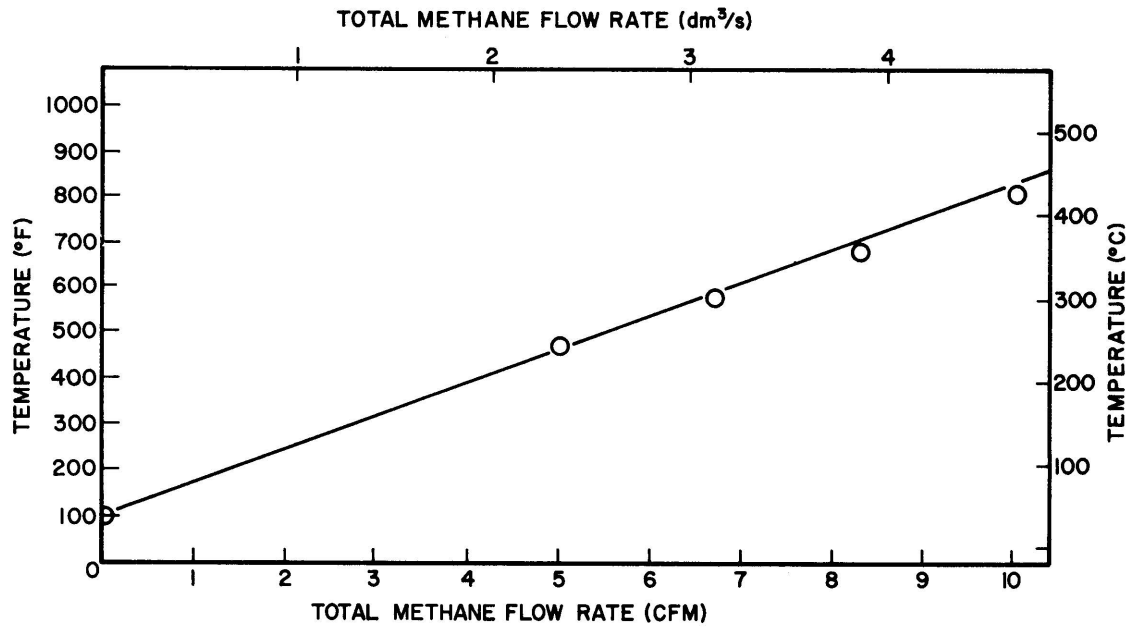


Figure 26. Temperature Rise of Fuel Contribution Thermocouple as a Function of Gas Flow

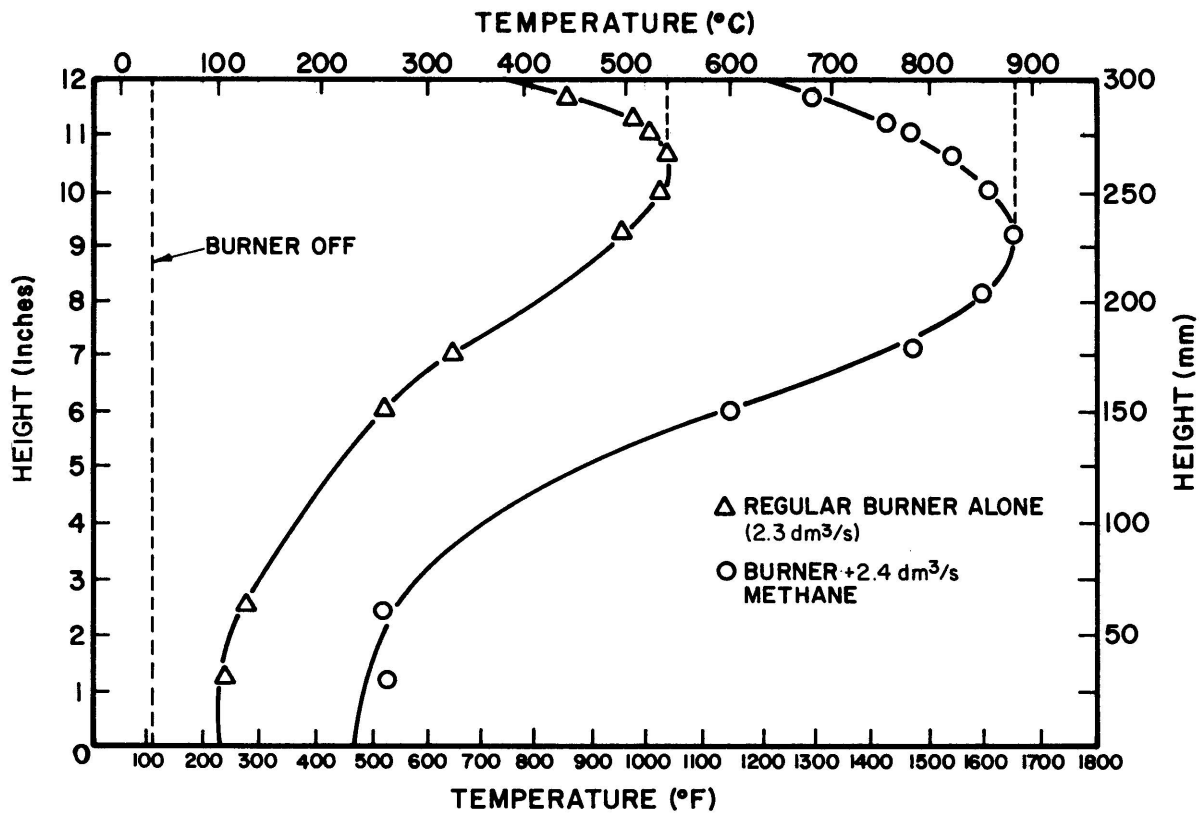


Figure 27. Vertical Temperature Profiles at 9 Feet at 5 Minutes Using Auxiliary Burner (1 foot = 0.305 meters)

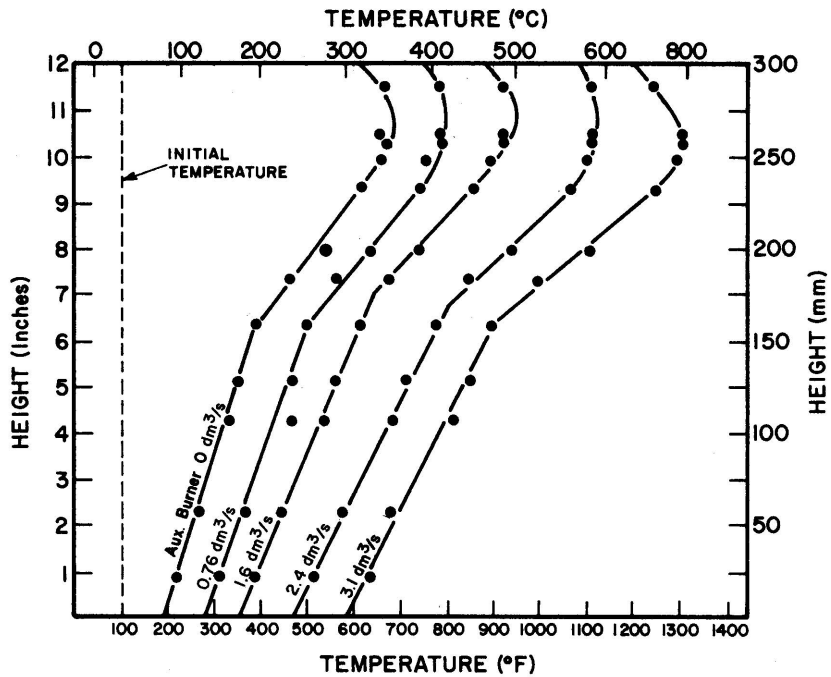


Figure 28. Vertical Temperature Profiles at 16 Feet at 5 Minutes Using Auxiliary Burner

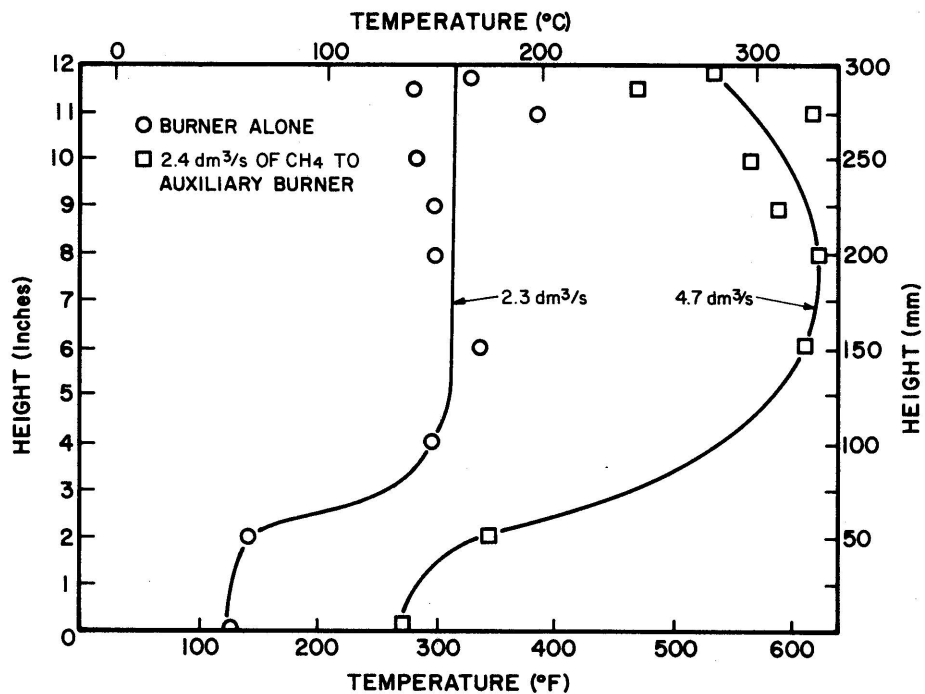


Figure 29. Temperature Distribution Along Wall at 14 Feet at 5 Minutes Using Auxiliary Burner (1 foot = 0.305 meters)

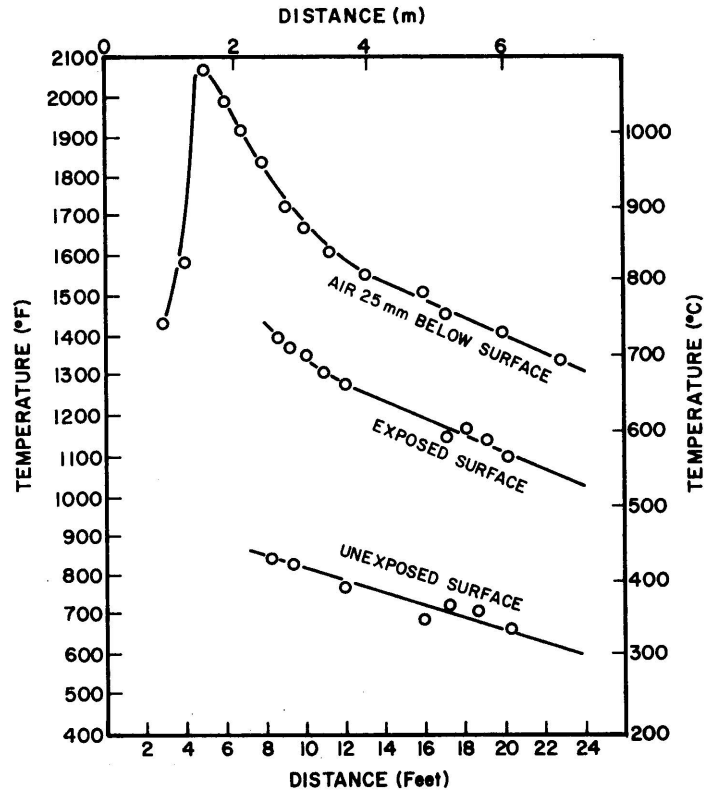


Figure 30. Temperatures for AMB Under Full Flame Exposure at 20 Minutes Using Auxiliary Burner

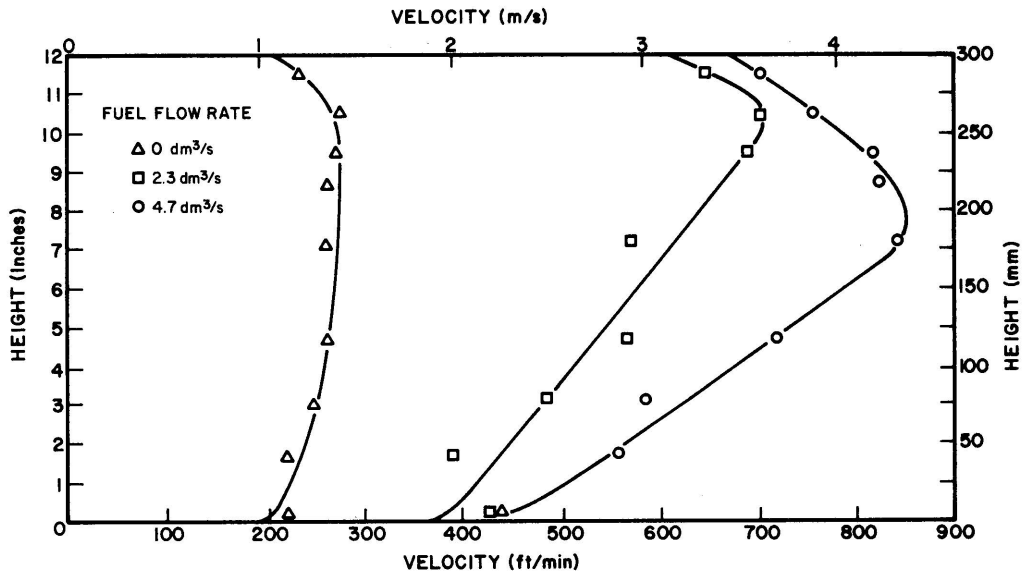


Figure 31. Vertical Velocity Profiles at 9 Feet at 5 Minutes Using Auxiliary Burner (1 foot = 0.305 meters)

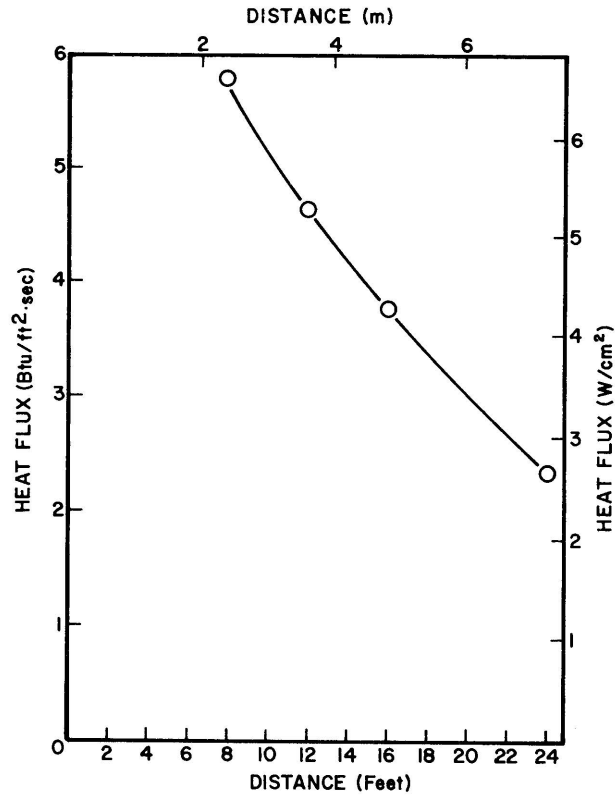


Figure 32. Incident Heat Flux Distribution Along an AMB Specimen Fully Covered with Flame at 20 Minutes

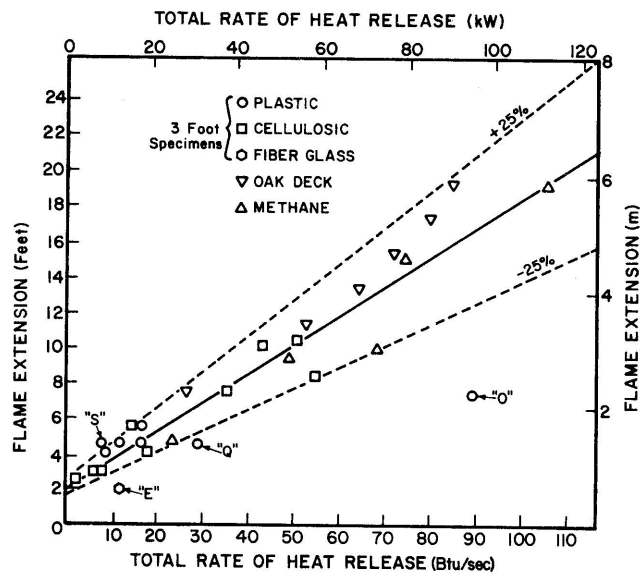


Figure 33. Flame Distance Versus Fuel Generation Rate in the Tunnel (1 foot = 0.305 meters) (For Identification of Specimens S, E, Q and O see Table 3)

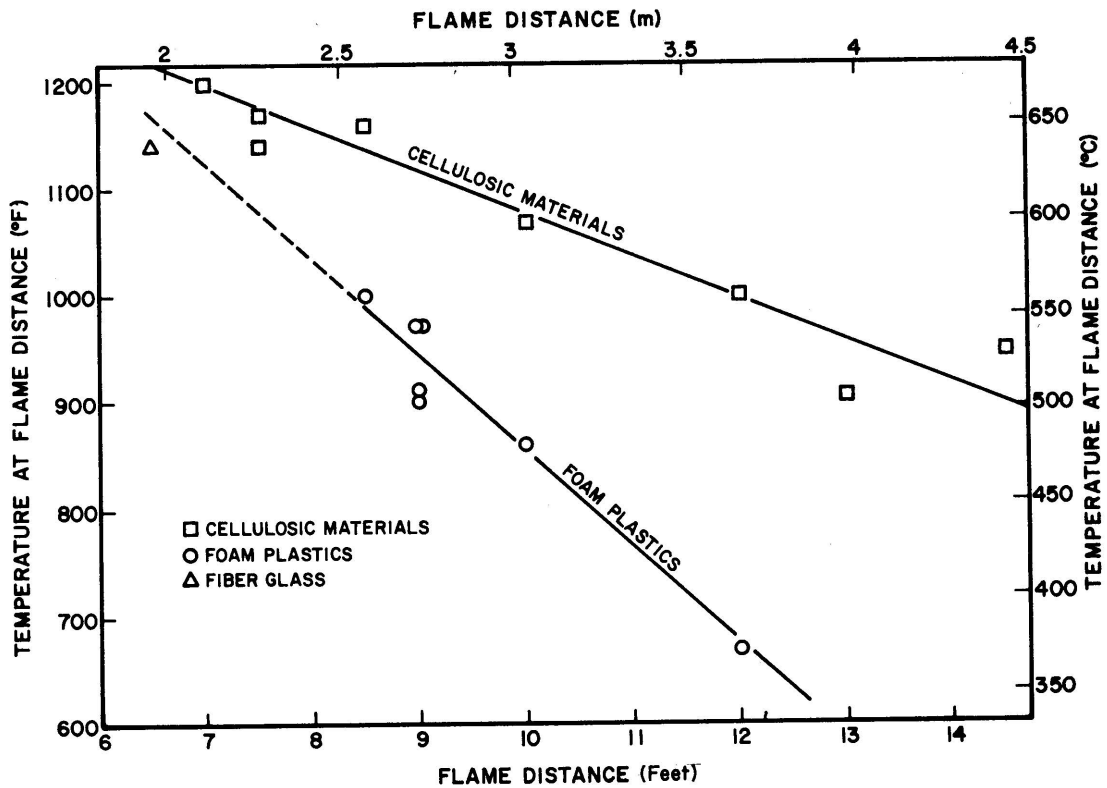


Figure 34. Air Temperatures at Called Flame Distances for Three-Foot Specimens

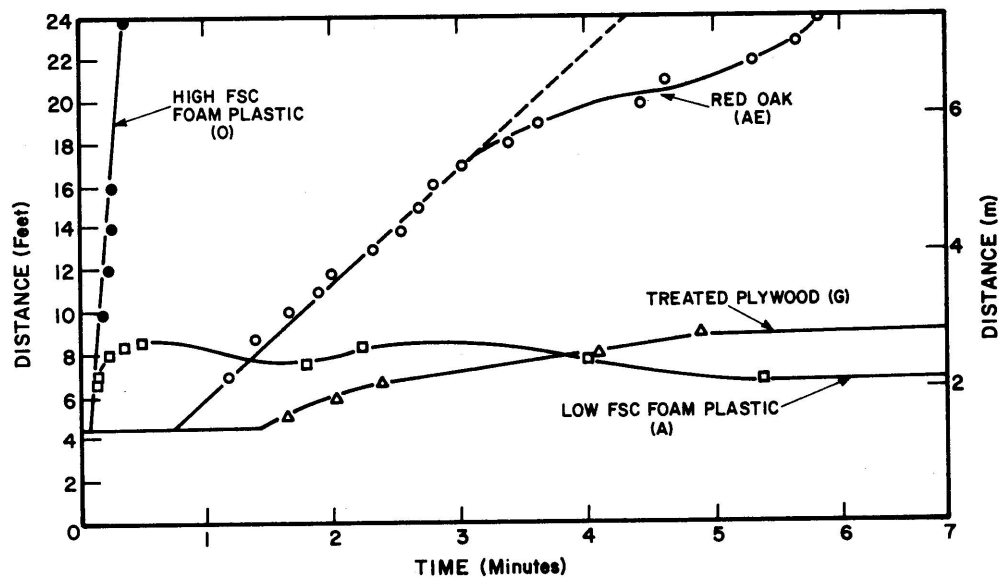


Figure 35. Flame Spread Distance Versus Time for Four Materials

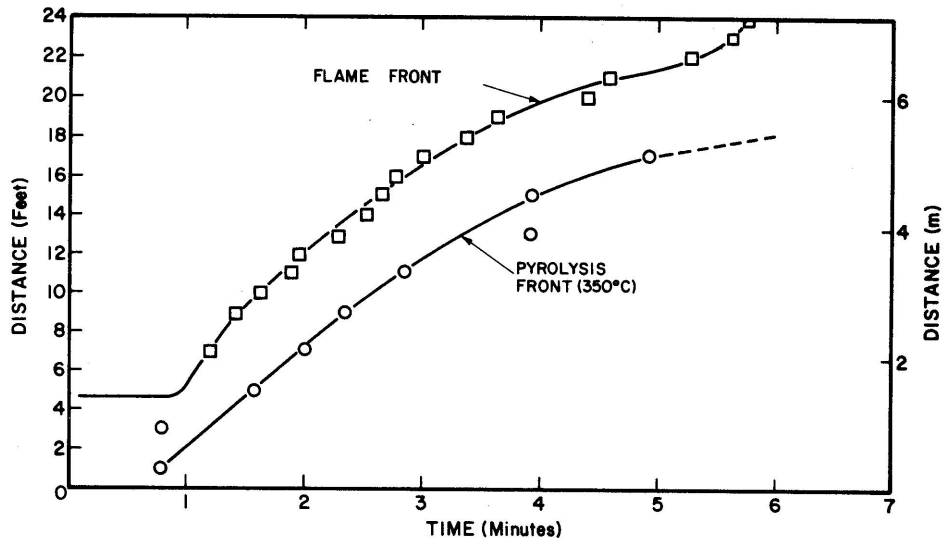


Figure 36. Relationship Between Flame Front and Pyrolysis Zone for Red Oak Deck in the Tunnel

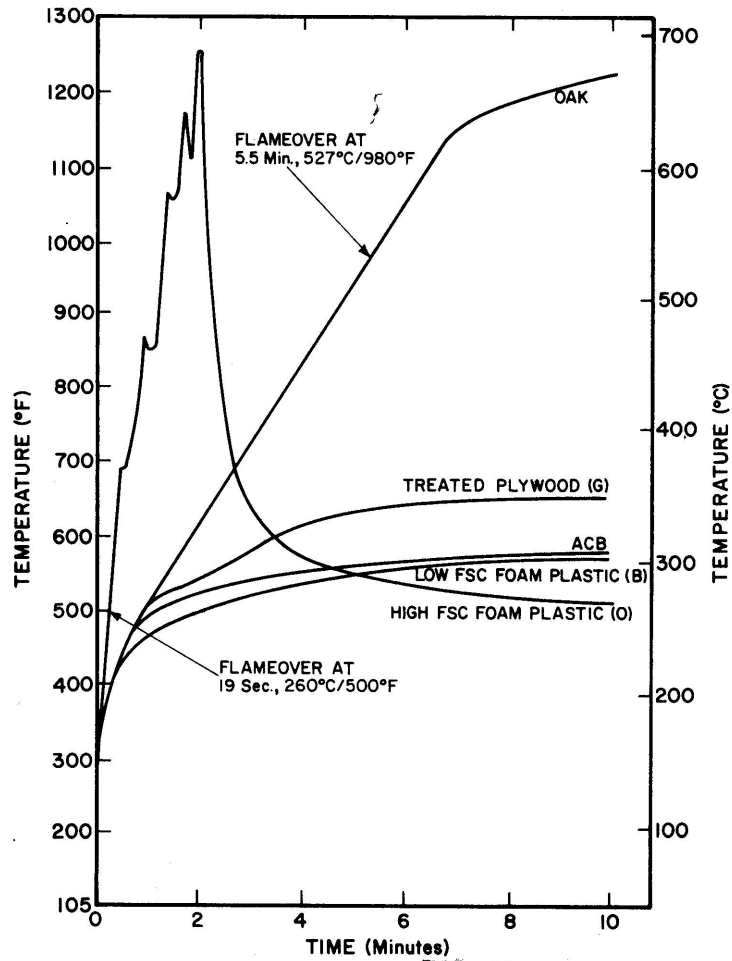


Figure 37. Temperature Versus Time on Heat Contribution Thermocouple for Five Materials

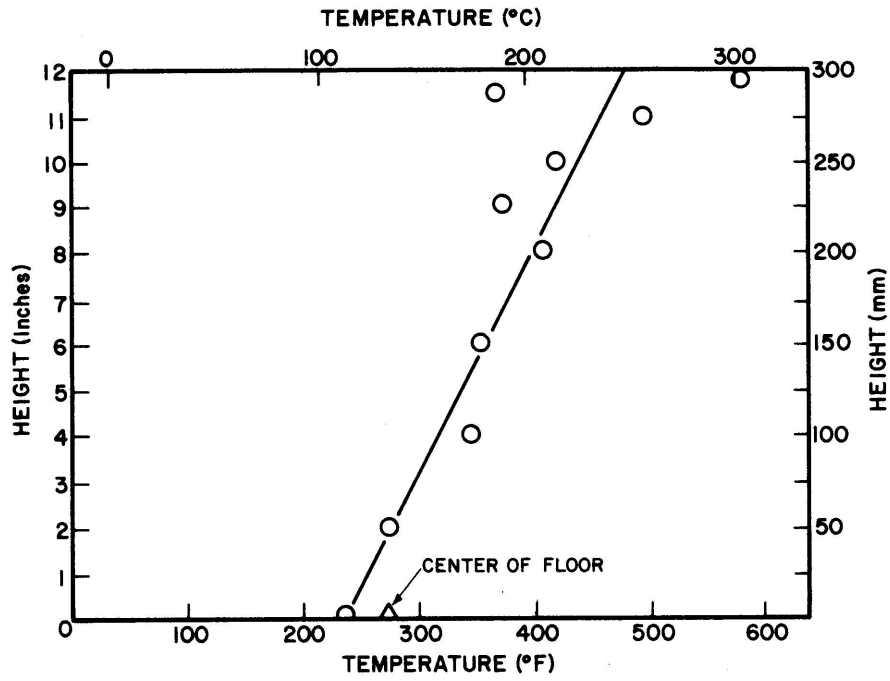


Figure 38. Temperature Distribution Along Wall at 14 Feet at 5 Minutes for Type B Specimen

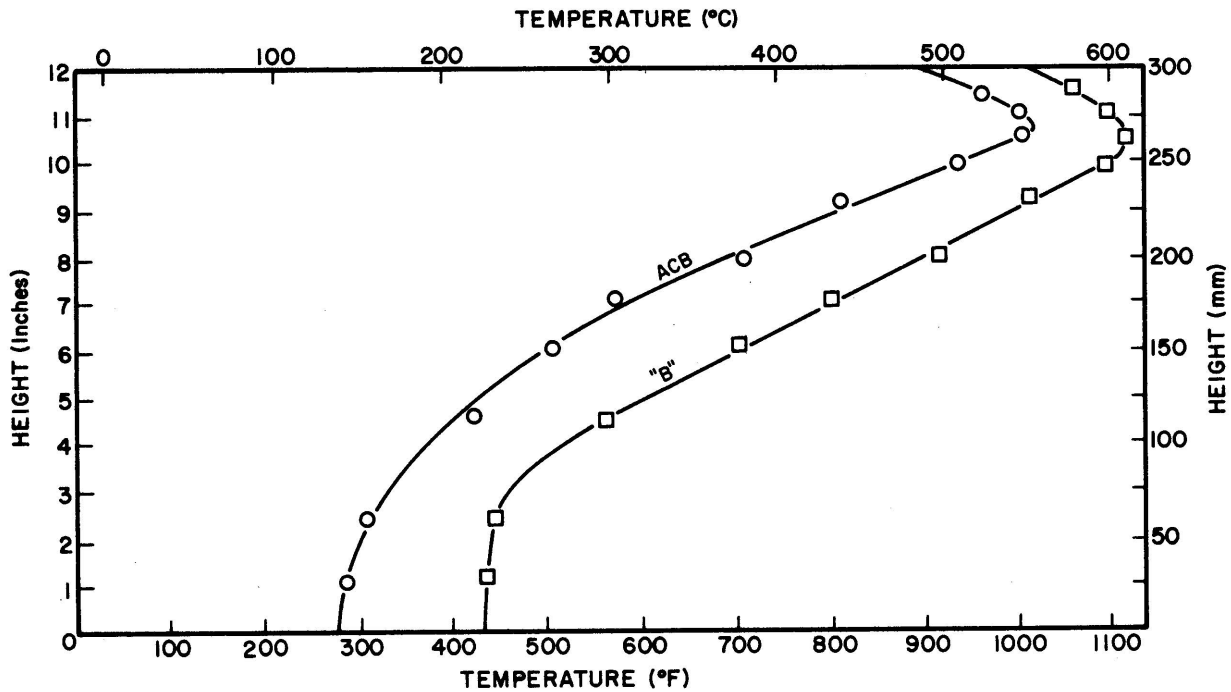


Figure 39. Vertical Temperature Profile at 9 Feet at 5 Minutes for Specimens of ACB and Type B (F.R. Polyurethane FSC 28) (1 foot = 0.305 meters).

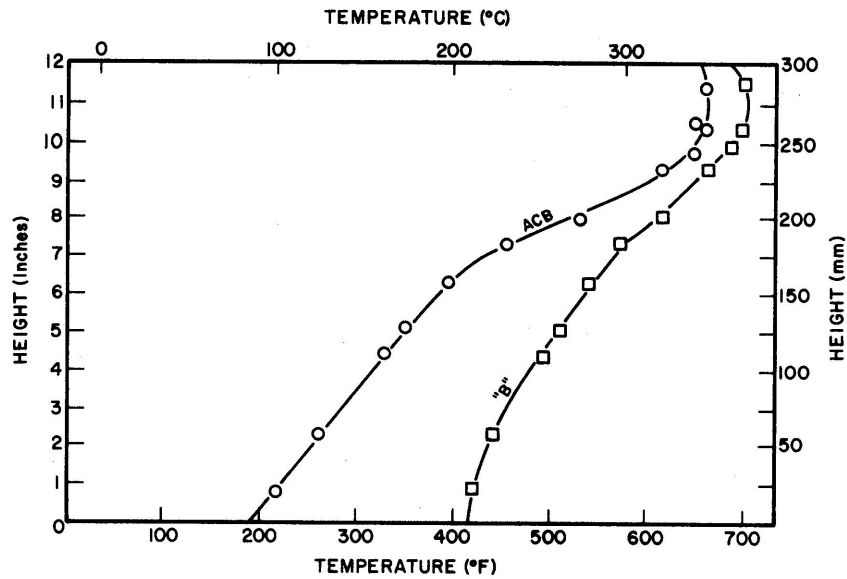


Figure 40. Vertical Temperature Profiles at 16 Feet at 5 Minutes for Specimens of ACB and Type B

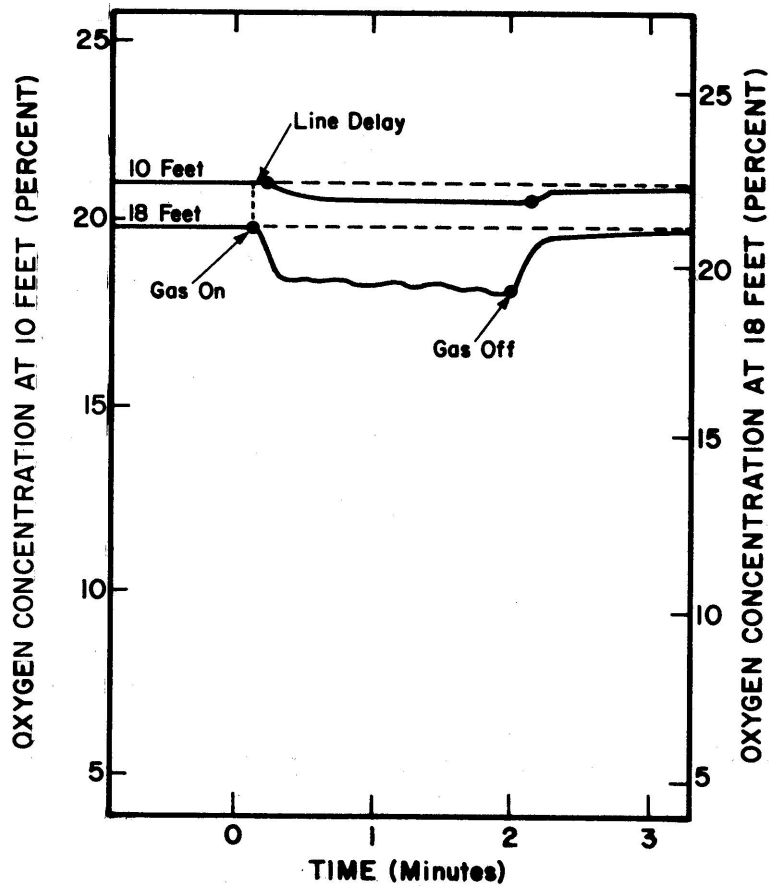


Figure 41. Chart Record of Oxygen Concentration on the Floor of the Tunnel at 10 and 18 Feet for a Type B Specimen (F.R. Polyurethane FSC 28). (1 foot = 0.305 meters)

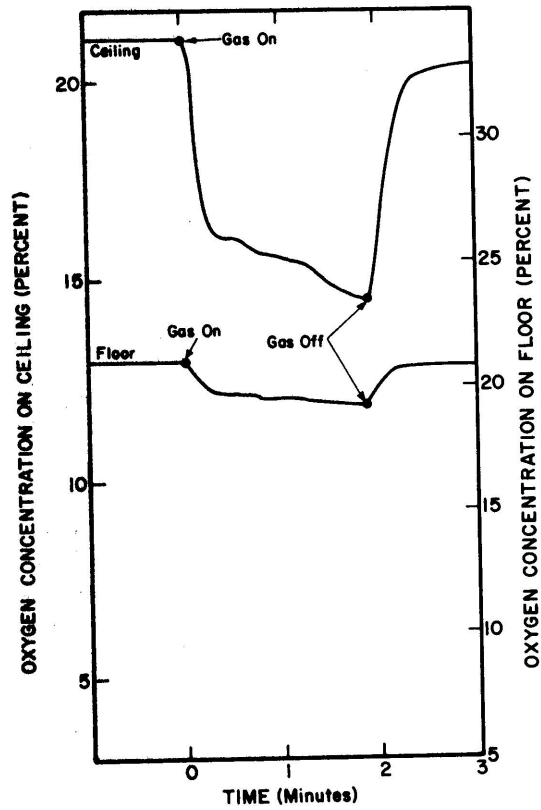


Figure 42. Chart Record of Oxygen Concentration on Floor and Ceiling at 22 Feet for a Type B Specimen (F.R. Polyurethane FSC 28) (1 foot = 0.305 meters)

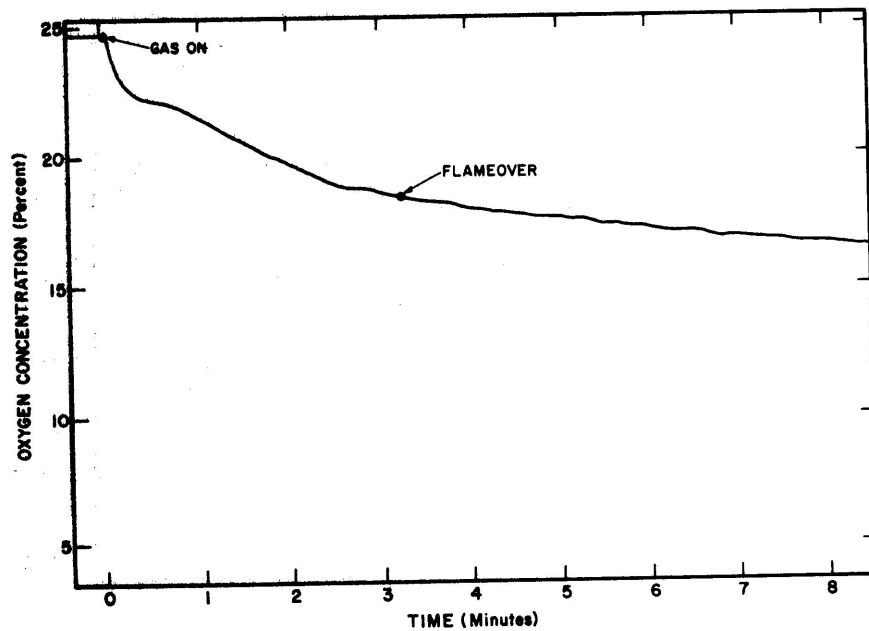


Figure 43. Chart Record of Oxygen Concentration in Duct for an Oak Specimen

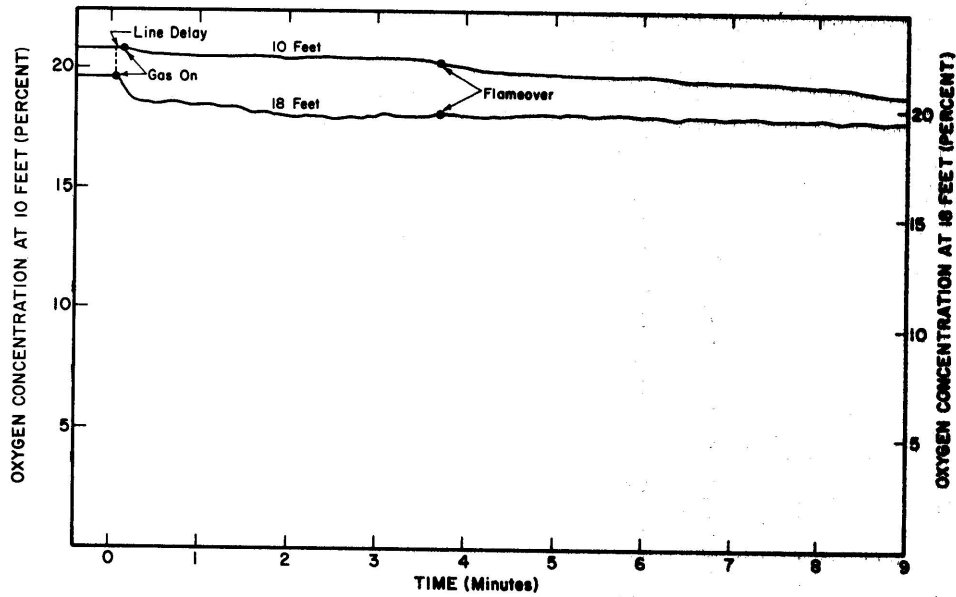


Figure 44. Chart Record of Oxygen Concentration on the Floor of the Tunnel at 10 and 18 Feet for an Oak Specimen (1 foot = 0.305 meters)

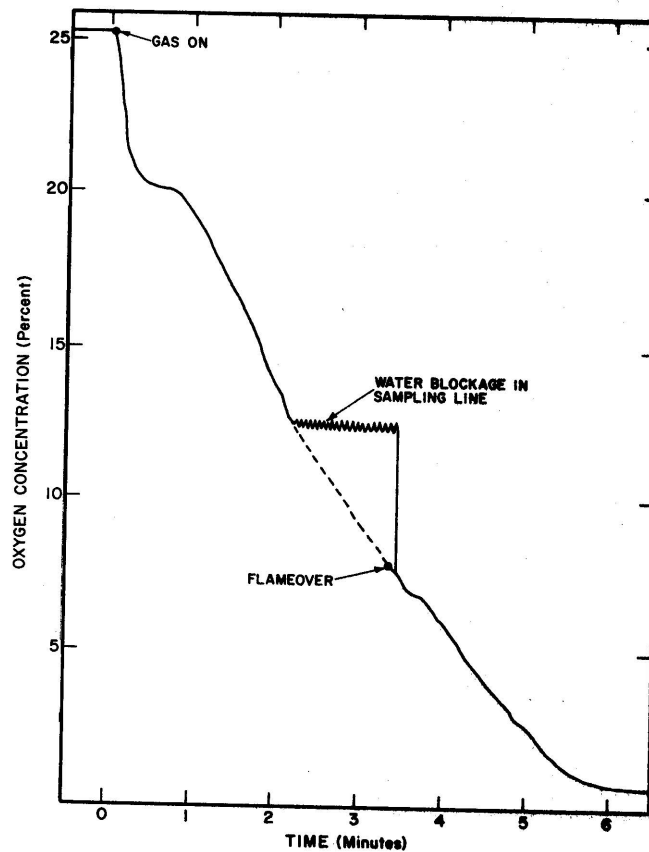


Figure 45. Chart Record of Oxygen Concentration at the Ceiling of the Tunnel at 22 Feet for an Oak Specimen (1 foot = 0.305 meters)

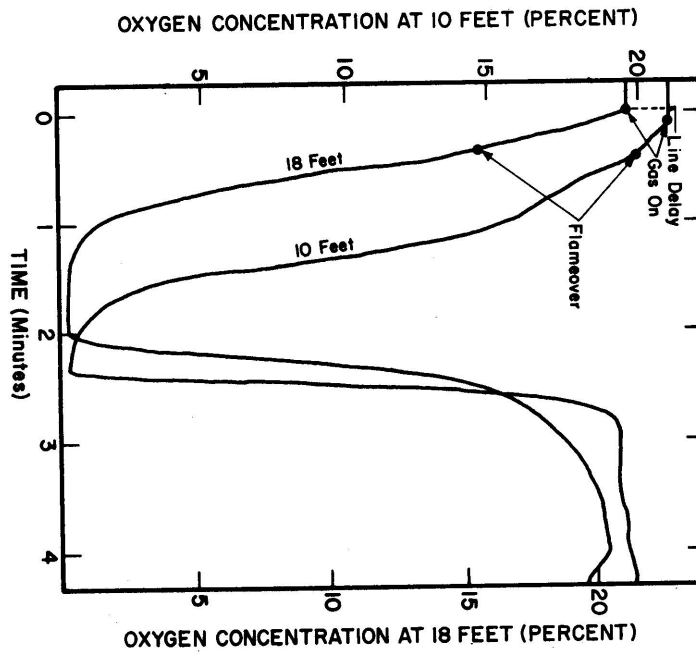


Figure 46. Chart Record of Oxygen Concentration on the Floor of the Tunnel at 10 and 18 Feet for a Type O Specimen

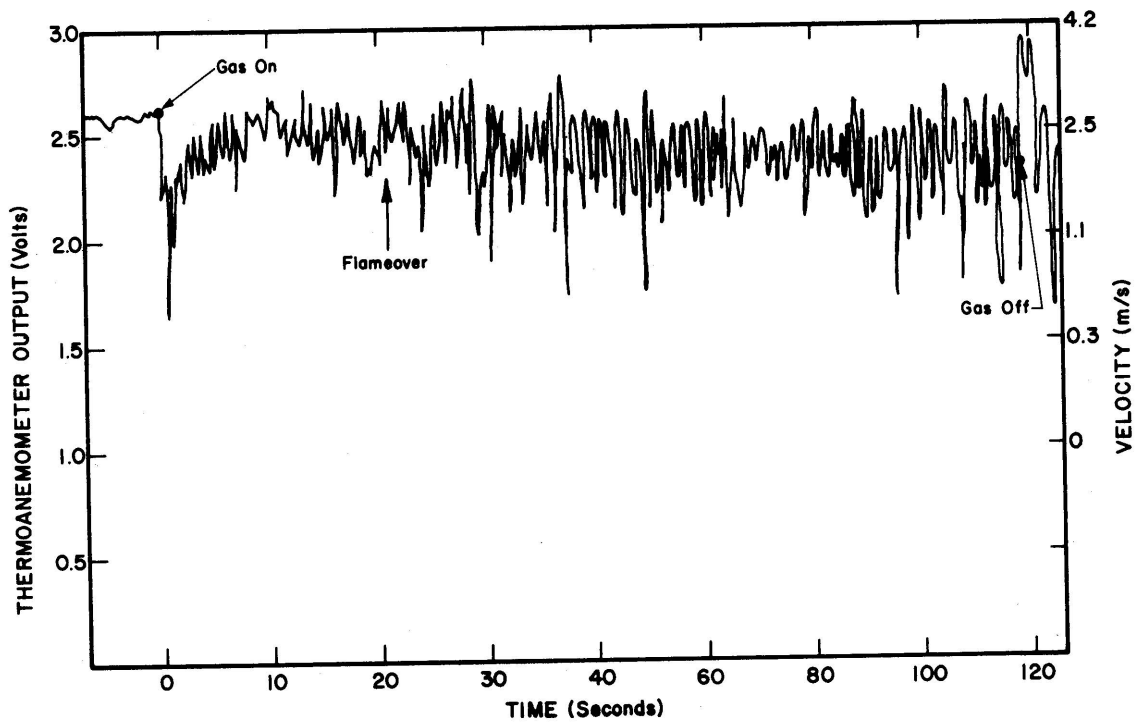


Figure 47. Chart Record of Inflow Velocity Data for a Type O Specimen

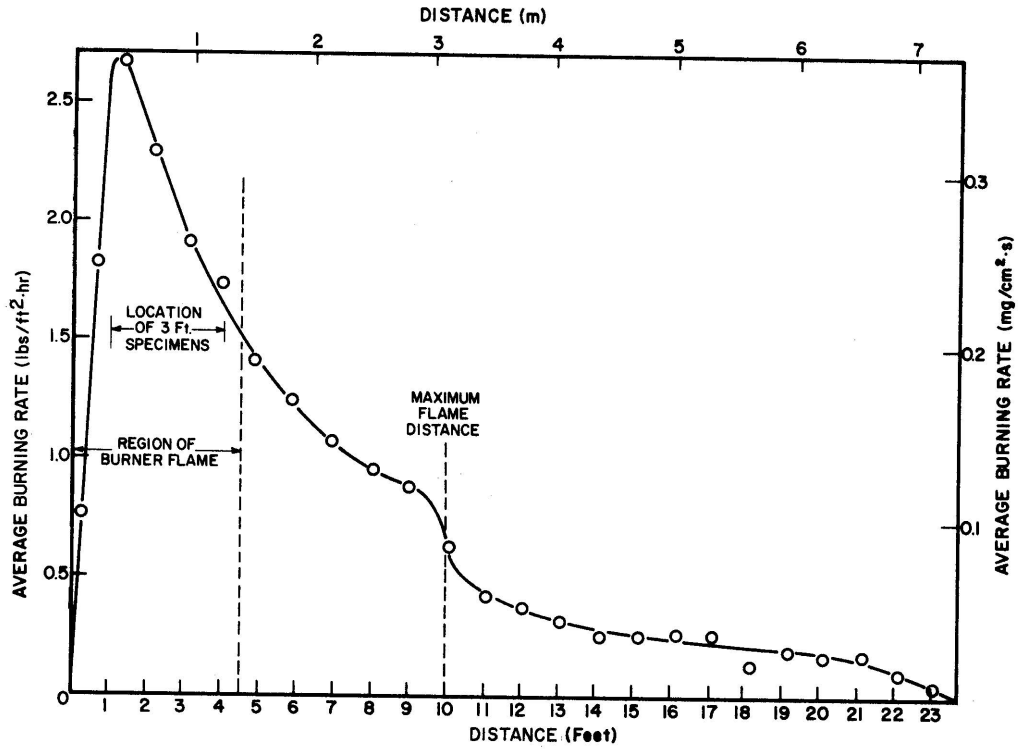


Figure 48. Average Burning Rate Distribution Along a Type B Specimen for a 5-Minute Period (F.R. Polyurethane FSC 28)

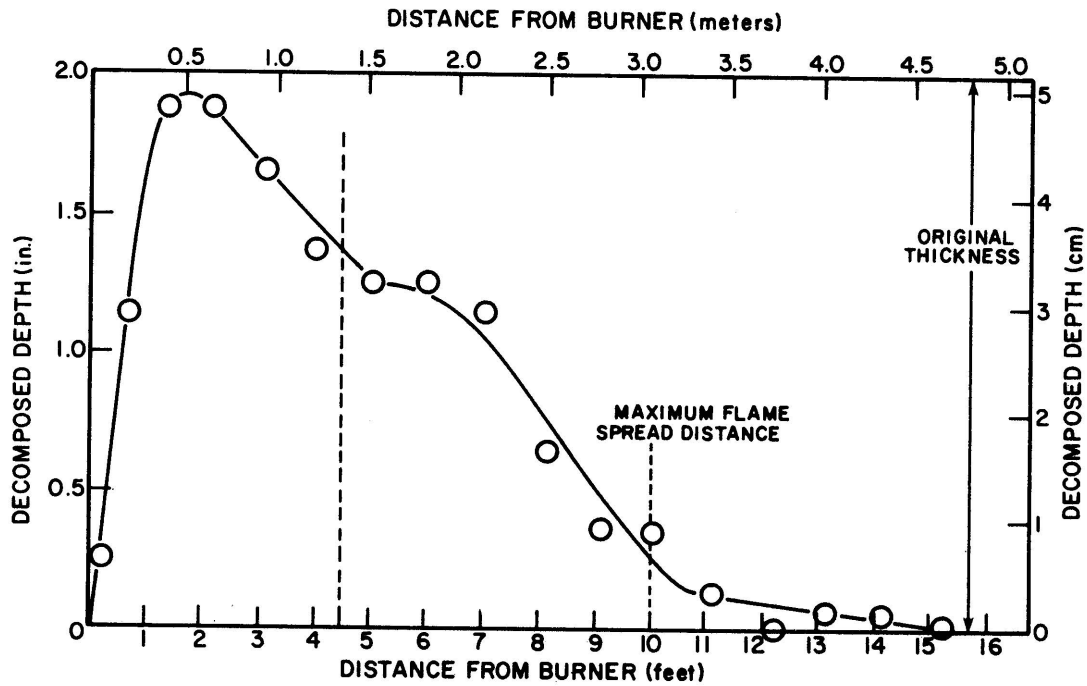


Figure 49. Decomposed Depth Versus Distance for Type B Specimen Over a 5-Minute Period

U.S. DEPT. OF COMM. BIBLIOGRAPHIC DATA SHEET	1. PUBLICATION OR REPORT NO. NBS TN-945	2. Gov't Accession No.	3. Recipient's Accession No.
4. TITLE AND SUBTITLE AN INVESTIGATION OF THE FIRE ENVIRONMENT IN THE ASTM E 84 TUNNEL TEST		5. Publication Date August 1977	6. Performing Organization Code
		8. Performing Organ. Report No.	
7. AUTHOR(S) William J. Parker		10. Project/Task/Work Unit No. 4926680	
9. PERFORMING ORGANIZATION NAME AND ADDRESS NATIONAL BUREAU OF STANDARDS DEPARTMENT OF COMMERCE WASHINGTON, D.C. 20234		11. Contract/Grant No.	
		12. Sponsoring Organization Name and Complete Address (Street, City, State, ZIP) same as No. 9	
14. Sponsoring Agency Code			
15. SUPPLEMENTARY NOTES			
<p>16. ABSTRACT (A 200-word or less factual summary of most significant information. If document includes a significant bibliography or literature survey, mention it here.)</p> <p>Measurements were made of heat flux, oxygen concentration, temperature, velocity and pressure in a series of instrumented ASTM E 84 tunnel tests using (1) standard length specimens, (2) 0.91-m (3-ft) long specimens, and (3) a reference specimen consisting of asbestos-cement board and an auxiliary controlled supply of methane. Five different flow rates of methane to the auxiliary burner provided constant and known heat inputs simulating the gaseous decomposition products from regular test specimens. Incident heat fluxes on an inert specimen surface as high as 6.3 W/cm² (5.5 Btu/ft²·s) were measured within the flame impingement zone with a water-cooled heat flux meter 0.61 m (2 ft) downstream from the burner. While oxygen depletion in the tunnel did not appear to be a dominating factor in controlling the flame spread, the oxygen depletion measured in the exhaust duct beyond the tunnel correlated with the total rate of heat production of the specimens. It appears that the differences in the observed burning behavior of materials in the tunnel test and in a room may be mainly due to differences in the incident heat flux distribution in the two cases. These distributions reflect the different geometries, orientations, and ignition sources. The potential for rapid flame spread of some low flame spread classification (FSC) low density materials is evident from observations of the flame propagation along these materials during the tunnel test, but is not adequately reflected in the flame spread classification.</p>			
17. KEY WORDS (six to twelve entries; alphabetical order; capitalize only the first letter of the first key word unless a proper name; separated by semicolons) ASTM E 84; fire tests; flame spread; heat flux; heat release rate; smoke; Steiner Tunnel Test; oxygen depletion.			
18. AVAILABILITY <input checked="" type="checkbox"/> Unlimited <input type="checkbox"/> For Official Distribution. Do Not Release to NTIS <input checked="" type="checkbox"/> Order From Sup. of Doc., U.S. Government Printing Office Washington, D.C. 20402, SD Cat. No. C13.46: 945 <input type="checkbox"/> Order From National Technical Information Service (NTIS) Springfield, Virginia 22151		19. SECURITY CLASS (THIS REPORT) UNCLASSIFIED	21. NO. OF PAGES 75
20. SECURITY CLASS (THIS PAGE) UNCLASSIFIED		22. Price	

